Western Graduate&PostdoctoralStudies

Western University
Scholarship@Western

Electronic Thesis and Dissertation Repository

9-16-2016 12:00 AM

# Effect of Local Bed Hydrodynamics on the Distribution of Liquid in a Fluidized Bed

Lingchao Li, *The University of Western Ontario*

Supervisor: Franco Berruti, *The University of Western Ontario*
Joint Supervisor: Cedric Briens, *The University of Western Ontario*
A thesis submitted in partial fulfillment of the requirements for the Master of Engineering Science degree in Chemical and Biochemical Engineering
© Lingchao Li 2016

Follow this and additional works at: https://ir.lib.uwo.ca/etd

Part of the Other Chemical Engineering Commons

## Recommended Citation

Li, Lingchao, "Effect of Local Bed Hydrodynamics on the Distribution of Liquid in a Fluidized Bed" (2016). *Electronic Thesis and Dissertation Repository*. 4120.
https://ir.lib.uwo.ca/etd/4120

This Dissertation/Thesis is brought to you for free and open access by Scholarship@Western. It has been accepted for inclusion in Electronic Thesis and Dissertation Repository by an authorized administrator of Scholarship@Western. For more information, please contact wlswadmin@uwo.ca.

# Abstract

In an industrial Fluid Coker™, liquid bitumen is injected into a bed of hot coke particles through spray nozzles, grouped in several banks at different vertical positions. The main objective of this thesis is to determine whether significant improvements in liquid-solid contact could be achieved by optimizing the location of the spray nozzles.

In the coker regions where bitumen is injected, the gas is a mixture of product vapors and steam. Steam introduced at different levels rises through the coker: the stripping steam is injected near the bottom, then the attrition steam above the stripper and finally the bitumen atomization steam. As a result, the cross-sectional averaged gas velocity greatly varies vertically, from the lowest spray bank to the highest spray bank. In addition, there are large radial variations in gas velocity, as gas bubbles tend to concentrate in the central region of the bed.

In this study, the impacts of gas velocity and uneven gas distribution on liquid-solid contact were investigated. The effects of spray pulsations and atomization gas flowrate on liquid distribution were also studied. Effects of bed hydrodynamics on the initial liquid distribution and on the subsequent drying were studied separately.

The results indicate that jet pulsations or increasing the atomization gas flowrate improve the liquid distribution. Large improvements in liquid distribution were achieved by increasing the superficial gas velocity and also increasing the gas velocity at the end of the spray jet cavity, for all types of spray jets, pulsating or non-pulsating.

Key words: Fluid Coker™, liquid distribution, gas velocity, gas distribution, jet stability, gas to liquid ratio, agglomerate formation

# Acknowledgement

I would like to thank Dr. Cedric Briens and Dr. Franco Berruti for their support and mentorship during these past two years. The chance they offered to work in an industrially related program is greatly appreciated.

I would also like to thank the National Science and Engineering Research Council of Canada, Syncrude Canada and ExxonMobil for their generous financial support. Special thanks to Dr. Jennifer McMillan for her instructions and advice throughout my research.

I would like to thank all ICFAR staff members for their technical and administrative support. They made a very friendly working environment and a highly efficient team. I would like to thank Liliana Pardo for introducing me to the high velocity fluidized bed at the beginning of my program. I would also like to thank Francisco Sanchez for his help with my project and all advice as a sincere friend.

Finally, I would like to thank my parents for their support through all times in this new living and working environment. Without you, I wouldn't have achieved what I have today.

# Table of contents

Abstract ..... i

Acknowledgement ..... ii

Table of contents ..... iii

List of tables ..... vii

List of figures ..... viii

Lists of symbols ..... xiii

Introduction ..... 1

1.1 Fluid Coking™ ..... 1

1.2 Bed hydrodynamics ..... 2

1.3 Liquid distribution and agglomeration ..... 4

1.4 Spray performance ..... 6

1.4.1 Atomization gas to liquid ratio (GLR) ..... 6

1.4.2 Spray stability ..... 7

1.5 Thesis Objectives ..... 8

Experimental setup and methodology ..... 10

2.1 Equipment and material ..... 10

2.2 Bed conductance measurements ..... 14

2.3 Cold simulation experimental model ..... 15

2.3.1 Agglomerate size distribution ..... 16

2.3.2 Initial liquid to solid ratio ..... 18

2.4 Jet stability measurement ..... 18

2.5 Jet expansion angle ..... 22

Effect of high gas velocity on the distribution of liquid in a fluidized bed ..... 25

3.1 Experimental setup and methodology ..... 25

3.2 Results and discussion ..... 26

3.2.1 Preliminary tests ..... 26

3.2.2 Effect of gas velocity during injection ..... 27

3.2.3 Effect of gas velocity during drying ..... 33

Effect of local gas velocity on the distribution of liquid in a fluidized bed ..... 36

4.1 Experimental setup and methodology ..... 36

4.1.1 Initial gas distribution ..... 37

4.1.2 Measurement of bubble gas flow in bed ..... 38

4.2 Results and discussion ..... 42

4.2.1 Radial profiles of bubble gas distribution ..... 42

4.2.2 Confirmation of gas distribution by entrainment tests ..... 49

4.2.3 Effect of gas distribution on liquid distribution ..... 51

Effect of improvements in nozzle performance on the distribution of liquid in a fluidized bed for various bed hydrodynamics ..... 54

5.1 Experimental setup and methodology ..... 54
5.1.1 Jet stability ..... 54
5.1.2 Gas to liquid ratio (GLR) ..... 58
5.1.3 Jet expansion angle ..... 58
5.2 Results and discussion ..... 59
5.2.1 Spray stability ..... 59
5.2.2 Effect of spray stability on liquid distribution ..... 60
5.2.3 Effect of gas velocity on liquid distribution for pulsating spray ..... 70
5.2.4 Effect of GLR on liquid distribution ..... 71
Conclusions and Recommendations ..... 77
6.1 Conclusions ..... 77
6.2 Recommendation ..... 78
References ..... 80
Appendices ..... 84
Data Acquisition ..... 84
Arduino ..... 106
Matlab Programs ..... 109
Pixel values ..... 109
Pixel values-Simulink ..... 113
Color analysis ..... 114

Color analysis-Simulink..... 120

Curriculum Vitae ..... 122

# List of tables

Table 4-1 Mass of solids entrained in left and right internal cyclones at different gas distributions ..... 50

Table 5-1 Linear velocities of liquid and atomization gas in different sizes of conduits ..... 57

Table 5-2 Free moisture fraction for pulsating and stable spray at different conditions ..... 69

# List of figures

Figure 1.1 Process flow diagram of fluid coking [1] ..... 1

Figure 1.2 Mechanism of agglomerate formation in a gas-solid fluidized bed [11] ..... 4

Figure 1.3 Schematic of granulation processes [12] ..... 5

Figure 1.4 Schematic diagram of feed-coke interaction [13] ..... 6

Figure 2.1 Schematic diagram of high gas velocity fluidized bed (front view) ..... 10

Figure 2.2 Schematic diagram of high gas velocity fluidized bed (lateral view) ..... 11

Figure 2.3 Picture of the sparger ..... 12

Figure 2.4 Schematic diagram of the sparger in the fluidized bed. The direction of gas entering the fluidized bed is parallel to the angled wall. ..... 12

Figure 2.5 Diagram of TEB spray nozzle ..... 13

Figure 2.6 Schematic diagram of injection system ..... 13

Figure 2.7 Size distribution of silica sand for experiments ..... 14

Figure 2.8 The electrical circuit system for conductance measurement ..... 15

Figure 2.9 Calibration curve for blue dye ..... 17

Figure 2.10 A single pixel in the original photo of the spray ..... 19

Figure 2.11 A single pixel in the photo of the spray transferred into gray scale ..... 19

Figure 2.12 Amount of pixels for each Gray Intensity for pure background ..... 20

Figure 2.13 Amount of pixels for each Gray Intensity ..... 21

Figure 2.14 Schematic diagram of jet expansion angle θ ..... 22

Figure 2.15 Geometry of jet expansion angle calculation ..... 23

Figure 2.16 Photo of the jet, GLR=1%, $F_L$=23.4 g/s ..... 23

Figure 2.17 Gray intensity values in the pixels where x=100, GLR=1% when x=100, y represents the vertical locations of pixels. ..... 24

Figure 3.1 Conductance signal for injection of 180 g $H_2O$ at room temperature ..... 26

Figure 3.2 Conductance signal for injection of 150 g Gum Arabic solution at 130 °C..... 27

Figure 3.3 Cumulative weight percentage of agglomerates in bed solid mass for various $V_{gi}$ while $V_{gd}$ is constant at 0.18 m/s ..... 28

Figure 3.4 The effect of $V_{gi}$ on amount of macro and micro agglomerates while $V_{gd}$ is constant at 0.18 m/s..... 29

Figure 3.5 Cumulative fraction of water trapped in agglomerates various $V_{gi}$ while $V_{gd}$ is constant at 0.18 m/s..... 30

Figure 3.6 Effect of $V_{gi}$ on the total amount of free moisture ..... 31

Figure 3.7 Initial L/S ratio in macro and micro agglomerates at various $V_{gi}$ at constant $V_{gd}$=0.18 m/s..... 32

Figure 3.8 Effect of increasing $V_{gd}$ on the amount of agglomerates at different $V_{gi}$ (0.18, 2.2 m/s) ..... 33

Figure 3.9 Effect of $V_{gd}$ on liquid to solid ratio when $V_{gi}$= 0.18 m/s and $V_{gi}$= 2.2 m/s ..... 34

Figure 3.10 Effect of $V_{gd}$ on amount of agglomerates when $V_{gi}$= 0.18 m/s and $V_{gi}$=2.2 m/s ..... 35

Figure 4.1 Schematic diagram of triboelectricity measurement system ..... 37

Figure 4.2 Top view of the locations of the 20 sonic nozzles..... 37

Figure 4.3 Top view of locations of tribo probes..... 39

Figure 4.4 Raw signal of triboelectricity measurement, superficial gas velocity 1m/s ..... 40

Figure 4.5 Power spectra of triboelectricity measurement for a low bubble gas flowrate ..... 41

Figure 4.6 Power spectra of triboelectricity measurement for a high bubble gas flowrate ..... 41

Figure 4.7 Correlation between the real average volumetric flux of bubble gas and the average volumetric flux calculated..... 43

Figure 4.8 Group 1 gas distributions, (a) 0.6-0.4 m/s, (b) 0.1-0.9 m/s, (c) 0.9-0.1 m/s..... 44

Figure 4.9 Profiles of gas bubble flow for Group 1 gas distributions. (The profile was measured without the jet)..... 45

Figure 4.10 Group 2 gas distributions, (a) 0.6-0.4 m/s, (b) 0.2-0.8 m/s, (c) 0.8-0.2 m/s..... 45

Figure 4.11 Profiles of gas bubble flow for Group 2 gas distributions..... 46

Figure 4.12 Group 3 gas distributions, (a) 0.6-0.4 m/s, (b) 0.3-0.7 m/s, (c) 0.7-0.3 m/s..... 46

Figure 4.13 Profiles of gas bubble flow for Group 3 gas distributions..... 47

Figure 4.14 Summary of bubble gas flow radial profiles of various gas distributions..... 48

Figure 4.15 schematic diagram of the high gas velocity fluidized bed ..... 49

Figure 4.16 Fraction of free moisture in mass of liquid injected (data for even distribution is obtained from section 3.2.2) ..... 51

Figure 4.17 weight percentage of agglomerates in bed mass ..... 52

Figure 4.18 liquid to solid ratio in agglomerates for gas distributions..... 53

Figure 5.1 Injection system for pulsating spray..... 55

Figure 5.2 Injection system for stable spray ..... 55

Figure 5.3 Flow pattern map of Taitel and Dukler [30]. The dotted line refers to the modified transition line between the intermittent and annular regimes, as proposed by Barnea et al [31]. 56

Figure 5.4 Pictures of spray (pulsating spray, t=0 is the beginning of injection) ..... 58

Figure 5.5 Stability analysis for pulsating spray, GLR=2.2%, $F_L$=21.4 g/s ..... 59

Figure 5.6 Stability analysis for stable spray GLR=2.2%, $F_L$=21.4 g/s..... 60

Figure 5.7 Cumulative Wt% of agglomerates in bed mass GLR=2.2%, $F_L$=21.4 g/s (two experiments for each condition)..... 61

Figure 5.8 Initial L/S ratio in agglomerates (g/g) GLR=2.2%, $F_L$=21.4 g/s..... 62

Figure 5.9 Cumulative fraction of water trapped in agglomerates GLR=2.2%, $F_L$=21.4 g/s..... 62

Figure 5.10 Cumulative Wt% of agglomerates in bed mass GLR=2.2%, $F_L$=21.4 g/s ..... 63

Figure 5.11 Initial L/S ratio in agglomerates (g/g) GLR=2.2%, $F_L$=21.4 g/s..... 64

Figure 5.12 Cumulative fraction of water trapped in agglomerates GLR=2.2%, $F_L$=21.4 g/s..... 64

Figure 5.13 Cumulative Wt% of agglomerates in bed mass GLR=2.2%, $F_L$=21.4 g/s ..... 65

Figure 5.14 Initial L/S ratio in agglomerates (g/g) GLR=2.2%, $F_L$=21.4 g/s..... 66

Figure 5.15 Amount of water trapped in agglomerates GLR=2.2%, $F_L$=21.4 g/s..... 66

Figure 5.16 Cumulative Wt% of agglomerates in bed mass GLR=2.2%, $F_L$=21.4 g/s ..... 67

Figure 5.17 Initial L/S ratio in agglomerates (g/g) GLR=2.2%, $F_L$=21.4 g/s..... 68

Figure 5.18 Initial L/S ratio in agglomerates (g/g) GLR=2.2%, $F_L$=21.4 g/s..... 68

Figure 5.19 Comparison between the amount of free moisture of stable spray and pulsating spray ..... 69

Figure 5.20 Cumulative weight fraction of water trapped in agglomerates, GLR=2.2%, $F_L$=21.4 g/s ..... 70

Figure 5.21 Stability analysis for open air spray at various GLRs, $F_L$=23.4 g/s ..... 71

Figure 5.22 Jet expansion angle for sprays of different GLRs in the open air ..... 72

Figure 5.23 Free moisture fraction in the water injected for different GLRs, $F_L$=23.4 g/s ..... 73

Figure 5.24 Cumulative fraction of water trapped in agglomerates in total amount of water injected for different GLRs, $F_L$=23.4 g/s ..... 73

Figure 5.25 Total fraction of agglomerates in bed mass for different GLRs, $F_L$=23.4 g/s ..... 74

Figure 5.26 Cumulative wt% of agglomerates in bed mass for different GLRs, $F_L$=23.4 g/s ..... 75

Figure 5.27 Liquid to solid ratio in agglomerates for different GLRs, $F_L$=23.4 g/s ..... 76

# Lists of symbols

$d_{aggl}$ Diameter of agglomerates (μm)

$d_p$ Particle diameter (μm)

f Average frequency

GLR Gas to liquid ratio

i Gray intensity

$L_{jet}$ Jet penetration distance (m)

$m_d$ Mass of dye (g)

$m_{GA}$ Mass of Gum Arabic (g)

$m_p$ Mass of particles trapped in agglomerates (kg)

$m_R$ Representative sample taken from $m_{<600\mu m}$ (g)

$m_{sand}$ Total mass of individual particles and agglomerates (g)

$m_{\mu aggl,\ i}$ Total mass of micro-agglomerates in the bed for a given size cut (g)

$m_{\mu aggl,\ Ri}$ Mass of micro-agglomerates in the sample for a given size cut (g)

$m_{<600\mu m}$ Bed mass after removal of agglomerates larger than 600 μm

P Power spectral density

$q_{bi}$ local volumetric flux of bubble gas, $m^3/(s \cdot m^2)$

$\overline{q_b}$ Cross-sectional average volumetric flux of bubble gas, $m^3/(s \cdot m^2)$

$U_{GS}$ Linear velocity of gas in the conduit

$U_{LS}$ Linear velocity of liquid in the conduit

$u_{mf}$ Minimum fluidization velocity

$x_f$ Fraction of particles smaller than 355 μm in $m_{sand}$

$x_{bed}$ Fraction of particles smaller than 355 μm in initial particle size distribution (PSD)

$V_g$ Gas velocity, m/s

$V_{gi}$ Superficial velocity during liquid injection, m/s

$V_{gd}$ Superficial velocity during drying, m/s

α Coefficient for correlation of power spectral density, frequency and local volumetric flux of bubble gas flow

β Coefficient for correlation of power spectral density, frequency and local volumetric flux of bubble gas flow

γ Coefficient for correlation of power spectral density, frequency and local volumetric flux of bubble gas flow

λ Local cross-sectional area for volumetric flux of bubble gas, $m^2$

θ Spray expansion angle

# Introduction

The present work addresses factors that could help improve the distribution of liquid injected into a solid-gas fluidized bed. Good liquid-solid contact is crucial to maintain good operability and maximize the yield of valuable liquid in Fluid Cokers™. The formation of undesired agglomerates needs to be minimized for better mass and heat transfer.

The key motivation of this study is to have a better understanding of impacts of different bed hydrodynamics on liquid distribution.

## 1.1 Fluid Coking™

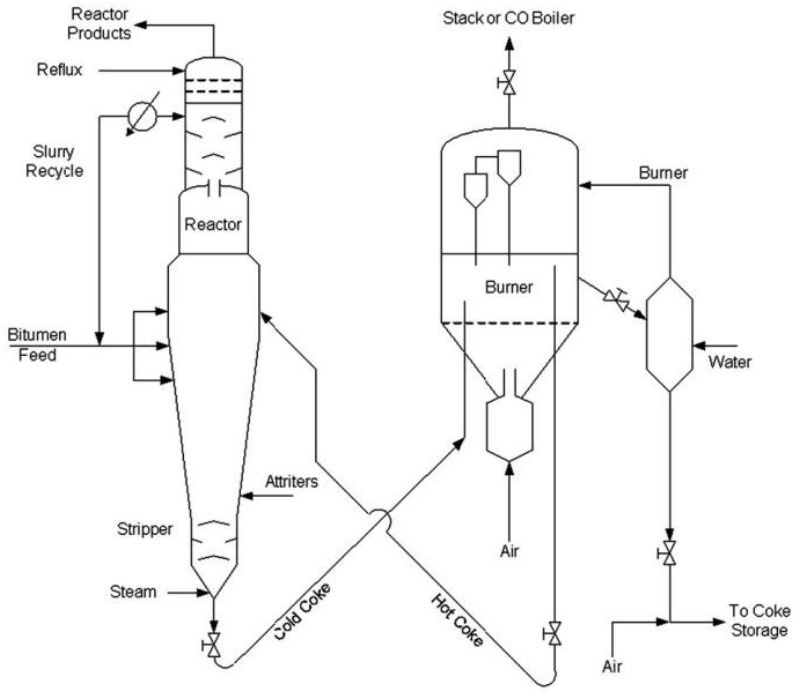


**Figure 0.1 Process flow diagram of fluid coking** [1]

Canada's oil sands are the world's largest known concentration of bitumen. The current estimate of the ultimately recoverable volume represents only 12 percent of the ultimate volume of bitumen in place (NEB, 2000). Fluid Coking™, which is mainly used to upgrade residues, has an important role in the oil sands industry.

Figure 1.1 provides a schematic diagram of the Fluid Coking™ process. A Fluid Coking unit is made up of 2 vessels, the coking vessel and the burner vessel. Liquid feedstocks can be heavy or reduced crudes or vacuum bottoms containing constituents that cannot be vaporized without decomposition. Feeds typically have an API between 0 to 20° and a Conradson carbon content of circa 5 to 40 weight percent. Liquid feedstock atomized with steam is sprayed into the reactor (coking vessel) after being preheated to 200 to 400 °C. It is very important to distribute the feed quickly and uniformly over particles in the bed. Spray nozzles are located at multiple points both circumferentially and vertically to avoid excessive concentration of liquid in a part of the bed. The average superficial velocity of the rising gases varies with height and is usually between 0.3 and 0.9 m/s. The temperature in the reactor is preferably maintained between 480 °C to 540 °C while the gauge pressure is between 0 to 3.5 bar. [3]

In the fluid bed reactor, the feed is converted to hot hydrocarbon vapor, permanent gases and solid coke. The gas and vapors pass through cyclones where most of the entrained particles are removed. Then the vapors enter a scrubber section in which remaining particles are removed and heavy liquids are condensed. At the base of the reactor, coke particles flow through the stripping section and interstitial product vapors are removed by a stripping gas, e.g. steam. The coke particles flow down through a stand-pipe then up though a riser to the burner. A portion of the coke particles are burned with air to produce enough heat for the process. The remaining, reheated particles are then transported back to the reactor to supply the heat required for reaction. Net coke is removed as product coke. [4]

## 1.2 Bed hydrodynamics

In a Fluid Coker, superficial gas velocity increases with increasing height due to the steam from the stripper section and attrition nozzles, and the gases and vapors from the pyrolysis of feed injected at different levels.

By experimental simulation, Song et al. [5] found a strong radial profile of the gas velocity in Fluid Cokers: there is a core-annulus structure. In the annular region, the particles flow downwards, while in the core region, particles are carried upwards by gas bubbles. The bed

voidage increases gradually from the wall to the center of the bed without a sharp transition from the annular region and the core region. This means that in the core region the gas velocity is higher than the cross-sectional average superficial gas velocity at the same height.

Mohagheghi et al. [6] used a conductance method to investigate the effect of local hydrodynamics on liquid distribution in a gas-solid fluidized bed, and found that a higher fluidization velocity during liquid injection is beneficial for liquid-solid contact.

Pougatch et al. [7] developed a novel mathematical model to describe the spray jet and its contact with solid particles in a fluidized bed. Through analysis they found that increasing gas velocity improves liquid-solid contact in the region far from the tip of the nozzle. Increasing the gas velocity has no measurable influence on liquid-solid contact in the region near the nozzle tip.

Morales et al. [8] conducted injections with a liquid solution which uses Plexiglas$^{TM}$ as binder to investigate the effect bed hydrodynamics on liquid distribution. They found that increasing the gas velocity in fluidized bed reduces the total amount of agglomerates. A higher gas velocity increases the amount of smaller, micro agglomerates but decreases the amount of larger, macro agglomerates, which are more problematic in the industrial process. However, the impacts of gas velocity on initial liquid distribution and on agglomerate breakage were not separated.

Weber et al. [9] investigated various factors that can possibly affect the agglomerate behavior in a fluidized bed. They found that agglomerate destruction is a complex process which is determined by several parameters, i.e. superficial gas velocity, initial agglomerate size, liquid concentration and liquid physical properties. Increasing the superficial velocity can switch the agglomerate size reduction mechanism to the more effective fragmentation regime. In accordance with this conclusion, Mohagheghi[6] utilized the capacitance method to confirm that increasing the gas velocity after liquid injection accelerates the breakage of agglomerates.

The study of Ariyapadi et al. [10] used X- rays to confirm that most of the agglomerates form at the end of the jet, where the shear force is lower. This conclusion leaves space for more study to investigate the mechanism of agglomerate formation which will be dealt with in Chapter 3.

## 1.3 Liquid distribution and agglomeration

Particle agglomeration occurs when liquid is sprayed into a gas-solid fluidized bed. Undesired agglomerates in a Fluid Coker need to be minimized for better mass and heat transfer.

Bruhns and Werther [11] proposed a model for the mechanism of the injection of liquid reactants into a fluidized bed reactor. When the liquid is sprayed into the fluidized reactor, no instantaneous liquid evaporation occurs at the nozzle tip even though the bed temperature is higher than the boiling point of the liquid. The liquid jet penetrates the bed and wets the particles entrained into the region of liquid – solid interaction. Agglomerates formed in this region are then transported into other parts of the bed. Due to the shear forces in the fluidized bed, resulting from gas bubbles, and the agglomerates are susceptible to breakup.

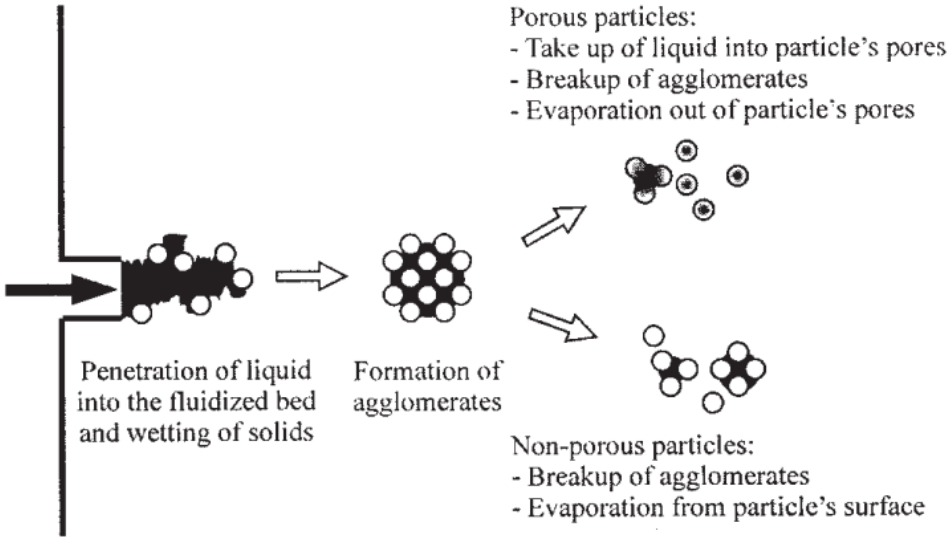


**Figure 0.2 Mechanism of agglomerate formation in a gas-solid fluidized bed** [11]

Iveson et al [12] proposed a description of wet granulation in which they adopted a modern approach instead of the complex traditional description which consists of a number of competing mechanisms. The modern model consists of three key rate processes: wetting and nucleation, consolidation and growth, and breakage and attrition.

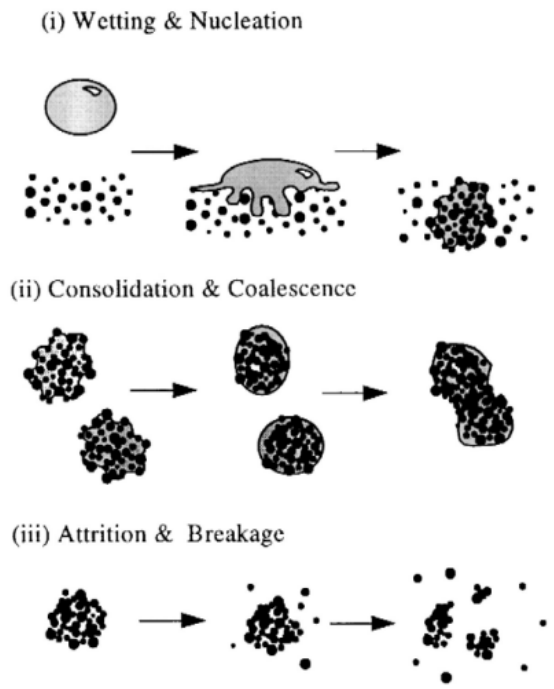


**Figure 0.3 Schematic of granulation processes** [12]

1. Wetting and nucleation. The liquid binder is sprayed into the fluidized bed and is distributed on the particles to give a distribution of nuclei granules;

2. Consolidation and growth. Granules collide with other granules, dry feed powder or the equipment which leads to granule compaction and growth;

3. Attrition and breakage. Wet or dried agglomerates break up due to impact, erosion or compaction.

Based on the description above and other previous researches, Gray [13] also proposed a mechanism for feed interaction with the bed particles in a Fluid Coker.

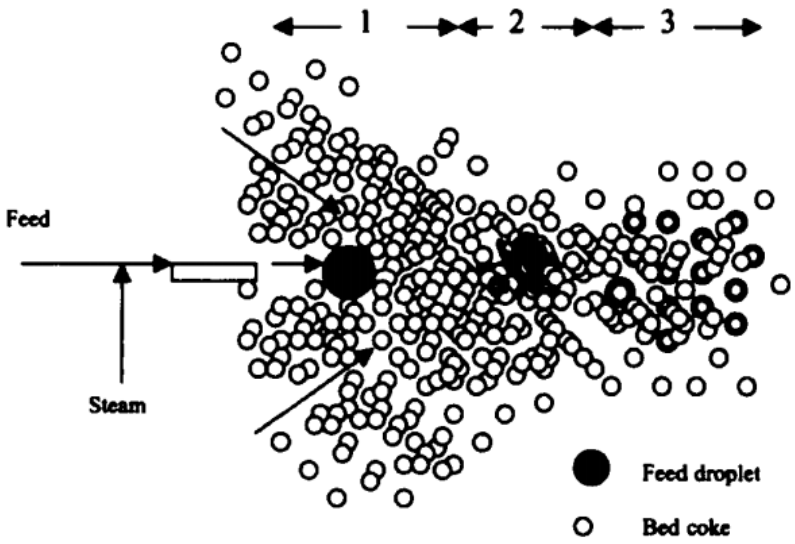


**Figure 0.4 Schematic diagram of feed-coke interaction** [13]

In the first step, the liquid feed is atomized and introduced into the fluidized bed. Secondly, a feed drop entering the bed collides with several particles since the particles are smaller. Particles wrapped by the drop form a wet granule. In the last step, due to gas velocities in the fluid bed (0.3-1.5 m/s), the granule tends to be broken up by shear forces. This mechanism results in uniformly coated particles. The thickness of liquid film depends on the local voidage of the fluidized bed and the liquid fraction in the void volume.

## 1.4 Spray performance

### 1.4.1 Atomization gas to liquid ratio (GLR)

Farkhondehkavaki et al. [14] used various methods to characterize the amount of free moisture(individual particles coated with liquid) in a fluidized bed after liquid addition. Using conductance method, she found that increasing the atomization Gas to Liquid ratio (GLR) of the liquid injection with a TEB nozzle (a typical commercial nozzle for Fluid Cokers$^{TM}$[15]) from 0 % to 2 % contributes to an increase in the amount of free moisture. And even the GLR of 2 % is not perfect because, with full-scale commercial spray nozzles, more than 50 % of injected liquid is still trapped in agglomerates just after the injection.

ZirGachian et al. [16] applied a novel measurement method employing electrical conductance in a large scale fluidized bed of 7 tons of silica sand. They conducted liquid injections with an industrial scale TEB nozzle. They showed that raising the GLR from 0 % to 5.59 % can greatly improve the efficiency of liquid-solid contact.

Portoghese et al. [17] developed a new method to characterize the efficiency of the injection of liquid sprayed into a fluidized bed. A Nozzle Performance Index (NPI) was derived from triboelectric signals for nozzles injecting air-atomized water into a gas–solid fluidized bed. Using this method, they also found that increasing the GLR would be beneficial to liquid distribution. The optimal GLR, however, depends on the nozzle size and operating liquid flowrate. It is also suggested that a better jet-bed interaction is obtained from 2 factors:

1. Finer liquid droplets at the nozzle tip
2. A higher rate of solid entrainment into the jet cavity caused by a larger expansion angle of the gas-liquid jet

Leach et al. [18] utilized a conductance method to characterize the performance of various atomizing feed nozzles at different GLRs. For the patented TEB nozzle which is widely used in the industrial process, it is reported that an optimal GLR exists at around 2.5 %. Increasing the GLR past 2.5% deteriorates the quality of liquid-solid contact. Leach et al. [18] also found that the impact of GLR is completely different for nozzles of different geometry.

Mohagheghi et al. [6] applied a new capacitance measurement method to characterize the liquid distribution in a fluidized bed. The results indicated as well that a higher GLR of the feed nozzle contributes to better contact between atomized liquid and fluidized particles.

### 1.4.2 Spray stability

Several researchers have studied the influence of spray pulsations on liquid distribution when liquid is injected into a gas-solid fluidized bed.

Sabouni, et al. [19] utilized a solenoid valve to introduce fluctuations of well-defined frequency to an atomized gas-liquid spray. They found that at three different GLRs, jet fluctuation improved liquid distribution. They also confirmed the significantly beneficial effect of pulsations on liquid-solid contact over a range of operating conditions i.e. different liquid flow rates, gas properties and spray nozzle geometry.

Later, the authors [20] created a plug flow before the gas-liquid mixture exited the nozzle tip. This resulted in a spray pulsation in the fluidized bed. The results indicated that pulsations can improve liquid distribution. The mechanism of the impact is likely relevant to the rapid expansion-contraction of the jet cavity. Subsequently they [21] also confirmed the beneficial impact of spray pulsations on liquid distribution for four different types of spray nozzles. It is suggested that the expansion-contraction of jet cavity would inhale more solids into the jet and also agitate the agglomerates, which contributes to a lower liquid to solid ratio and smaller sized agglomerates.

Leach et al. [22] tested the effect of spray pulsations in a large scale fluidized bed containing 8800 kg of silica sand. Also different from the above-mentioned studies, they introduced spray pulsations in a commercial-scale spray nozzle. It is reported that large amplitude pulsations with a frequency ranging from 1-5 Hz resulted in less agglomerate formation and better contact between liquid and particles throughout the bed.

## 1.5 Thesis Objectives

The objective of this study is to investigate the effect of local bed hydrodynamics on the liquid distribution in a fluidized bed.

The impacts of increasing gas velocity during liquid injection and after injection are studied separately to understand the initial liquid distribution and agglomerate breakage in the fluidized bed. The effect of the “radial” profile (more precisely lateral profile, since the column has a rectangular cross-section) of the gas velocity on liquid distribution is investigated to whether it is beneficial to have a higher gas velocity at the tip of the nozzle or the end of the jet. The effects of the GLR and jet stability on liquid distribution at different superficial velocities are also studied.

The cold simulation experimental model (Chapter 2), which was utilized to acquire the mass of agglomerates in different sizes and also the liquid concentration in agglomerates, serves as a more direct method to characterize the liquid-solid contact than other methods previously developed, e.g. conductance and capacitance methods.

Chapter 3: The effects of high gas velocity during injection and also during agglomerate drying and breakup are determined separately. The lateral profile of the initial gas distribution is even for experiments in this study. The superficial velocity spans from 0.18 m/s to 2.2 m/s.

Chapter 4: When the superficial velocity in the freeboard is constant, the effect of laterally uneven gas distribution in various patterns on liquid distribution is investigated. The main objective is to observe whether having a higher gas velocity at the end of the jet or the beginning of the jet would be beneficial for liquid distribution.

Chapter 5: Effect of change in nozzle performance (e.g. GLR and stability) on liquid distribution in a fluidized bed for various bed hydrodynamics is studied. Pulsations were introduced into the spray by changing the geometry of the injection system. Bed hydrodynamics were changed at different nozzle performance conditions.

# Experimental setup and methodology

## 2.1 Equipment and material

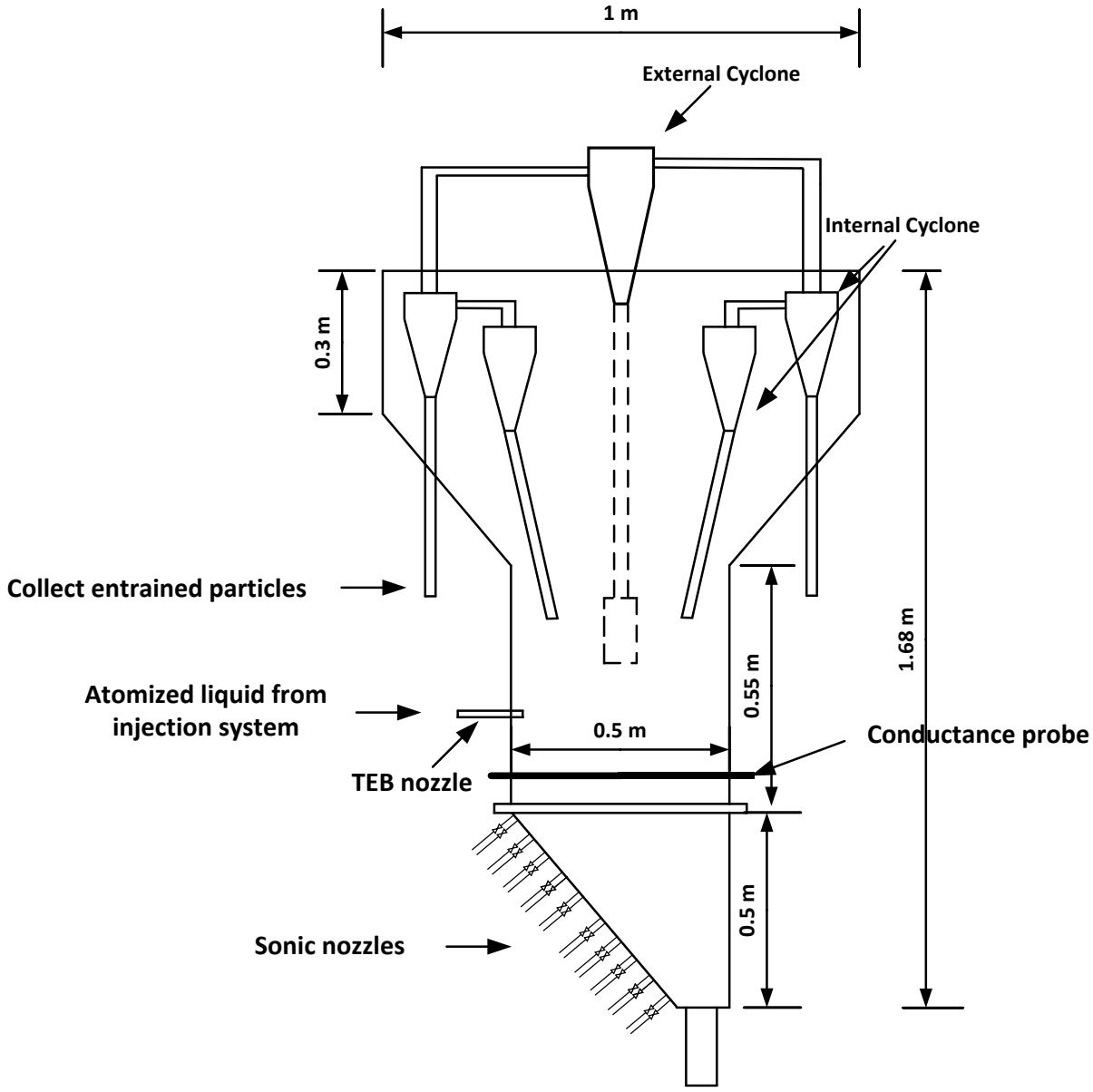


**Figure 0.1 Schematic diagram of high gas velocity fluidized bed (front view)**

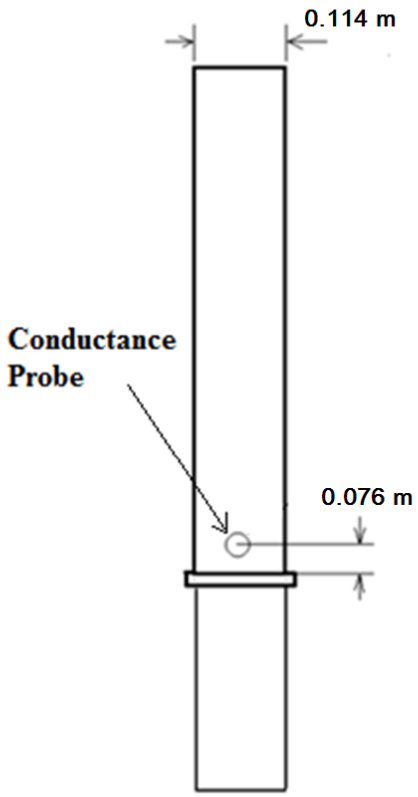


**Figure 0.2 Schematic diagram of high gas velocity fluidized bed (lateral view)**

As shown in Figure 2.1 and Figure 2.2, the high velocity fluidized bed consists of 2 major parts. The column height is 1.68 m with an expansion in the upper section. The bed width expands from 0.5 m to 1 m from the lower section to the higher section. The sonic nozzles are distributed on an angled slope, which results in an asymmetrical gas distribution in the fluidized bed when the open sonic nozzles are evenly distributed (described in Chapter 4).

The gas distributors consist of 20 tuyeres, each supplied by a dedicated sonic nozzle to maintain the required gas flow through each tuyere, independently of downstream conditions. The sonic nozzles are located well upstream of the bed to prevent excessive attrition of the bed solids. As shown in Figure 2.3, each tuyere consists of a hollowed bolt: the gas flows up through the hollowed bolt and out through three 3 mm holes at the top. The fluidization gas was air at ambient conditions.

**Figure 0.3 Picture of the sparger**

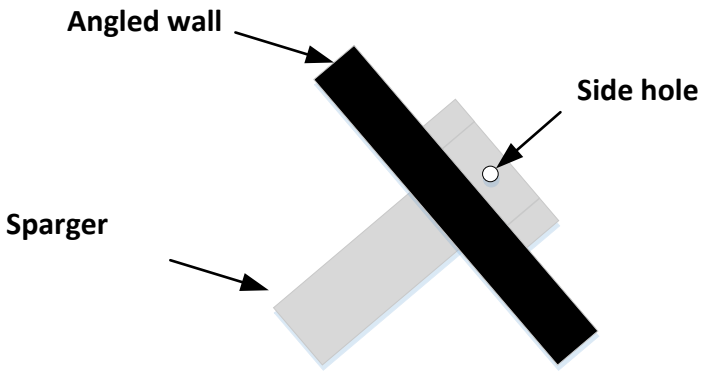


**Figure 0.4 Schematic diagram of the sparger in the fluidized bed. The direction of gas entering the fluidized bed is parallel to the angled wall.**

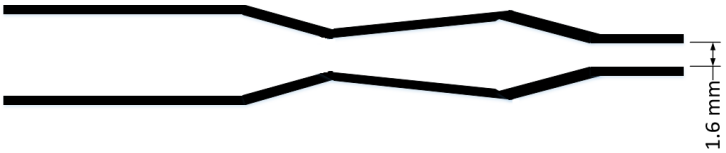


**Figure 0.5 Diagram of TEB spray nozzle**

For all the liquid injection experiments in this study, the spray nozzle used is a typical industrial TEB nozzle[15] with a throat diameter of 1.6 mm as shown in Figure 2.5. The flow of the mixture of liquid and atomization gas through the nozzle throat was always in the sonic regime.

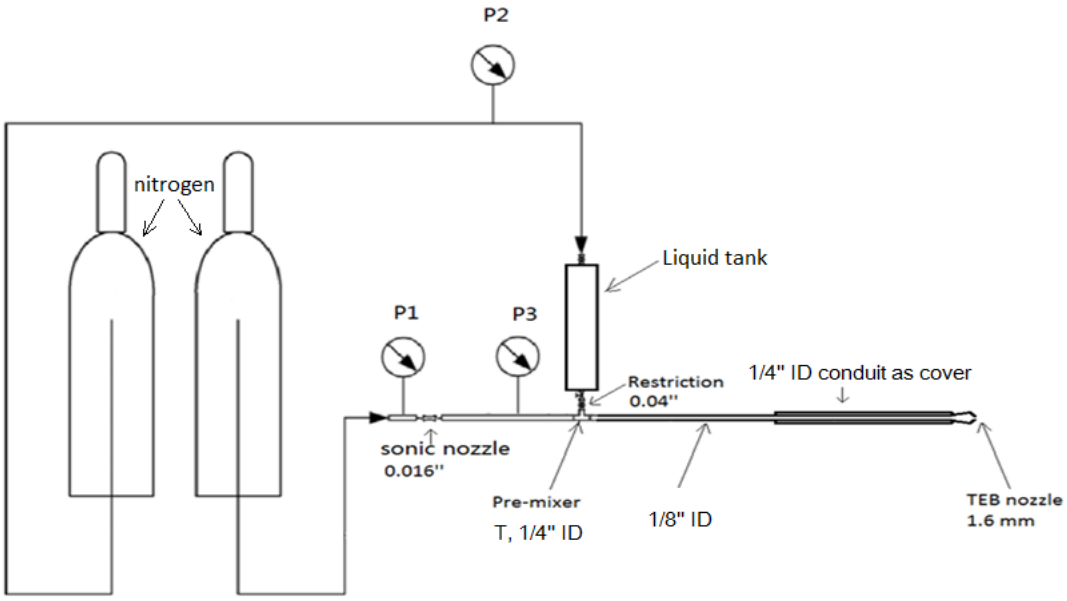


**Figure 0.6 Schematic diagram of injection system**

The injection system shown in Figure 2.6 produces a relatively stable spray. Pressures for atomization gas and liquid tank are adjusted by regulators to achieve the required liquid and gas flowrates. In chapter 5, changes were made to the geometry of the system to produce a pulsating spray.

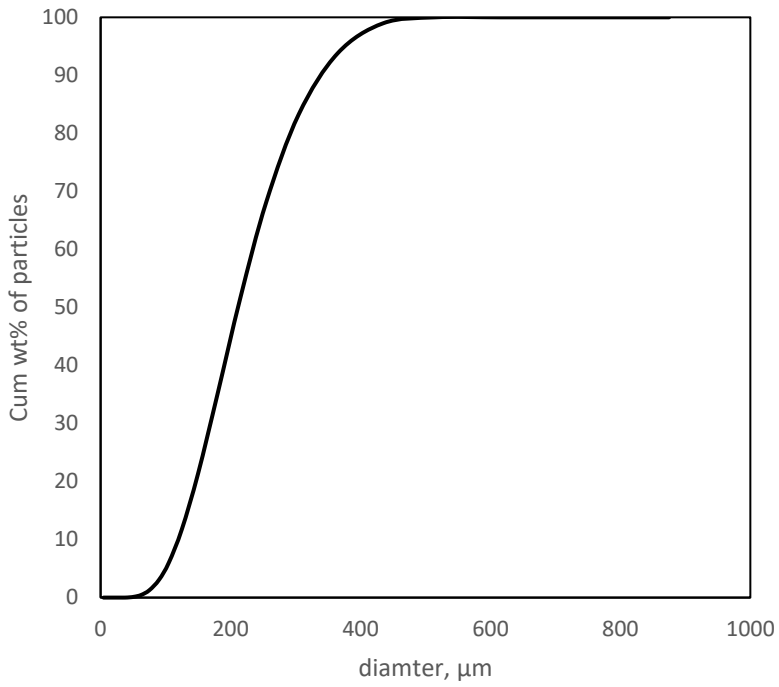


**Figure 0.7 Size distribution of silica sand for experiments**

The fluidized bed solids consisted of 80 kg of silica sand with a bulk density of 2650 kg/m$^3$ and a Sauter mean diameter of 190 µm, with the cumulative size distribution shown in Figure 2.7. The minimum fluidization velocity for the bed is 0.03 m/s[23].

## 2.2 Bed conductance measurements

The electrical circuit system is shown in Figure 2.8. The conductance method utilizes the principle that the bed conductivity increases with increasing amount of free moisture in the bed[24].

A conductance probe, which is a stainless steel rod isolated from the bed walls, is placed across the fluidized bed as shown in Figure 2.1. A function generator supplies an AC current to the circuit, with a frequency of 100 Hz and a total voltage of 7 V. When the resistance of the fluidized bed changes, the voltage on the resistor changes accordingly.

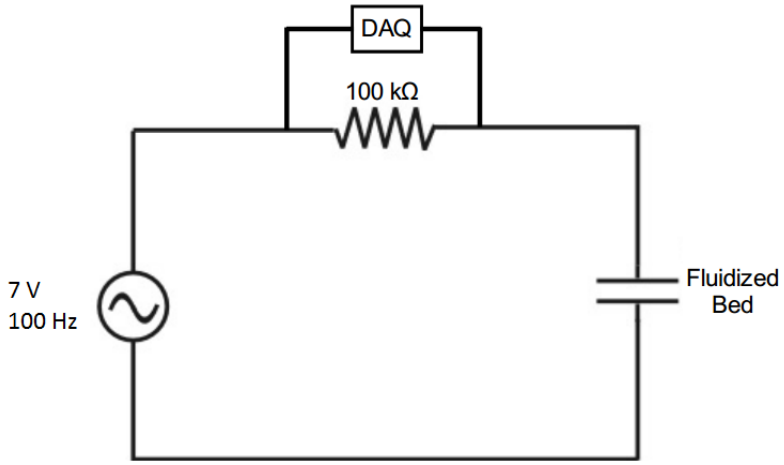


**Figure 0.8 The electrical circuit system for conductance measurement**

## 2.3 Cold simulation experimental model

Pardo et al. [25] developed a cold simulation, experimental method to simulate the process of agglomerate formation in a Fluid Coker$^{TM}$. A binder solution with dyes is injected into the fluidized bed so that the sizes of agglomerates and the initial liquid to solid ratio (L/S) can be retrieved afterwards. For this study, one dye of blue color is used since there is only one injection in each experiment.

The binder solution consists of 92 wt% water, 6 wt% Gum Arabic, 2 wt% blue with a total mass of 150 g injected in each experiment. The mass of liquid is chosen to avoid bogging. The pH of the solution is adjusted to 3.0 using hydrochloric acid in order to adjust the viscosity of the liquid into the range of bitumen viscosity at injection conditions[25]. The liquid mass flowrate is kept at 24.2 g/s during injection and GLR is 2%. At the beginning of injection, the bed temperature is 135 °C. The gas velocity during injection and afterwards can be adjusted using pressure regulators and opening/closing the valves upstream of each sonic nozzle. After each experiment, the sand and agglomerates are cooled overnight.

### 2.3.1 Agglomerate size distribution

The agglomerates are separated into 9 different size cuts by sieving. The 6 size cuts for macro-agglomerates are shown below.

$$d_{aggl} \geqslant 9500\ \mu m$$

$$9500\ \mu m > d_{aggl} \geqslant 4000\ \mu m$$

$$4000\ \mu m > d_{aggl} \geqslant 2000\ \mu m$$

$$2000\ \mu m > d_{aggl} \geqslant 1400\ \mu m$$

$$1400\ \mu m > d_{aggl} \geqslant 850\ \mu m$$

$$850\ \mu m > d_{aggl} \geqslant 600\ \mu m$$

Agglomerates recovered by sieving that have a diameter smaller than 600 µm, are mixed with sand particles, and are called micro-agglomerates.

The 3 size cuts for micro-agglomerates are as below.

$$600\ \mu m > d_{aggl} \geqslant 500\ \mu m$$

$$500\ \mu m > d_{aggl} \geqslant 425\ \mu m$$

$$425\ \mu m > d_{aggl} \geqslant 355\ \mu m$$

The agglomerates in the above-mentioned size cuts will also be dissolved in water. The mass of water for dissolution is generally 3 times the mass of agglomerates. The concentration of blue in the solution is determined by using a spectrophotometer (Thermo Scientific Evolution 220 UV-Visible Spectrophotometer) to measure the absorbance at 630 µm (wavelength of blue light). The correlation between the absorbance and the blue concentration is obtained by calibration, and is shown in Figure 2.9.

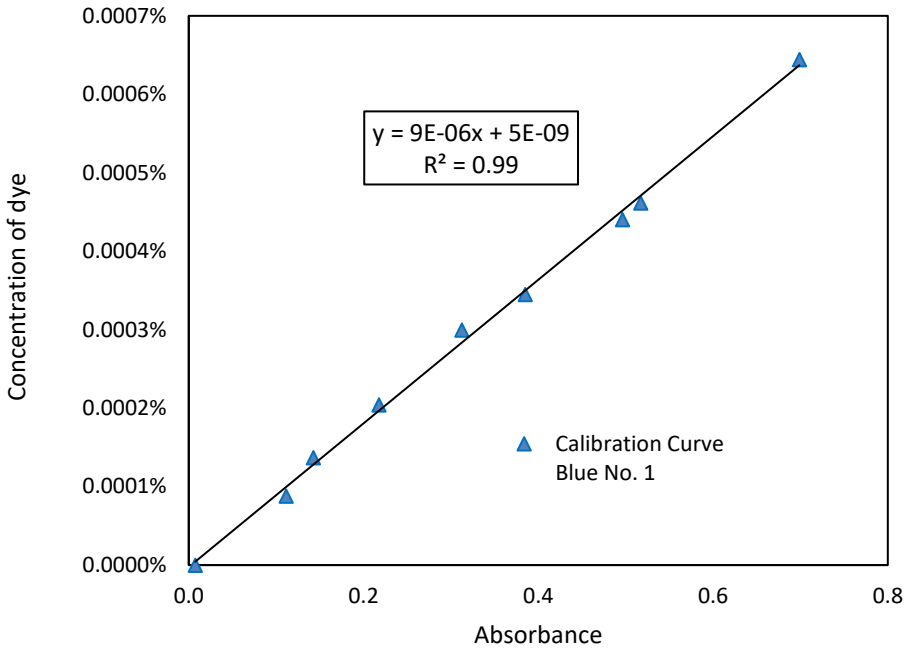


**Figure 0.9 Calibration curve for blue dye**

After retrieving the macro agglomerates through sieving, a sample of 5 kg of sand and micro agglomerates is taken and sieved. The size distribution of the sand particles trapped in agglomerates is assumed to be the same as the initial sand particles. Thus, the particles trapped in micro agglomerates can be used as a tracer to calculate the mass of agglomerates. Use size cut 425 µm > $d_p \geqslant$ 355 µm as an example.

$$m_p = m_{sand} \frac{x_f}{x_{bed}} \qquad 2\text{-}1$$

Then the mass of micro-agglomerates in the sample ($m_{\mu agg}$,$R_i$) could be calculated for each size cut, considering that the agglomerates consist of sand, dye and gum. Therefore, the mass of agglomerates in the sample could be defined as:

$$m_{\mu aggl,R_i} = m_p + m_{GA} + m_d \qquad 2\text{-}2$$

Subsequently the total mass of micro agglomerates between 355 µm and 425 µm in the bed mass can be calculated as[25]

$$m_{\mu agg,i} = m_{\mu agg,R_i} \frac{m_{<600\mu m}}{m_R} \quad 2\text{-}3$$

### 2.3.2 Initial liquid to solid ratio

The blue dye is used as a tracer to calculate the amount of Gum Arabic and water initially, trapped in agglomerates, before evaporation of the water. Thus the ratio between blue dye, Gum Arabic and water is 2 : 6 : 92. Obtaining the amount of blue in agglomerates in each size cut, we can then calculate the amount of water and Gum Arabic trapped in agglomerates. Knowing the mass of sand particles, the initial liquid to solid mass ratio in agglomerates can be calculated as below.

$$\frac{\mathrm{L}}{\mathrm{S}} = \frac{100}{2}\frac{\mathrm{m_d}}{\mathrm{m_p}} \quad 2\text{-}4$$

## 2.4 Jet stability measurement

To characterize the frequency and amplitude of the jet pulsations, the spray nozzle is moved out of the column to spray in open air, so that a movie of its spray pattern can be taken (Figure 2.10). Frames are first changed from colors into grayscale. For every pixel in the image, the colour is characterized by Red, Green and Blue, each in the range from 1 to 256.

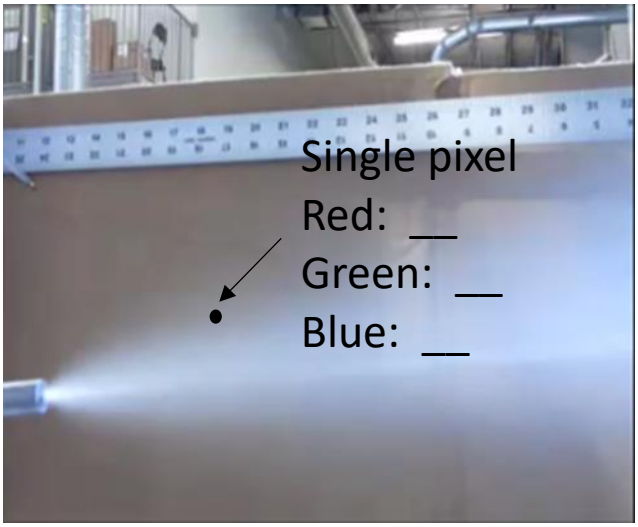


**Figure 0.10 A single pixel in the original photo of the spray**

Define Gray Intensity i as a combination of Red, Green and Blue.

$$i = 0.2989Red + 0.5870Green + 0.1140 \times Blue \text{ [26]} \quad 2\text{-}5$$

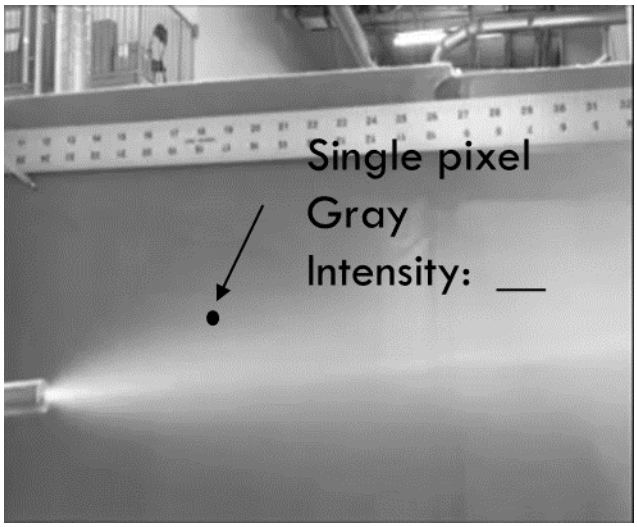


**Figure 0.11 A single pixel in the photo of the spray transferred into gray scale**

Within each frame, there is a variation in Gray Intensity at different pixels. Define Y(i) as the fraction of pixels for each Gray Intensity in the whole image. For pure background (pictures with no spray jet), the total number of pixels:

$$\sum_1^{256} Y_b(i) = 1 \quad 2\text{-}6$$

$Y_b(i)$ is derived from the average in 5 seconds before injection. Figure 2.12 shows typical results.

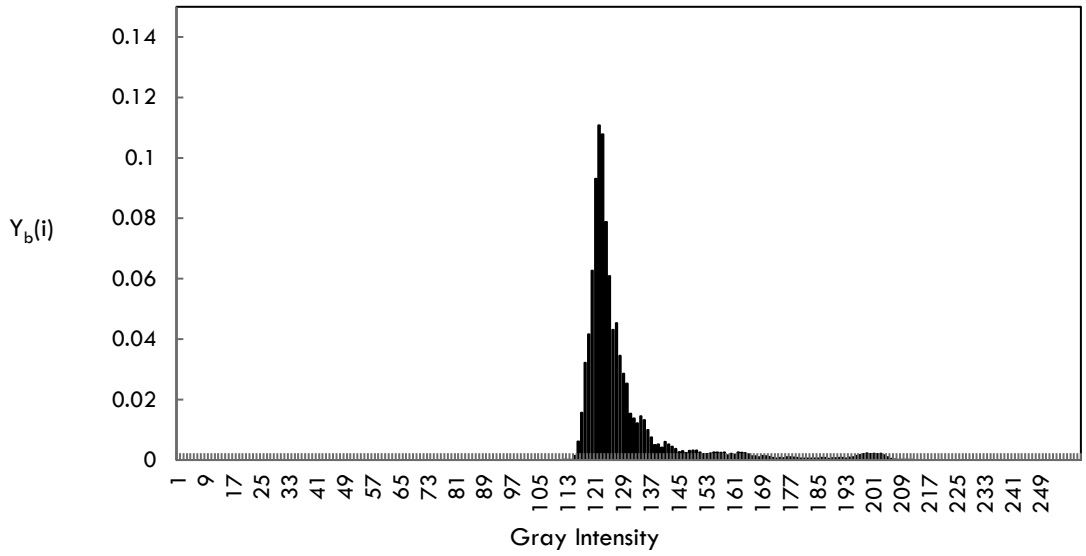


**Figure 0.12 Fraction of pixels for each Gray Intensity for pure background**

Zooming in on the image the total amount of pixels for pure spray can be obtained.

$$\sum_1^{256} Y_s(i) = 1 \qquad 2\text{-}7$$

$Y_s(i)$ is derived from the average in the 7 seconds of injection.

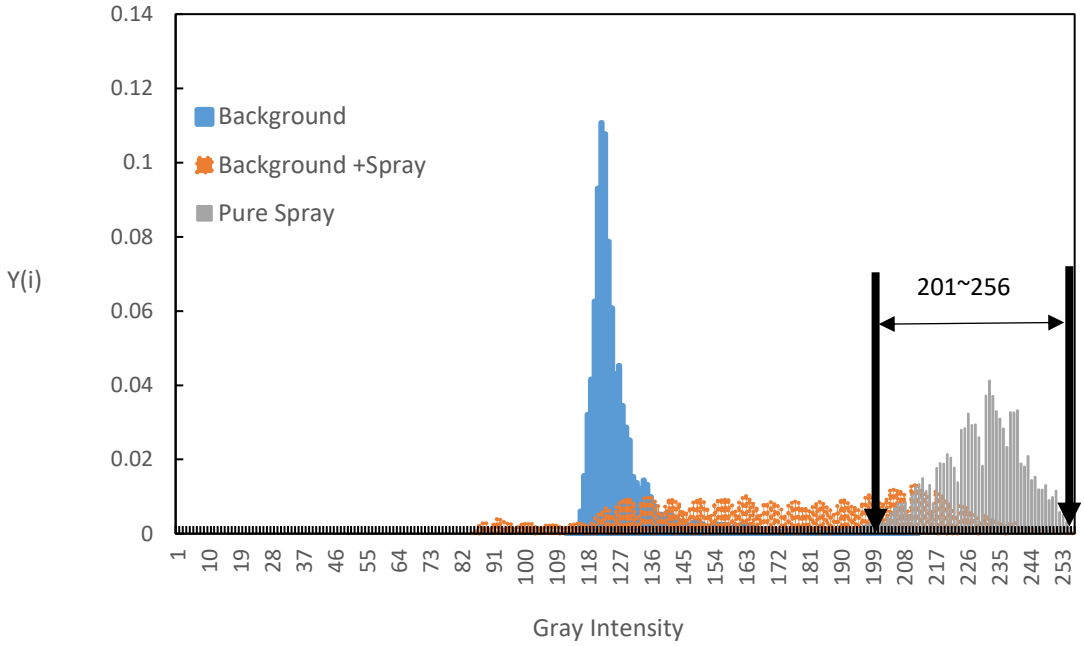


**Figure 0.13 Fraction of pixels for each Gray Intensity**

To cancel out the effect of background, choose the Gray Intensity range from 201 to 256 to analyze the stability of spray, since Figure 2.13 show a strong signal in this pixels range for the spray and a negligible signal for the background.

Define η as the proportion of spray in the whole image. The image is composed of the spray and the background.

$$\sum_{201}^{256} Y(i) = (1-\eta)\sum_{201}^{256} Y_b(i) + \eta \sum_{201}^{256} Y_s(i) \qquad 2\text{-}8$$

Define

$$\alpha = \sum_{201}^{256} \mathrm{Y(i)} \qquad 2\text{-}9$$

$\alpha_b$ characterizes the background, $\alpha_s$ characterizes the spray, and α characterizes the combination of background and spray:

$$\alpha = (1-\eta)\alpha_b + \eta\alpha_s \qquad 2\text{-}10$$

$$\alpha - \alpha_b = (\alpha_s - \alpha_b)\eta \quad (2\text{-}11)$$

If we take the time average of α and η, over the duration of spray:

$$\overline{\alpha} - \alpha_b = (\alpha_s - \alpha_b)\overline{\eta} \quad (2\text{-}12)$$

Dividing

$$\frac{\eta}{\overline{\eta}} = \frac{\alpha\text{-}\alpha_b}{\overline{\alpha}\text{-}\alpha_b} \quad (2\text{-}13)$$

$\eta/\bar{\eta}$ can effectively characterize the stability of different sprays. For a perfectly stable spray $\eta/\bar{\eta}$ should be equal to 1 constantly. In this way there is no need to calibrate for $\alpha_s$. Previous research also showed that the jet stability is not affected whether the injection is in the open air or in the fluidized bed[27].

## 2.5 Jet expansion angle

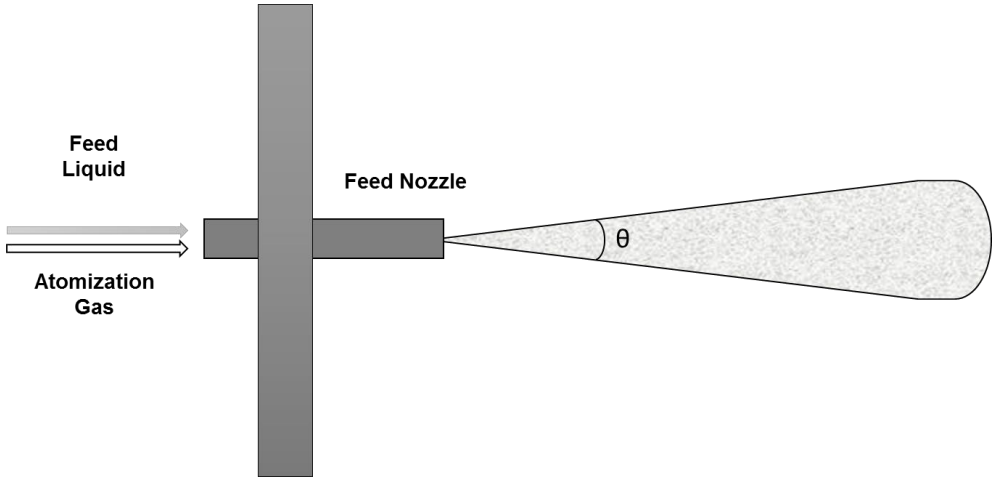


**Figure 0.14 Schematic diagram of jet expansion angle θ**

In order to investigate the impact of GLR, a video analysis method was developed to calculate the expansion angle of the jets in the open air injection. The jet expansion angle θ is defined as the angle of the spray from the nozzle tip, as shown in Figure 2.14. Each frame of the spray video has a total number of 854×480 pixels. In each second, the video contains 30 frames. A

Matlab program (see Appendix) was created to analyze the gray intensity for each pixel in each frame.

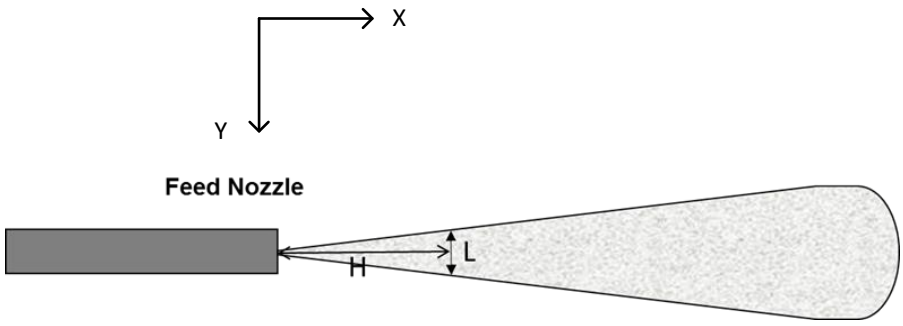


**Figure 0.15 Geometry of jet expansion angle calculation**

The intensity values of the 480 pixels which has the same x coordinate were acquired. As shown in Figure 2.15 the distance chosen from the nozzle tip is H. Then the intensity values at the same pixels are averaged as a function of time (15 frames, 0.5 s).

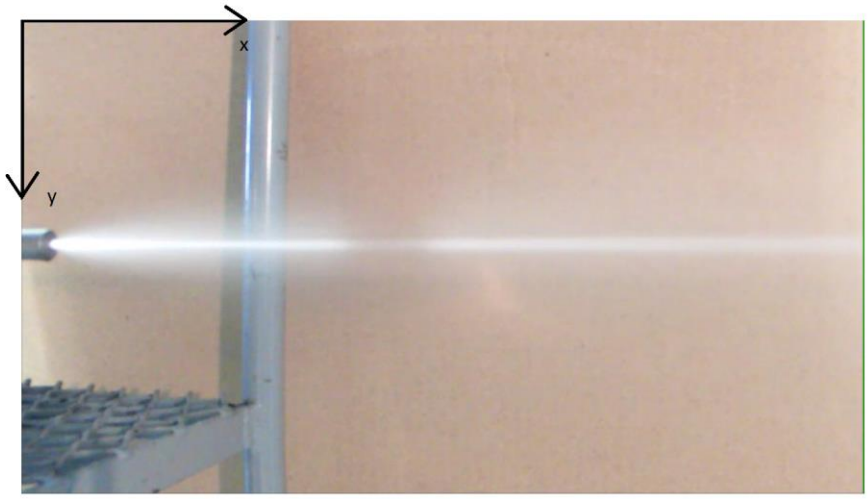


**Figure 0.16 Photo of the jet, GLR=1%, $F_L$=23.4 g/s**

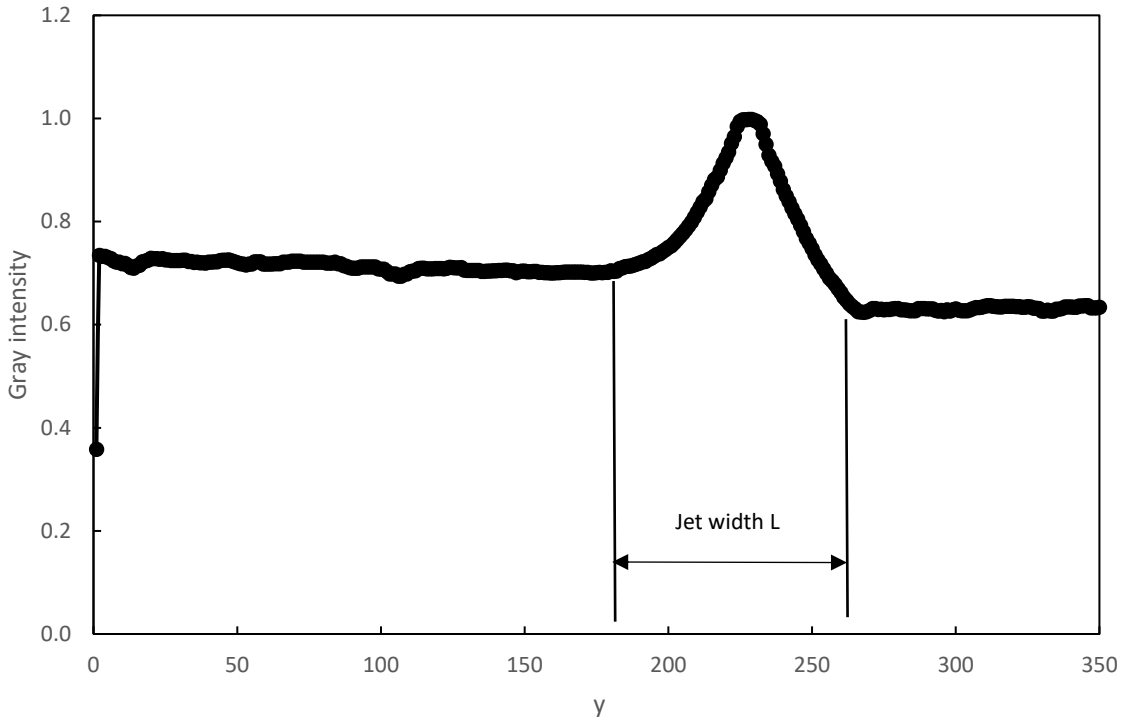


**Figure 0.17 Gray intensity values in the pixels where x=100, GLR=1% when x=100, y represents the vertical locations of pixels.**

From Figure 2.17 the value of L is acquired. The expansion angle is, then, calculated by the equation below:

$$\theta = 2 * \arctan(\frac{L}{2*H}) \qquad 2\text{-}14$$

# Effect of high gas velocity on the distribution of liquid in a fluidized bed

In a Fluid Coker™, superficial velocity increases as the height in the bed increases due to the steam from the stripper section, attrition nozzles, feedstocks injected at different levels and the vapors produced by pyrolysis.

Previous studies have pointed out that increasing the gas velocity in fluidized bed during liquid injection is beneficial for initial liquid-solid contact and also gas velocity has a significant impact on agglomerate breakup. The high gas velocity fluidized bed was specifically designed in order to achieve a superficial velocity up to 2.2 m/s.

## 3.1 Experimental setup and methodology

The equipment used is shown in Section 2.1. The fluidized bed is preheated to 135 °C before each experiment. Gas velocity is changed at two stages during each experiment to separately investigate the effect of gas velocity on initial liquid distribution and agglomerate breakage. Each experiment takes 3 min. The steps are shown below.

1) From 0-60 s it is preparation. The pressure regulator upstream of sonic nozzles is adjusted to make the gas velocity stable at $V_g$ = 0.18 m/s
2) From 60-90 s the bed is fluidized at the gas velocity during injection - $V_{gi}$
3) At 90 s the solenoid valve below injection tank is opened automatically and stays open for 8 s to make sure all liquid is injected
4) From 98 – 103 s the bed is fluidized at $V_{gi}$
5) From 103 – 180 s the the bed is fluidized at the gas velocity during drying - $V_{gd}$
6) The bed is defluidized at 180 s and heaters are switched off
7) Bed solids are left to cool overnight and then sieved to recover agglomerates

The stage of injection in each experiment corresponds to the feedstock spray region in a real coker since bitumen is continuously injected into the reactor. The stage of bed drying corresponds to the agglomerate breakup region in a real coker where no jet-bed interaction occurs but agglomerates exist.

The method to analyze the agglomerates is described in Chapter 2 as the cold simulation model. The injection system used for this chapter is as shown in Figure 2.6, which produces a relatively stable spray. A gum Arabic solution of 150 g is injected in each experiment.

## 3.2 Results and discussion

### 3.2.1 Preliminary tests

The conductance method (described in Chapter 2) is used to verify that the free moisture is instantly evaporated at a high temperature of 135°C.

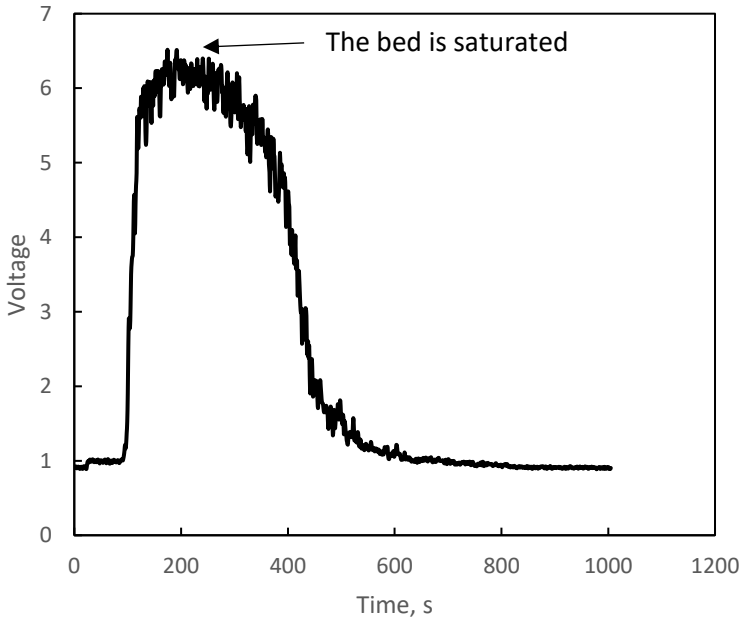


**Figure 0.1 Conductance signal for injection of 180 g $H_2O$ at room temperature**

The signal shows the conductance method is able to detect free moisture in the bed.

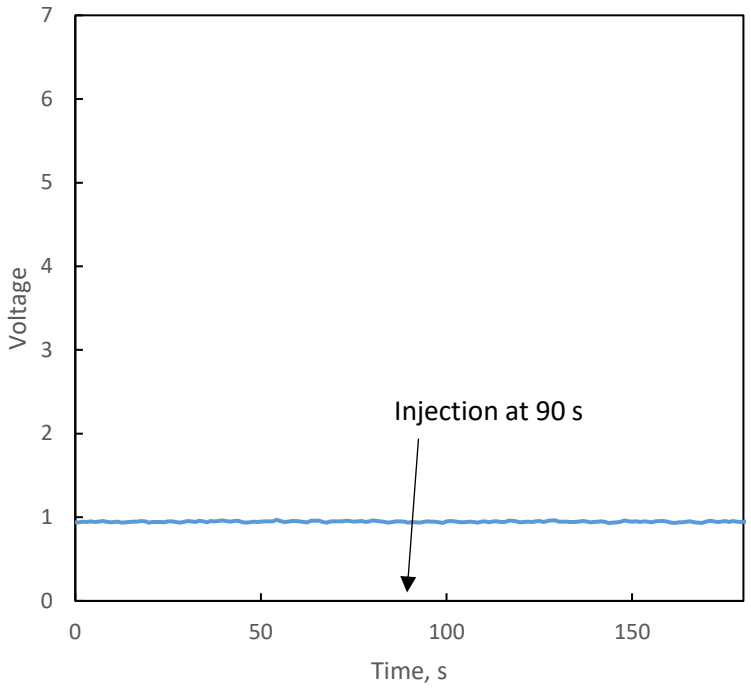


**Figure 0.2 Conductance signal for injection of 150 g Gum Arabic solution at 130 °C**

The injection duration is 7 seconds for 150 g of Gum Arabic solution. The voltage signal of the resistance in the circuit stayed constantly at 0.95 voltage. It shows that the free moisture is quickly evaporated in the bed when the temperature is at 130 °C.

## 3.2.2 Effect of gas velocity during injection

To understand the effect of gas velocity during injection on liquid distribution, $V_{gi}$ is varied from 0.18 m/s to 2.2 m/s. In a Fluid Coker$^{TM}$, the cross-sectional average superficial gas velocity varies from 0.24 m/s to approximately 0.9 m/s with the vertical position, and there are significant radial variations [5]: the range of gas velocity used in this study is, thus, set to include the range of velocities that could be expected in the spray region in the industrial case. Using the cold simulation experimental method, the amount and size distribution of agglomerates, and the initial liquid to solid ratio of agglomerates are obtained. The results in Figure 3.3 below show the cumulative weight percentage of agglomerates at different size cuts. When $V_{gi}$ increases from 0.18 m/s to 1.2 m/s the total amount of agglomerates decreases while further increase of $V_{gi}$ has minimal impact on the amount of agglomerates.

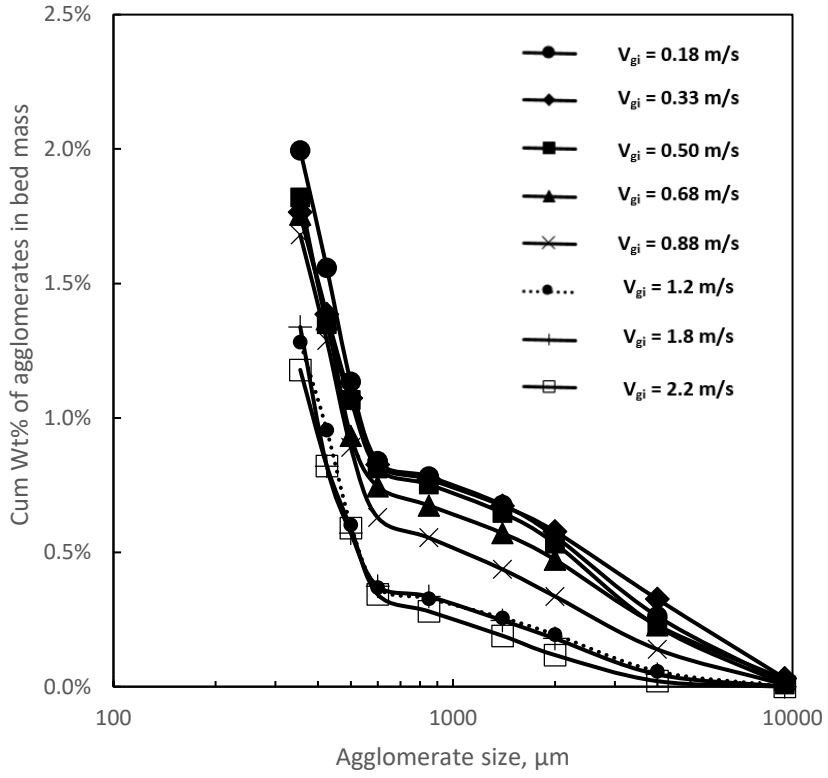


**Figure 0.3 Cumulative weight percentage of agglomerates in bed solid mass for various $V_{gi}$ while $V_{gd}$ is constant at 0.18 m/s**

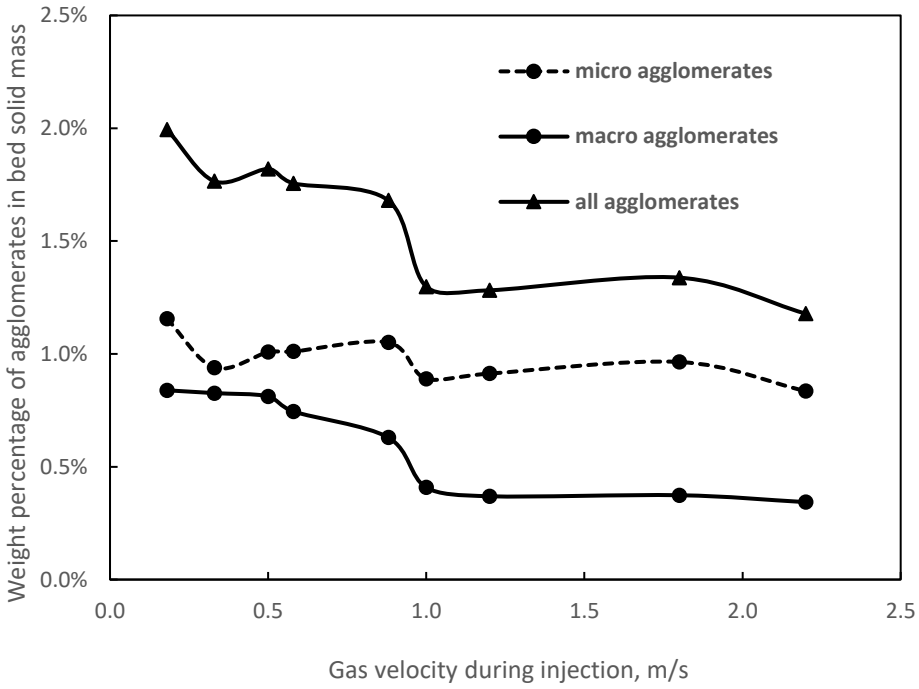


**Figure 0.4 The effect of $V_{gi}$ on amount of macro and micro agglomerates while $V_{gd}$ is constant at 0.18 m/s**

The results in figure 3.4 show that the increase of gas velocity during injection has no significant impact on the mass of micro agglomerates. The increase of gas velocity during injection from 0.18 m/s to 1.2 m/s contributed to the dropping of mass of macro agglomerates while at gas velocities higher than 1.2 m/s the mass of macro agglomerates remains at circa 0.37%. The total amount of agglomerates in the fluidized bed dropped drastically when gas velocity during injection changed from 0.18 m/s to 2.2 m/s. However, after the gas velocity reaches 1.2 m/s, the change in mass of agglomerates is minimal.

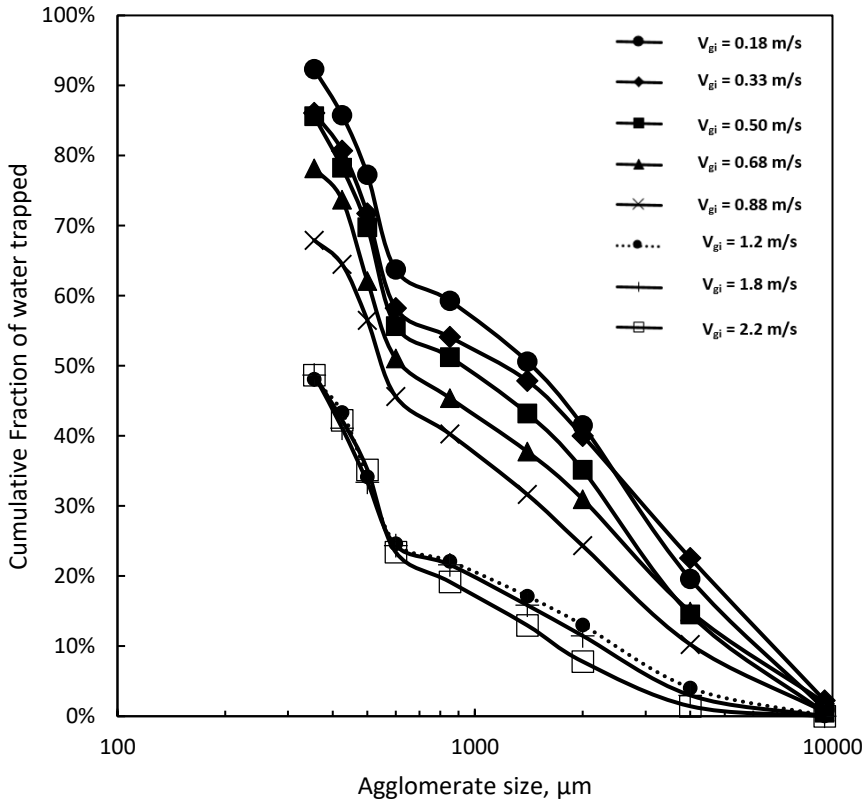


**Figure 0.5 Cumulative fraction of water trapped in agglomerates various $V_{gi}$ while $V_{gd}$ is constant at 0.18 m/s**

The results in Figure 3.5 indicate the cumulative fraction of water trapped in agglomerates at different size cuts. When $V_{gi}$ increases from 0.18 m/s to 1.2 m/s the total amount of agglomerates decreases while further increase of $V_{gi}$ has minimal impact on the amount of agglomerates.

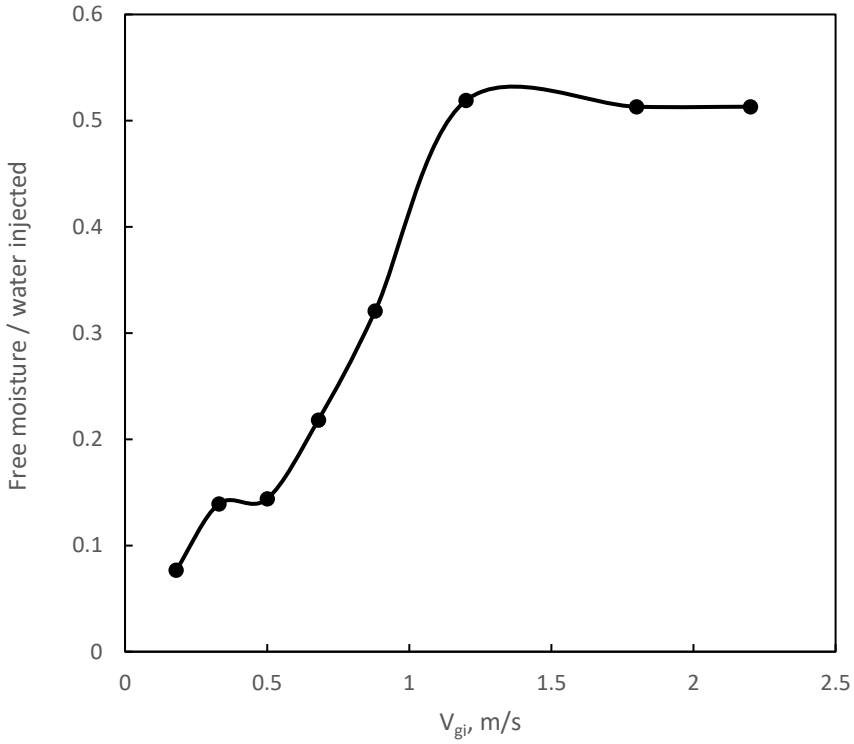


**Figure 0.6 Effect of $V_{gi}$ on the total amount of free moisture**

On one hand the fraction of free moisture in the total amount of liquid injected increases from 7.7% to 51.7% when gas velocity during injection rises from 0.18 m/s to 2.2 m/s. On the other hand, the quality of liquid to solid contact is hardly affected after the gas velocity reaches 1.2 m/s. It is suspected that a transition from bubbling regime to turbulent regime happened when the superficial gas velocity is at approximately 1.2 m/s. Tests of the pressure difference in the fluidized bed need to be conducted to confirm the possible transition.

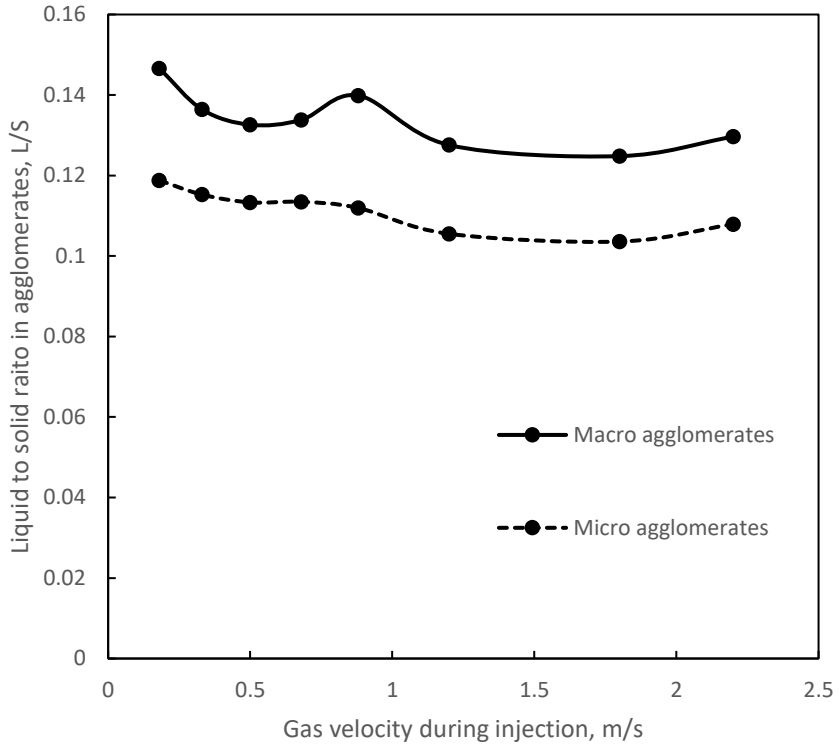


**Figure 0.7 Initial L/S ratio in macro and micro agglomerates at various $V_{gi}$ at constant $V_{gd}$=0.18 m/s**

Results in Figure 3.7 indicate that increasing the gas velocity during injection will slightly reduce the liquid to solid ratio in both macro and micro agglomerates while after $V_{gi}$ reaches 1.2 m/s the impact is minimal. When the superficial gas velocity increases, in the region where solids and liquid interact, the liquid was more evenly distributed onto the particles. This is possibly because the at a higher superficial gas velocity, the ratio below the liquid and solids in the interaction region since more gas bubbles enter the interaction region which carry more solids in the wakes.

## 3.2.3 Effect of gas velocity during drying

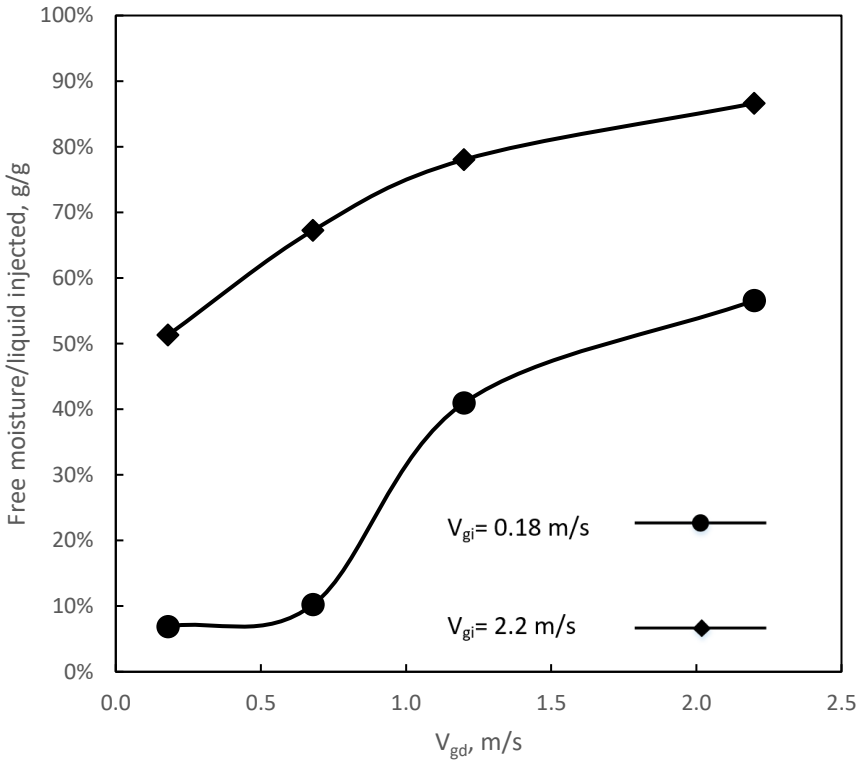


**Figure 0.8 Effect of increasing $V_{gd}$ on the amount of agglomerates at different $V_{gi}$ (0.18, 2.2 m/s)**

Figure 3.8 shows that increasing gas velocity during drying is beneficial for liquid distribution when $V_{gi}$ is either at 0.18 m/s or 2.2 m/s. A higher gas velocity during the drying stage contributes to the breakup of agglomerates which releases the liquid that was trapped in agglomerates.

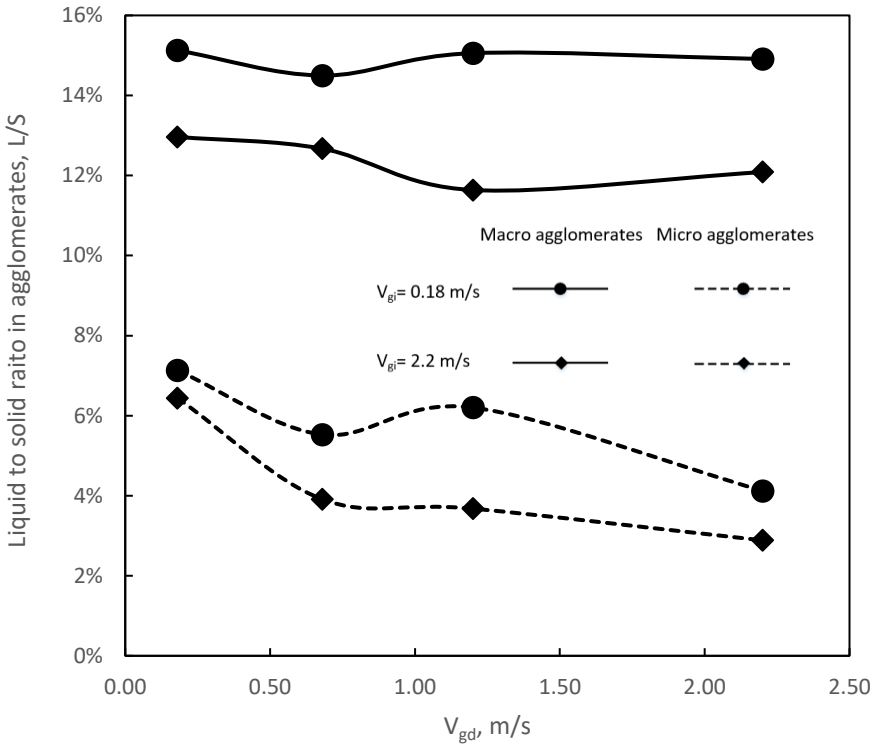


**Figure 0.9 Effect of $V_{gd}$ on liquid to solid ratio when $V_{gi}$= 0.18 m/s and $V_{gi}$= 2.2 m/s**

Figure 3.9 shows that increasing gas velocity during drying contributes to lower the liquid to solid ratio of the agglomerates when $V_{gi}$ is either at 0.18 m/s or 2.2 m/s. A higher gas velocity during the drying stage contributes to the breakup of agglomerates which releases the liquid that was trapped in agglomerates.

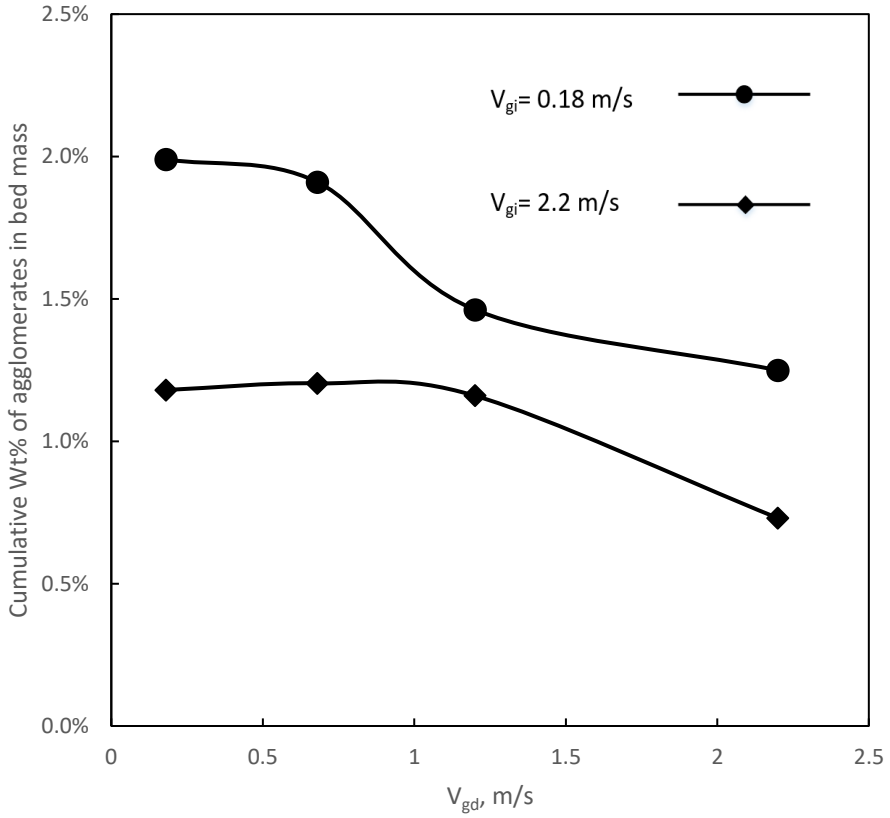


**Figure 0.10 Effect of $V_{gd}$ on amount of agglomerates when $V_{gi}$= 0.18 m/s and $V_{gi}$=2.2 m/s**

The results in Figure 3.10 indicate that increasing gas velocity during drying contributes to a lower amount of agglomerates when $V_{gi}$ is either at 0.18 m/s or 2.2 m/s. A higher gas velocity during the drying stage contributes to the breakup of agglomerates which makes the total amount of agglomerates lower.

# Effect of local gas velocity on the distribution of liquid in a fluidized bed

In a Fluid Coker™, superficial velocity increases as the height in the bed increases due to the steam from stripper section, attrition nozzles, feedstocks injected at different levels and the vapors produced by pyrolysis.

Previous studies have also found that a core-annulus structure exists in a fluid coker. In the annular region, the particles flow downwards and gas is carried down by the particles. In the core region gas rises rapidly and particles are carried upwards. The bed voidage increases gradually from the wall to the center of the bed without a sharp transition from the annular region and the core region. This means that in the core region the gas velocity is higher than superficial gas velocity at the same height. The location of feed nozzles in the bed determines the area which the sprays fall in.

The objective of this study is to better understand the effect on liquid distribution when the gas distribution changes at the same level as the jet. In comparison to the base case in which the initial gas distribution was even, gas velocity was increased in the region at the end of the jet or at the tip of the nozzle. Gum Arabic injections were conducted to characterize the liquid distribution with various gas distributions.

## 4.1 Experimental setup and methodology

The fluidized bed and injection systems used for this chapter are the same as described in Chapter 2 (Section 2.1). As in Chapter 3, 150 g of Gum Arabic solution is injected in each experiment. Local gas velocity is adjusted by changing the positions of open sonic nozzles. Triboprobes are installed at the bed wall to measure the lateral profile of gas bubble flow.

### 4.1.1 Initial gas distribution

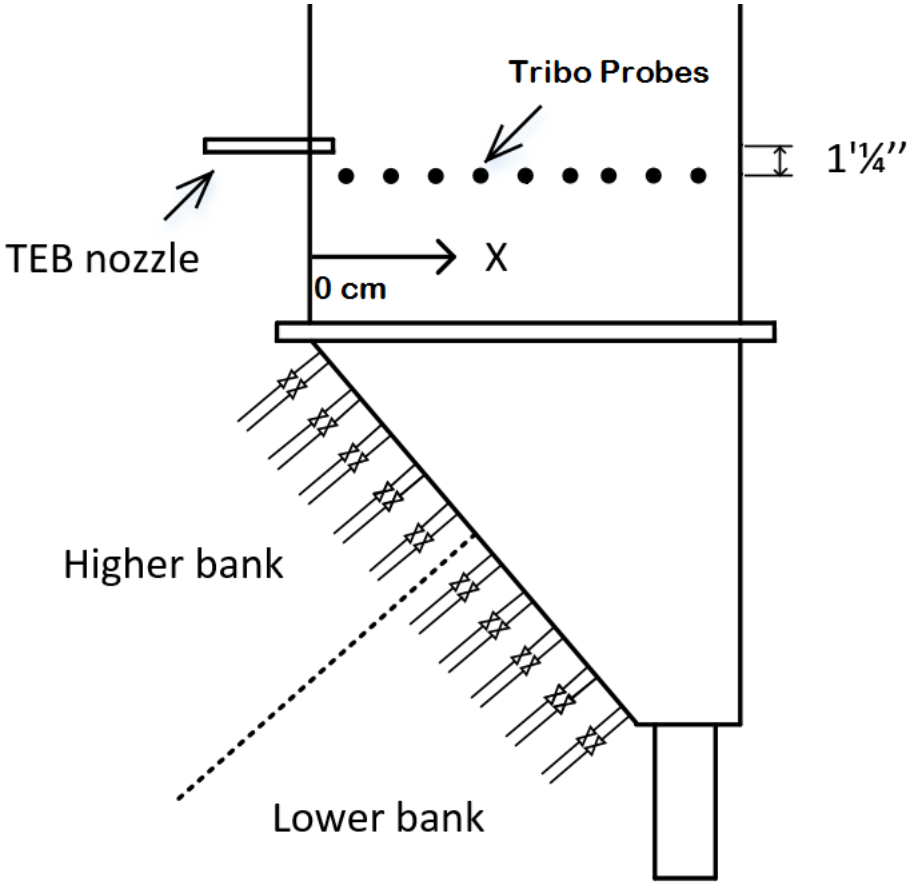


**Figure 0.1 Schematic diagram of triboelectricity measurement system**

The 20 sonic nozzles are defined into 2 banks. Each of the higher bank and the lower bank includes the 10 sonic nozzles. At a superficial gas velocity of 1 m/s, all the nozzles can provide the same gas velocity despite the different hydrostatic pressure in the bed.

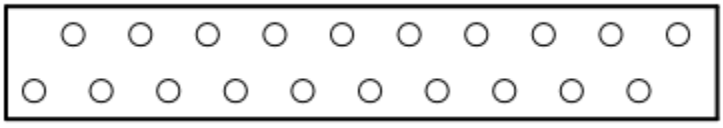

**Figure 0.2 Top view of the locations of the 20 sonic nozzles**

For each experiment 10 gas sonic nozzles will be opened. Each open sonic nozzle contributes to 0.1 m/s of the total superficial velocity in the freeboard. The locations of open sonic nozzles are varied to create different initial gas distributions, for all of which the superficial velocity in the freeboard is maintained at 1 m/s.

### 4.1.2 Measurement of bubble gas flow in bed

A triboelectricity method has been successfully utilized by Portoghese et al.[17] to characterize the liquid–solid contacting efficiency by detecting the bed wetted area. Better liquid-solid contacting during injection leads to a more uniform distribution of liquid on bed particles which results in a larger bed wetted area. A larger bed wetted area produces a more intense electric current.

In this study, a triboelectricity method is used to detect the gas bubble flow in the fluidized bed. 9 triboprobes were installed horizontally on the bed wall as shown in Figure 4.3. The bed width is 50 cm and the distance between each probe is 5 cm. The distance that the probes penetrated into the bed is 5 cm.

Triboelectric current is produced through the friction of the bed particles colliding with the probe surface. Both bubble size and bubble frequency can influence the intensity of collision between particles and the probes during a certain time. Larger bubbles carry a larger amount of solids in the wake. A higher local bubble frequency leads to more collisions. Both of these factors contribute to a stronger triboelectric current.

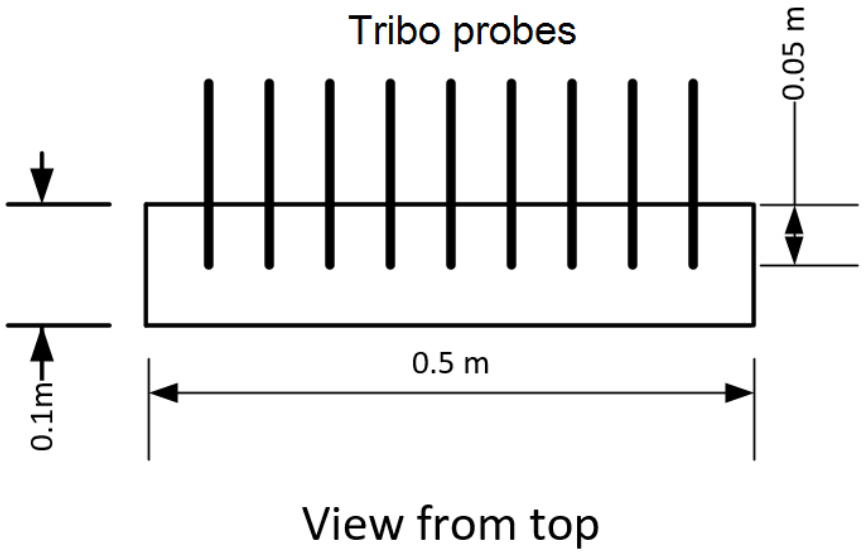


**Figure 0.3 Top view of locations of tribo probes**

A data acquisition system is connected to the triboelectric tubes via an amplifier to provide grounding, current-voltage conversion and amplification of the electrical signal. The triboelectric signal was acquired at a frequency of 1000 Hz. The range of the amplifier is chosen to be 0 to 200 mA.

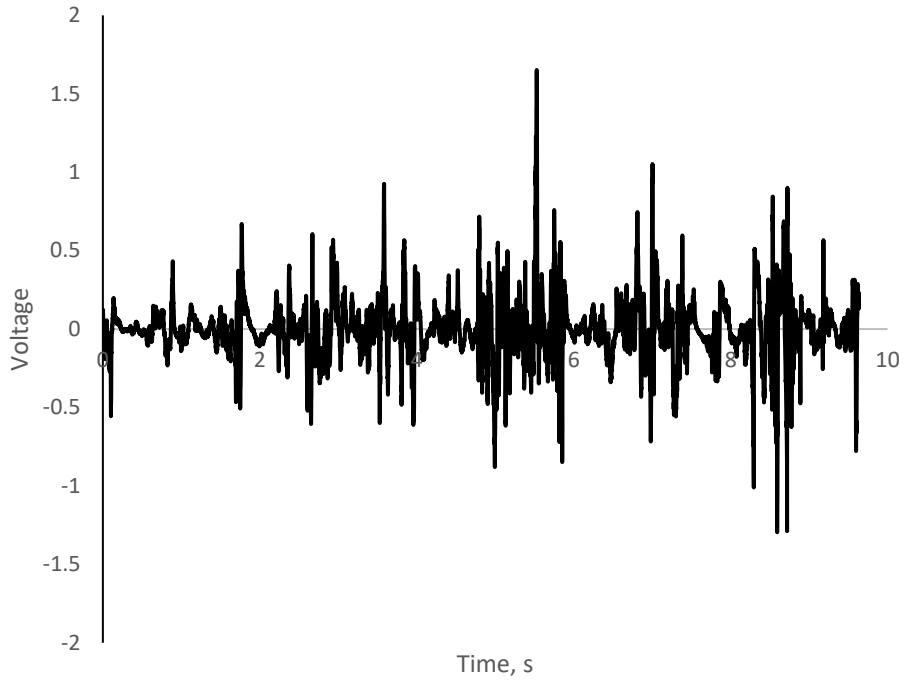


**Figure 0.4 Raw signal of triboelectricity measurement, superficial gas velocity 1m/s**

Figure 4.4 shows the raw signal of triboelectricity measurement. The frequency of the signal corresponds to the frequency of bubbles colliding with the tribo probe. The amplitude of the signal corresponds to the size of the bubble colliding with the tribo probe since larger bubbles carry more particles in the wakes.

Two parameters are derived from voltage signal over a frequency range of 0-100 Hz:

- Average Frequency (f)
- Power spectra density (P)

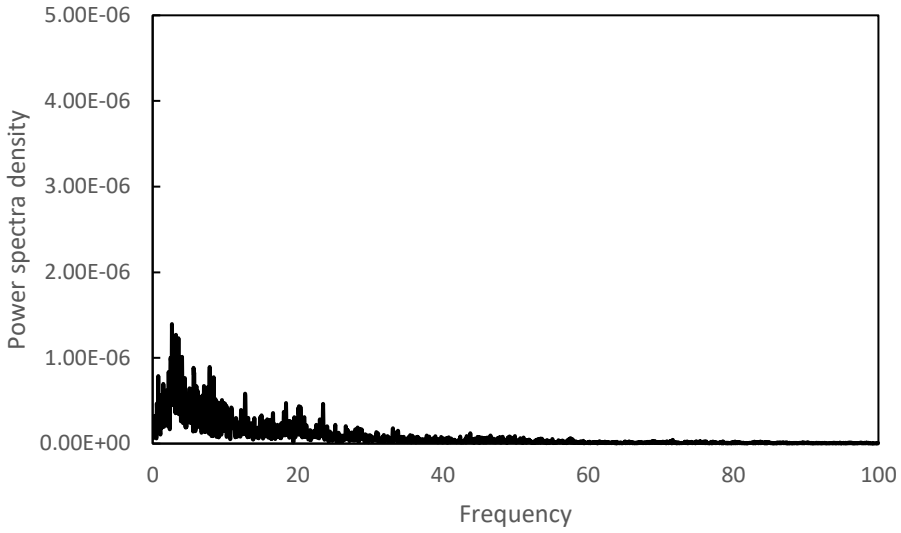


**Figure 0.5 Power spectra of triboelectricity measurement for a low bubble gas flowrate**

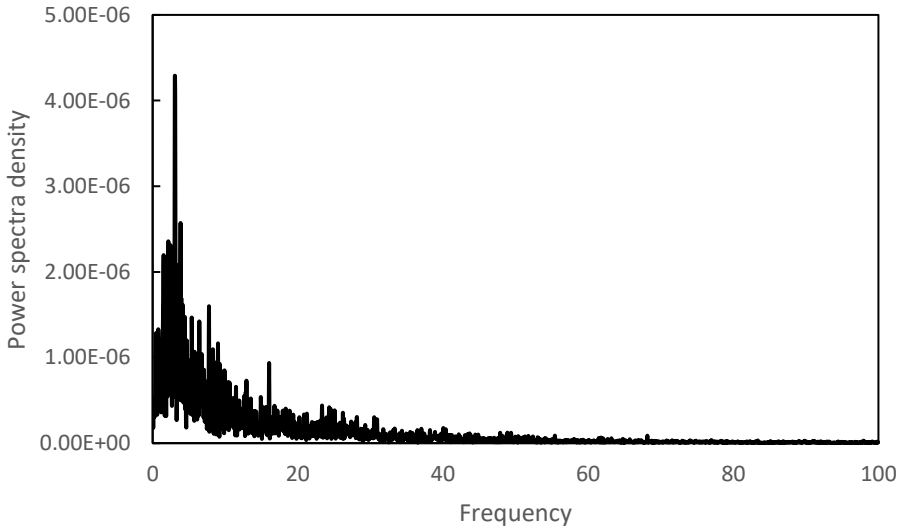


**Figure 0.6 Power spectra of triboelectricity measurement for a high bubble gas flowrate**

Local volumetric flux of gas bubble is defined as

$$q_{bi} = \alpha P_i^{\beta} f_i^{\gamma} \qquad 4\text{-}1$$

α, β, γ are coefficients for the correlation.

Cross-sectional average volumetric flux can be derived as

$$\overline{q_b} = \frac{1}{\sum \lambda_i}\left[\sum \lambda_i \, \alpha P_i^{\beta} f_i^{\gamma}\right] \quad 4\text{-}2$$

We are interested in

$$\frac{q_{bi}}{\bar{q}_b} = \frac{P_i^{\beta} f_i^{\gamma}}{\frac{1}{\sum \lambda_i}\left[\sum \lambda_i P_i^{\beta} f_i^{\gamma}\right]} \quad 4\text{-}3$$

α, β and γ are obtained by using data obtained at different superficial gas velocities, since for Group B powder:

$$\overline{q_b} = (\mathrm{V}_g - \mathrm{U}_{mf}) \quad 4\text{-}4$$

## 4.2 Results and discussion

### 4.2.1 Radial profiles of bubble gas distribution

Triboelectricity signals acquired at 9 superficial velocities in the bed were used to obtain the coefficients in Equation 4.1. The best fit for coefficients α, β and γ is the values that produce a minimum value of

$$\left\{(\mathrm{V}_g - \mathrm{U}_{mf}) - \frac{1}{\sum \lambda_i}\left[\sum \lambda_i \, \alpha P_i^{\beta} f_i^{\gamma}\right]\right\}^2$$

Through calculation and fitting using the solver function in Excel, we can find that

$$q_{bi} = 5.168 \times 10^{-5} P_i^{0.0949} f_i^{3.31} \quad 4\text{-}5$$

The correlation between the real average volumetric flux of bubble gas and the average volumetric flux calculated from Equation 4.5 and 4.2 is shown below. It shows a reasonably good fitting.

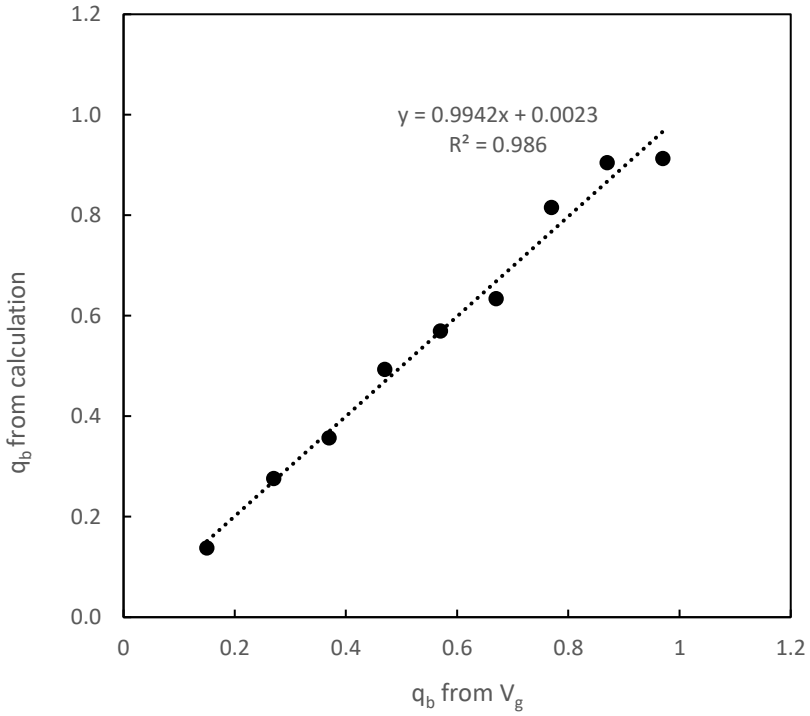


**Figure 0.7 Correlation between the real average volumetric flux of bubble gas and the average volumetric flux calculated**

The correlation for gas-liquid jets from Benjelloun [28] was used to calculated the average jet penetration $L_{jet}$.

Three groups of gas distributions are measured. The base case is even distribution as shown below(a). Since it has 6 sonic nozzles open in the higher bank and 4 nozzles open in the lower bank, it is defined as 0.6-0.4 m/s. In the same way case b would be defined as 0.1-0.9 m/s and case c as 0.9-0.1 m/s.

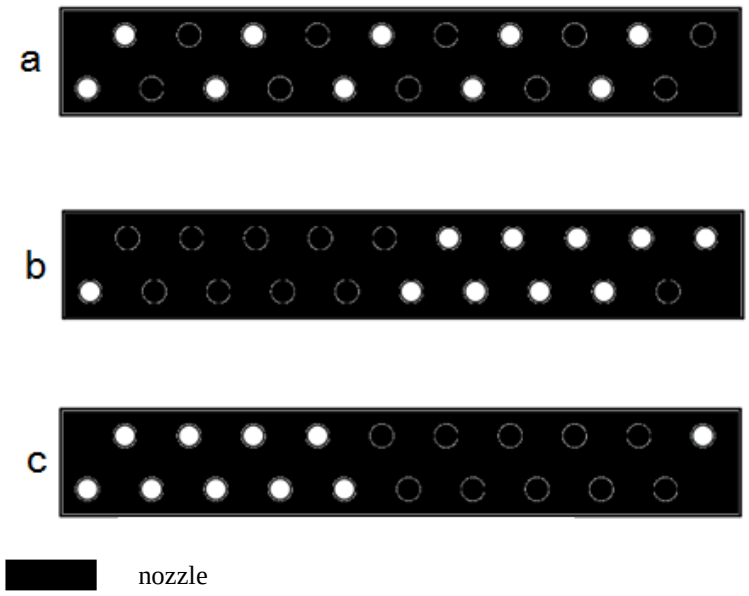


**Figure 0.8 Group 1 gas distributions, (a) 0.6-0.4 m/s, (b) 0.1-0.9 m/s, (c) 0.9-0.1 m/s**

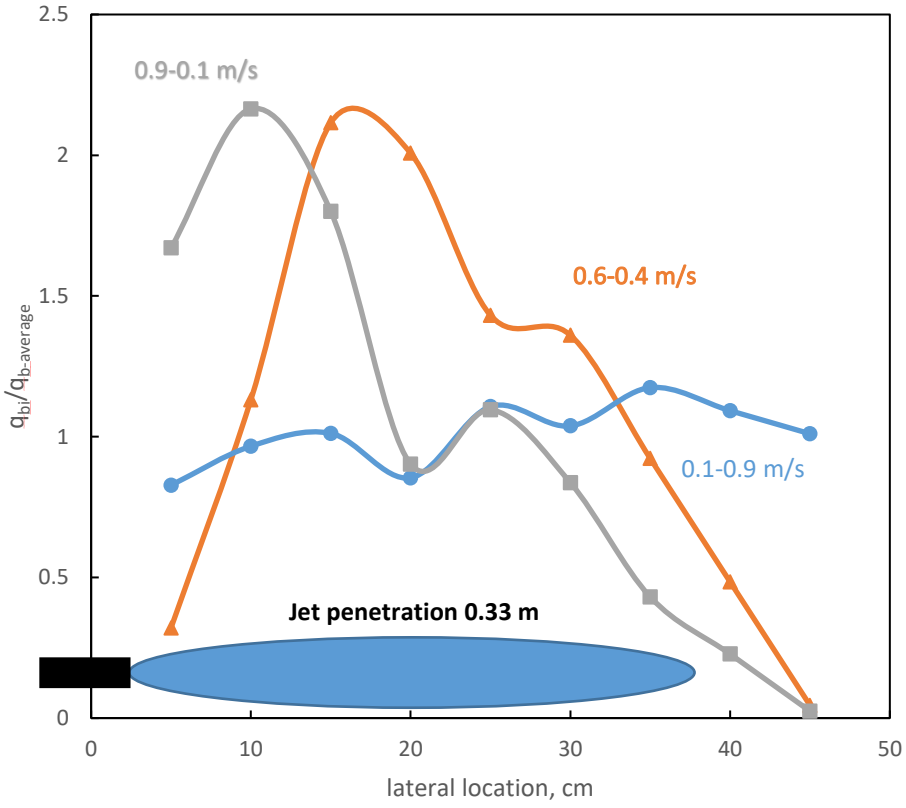

**Figure 0.9 Profiles of gas bubble flow for Group 1 gas distributions. (The profile was measured without the jet)**

The tribo probes were placed 1.25 inch below the injection nozzle vertically. For the even gas distribution 0.6-0.4 m/s, the gas distribution is bed is not symmetrical due to the angled slope for gas distributors. The center of the profile, where the bubble gas flowrate is the highest, is closer to the left wall of the fluidized bed than to the right wall. For gas distribution 0.1-0.9 m/s, gas flowrate is higher at the end of the jet and the profile is almost flat. For gas distribution 0.9-0.1 m/s, gas flowrate is higher at the tip of the nozzle.

The second group of gas distributions are shown below.

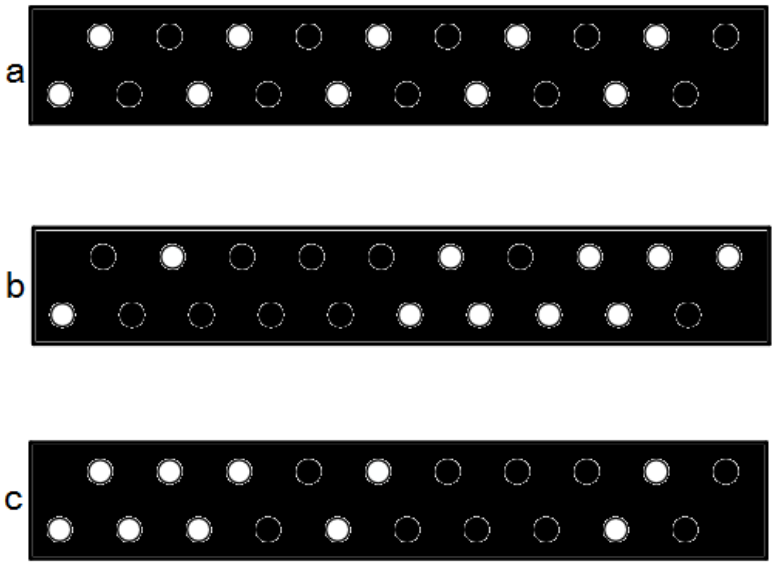


**Figure 0.10 Group 2 gas distributions, (a) 0.6-0.4 m/s, (b) 0.2-0.8 m/s, (c) 0.8-0.2 m/s**

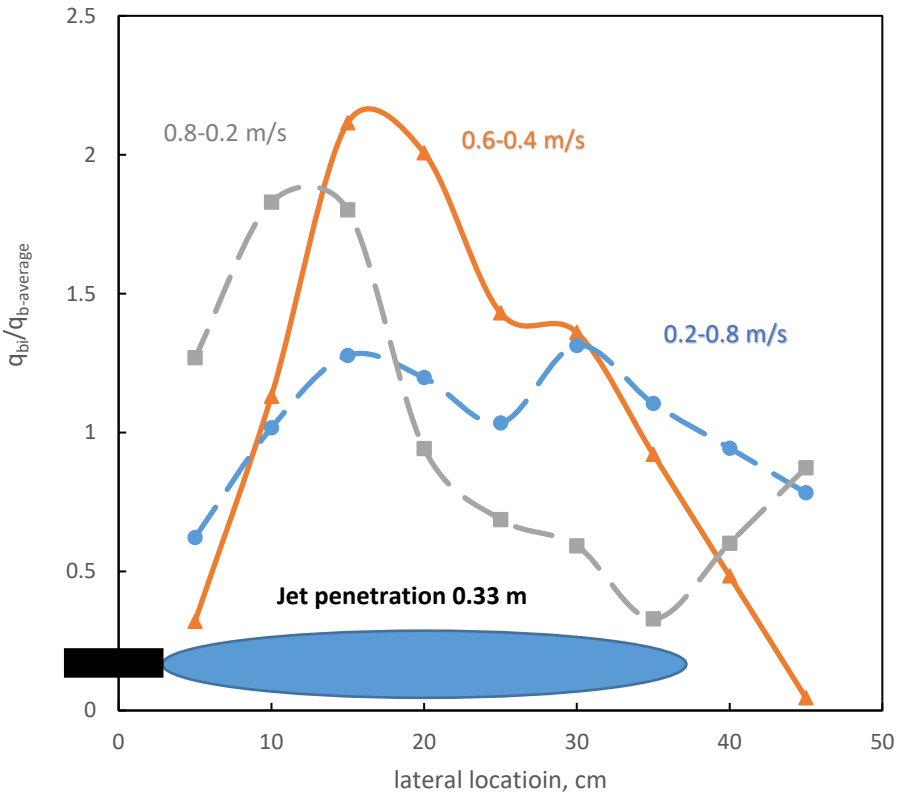


**Figure 0.11 Profiles of gas bubble flow for Group 2 gas distributions**

The third group of gas distributions are shown below.

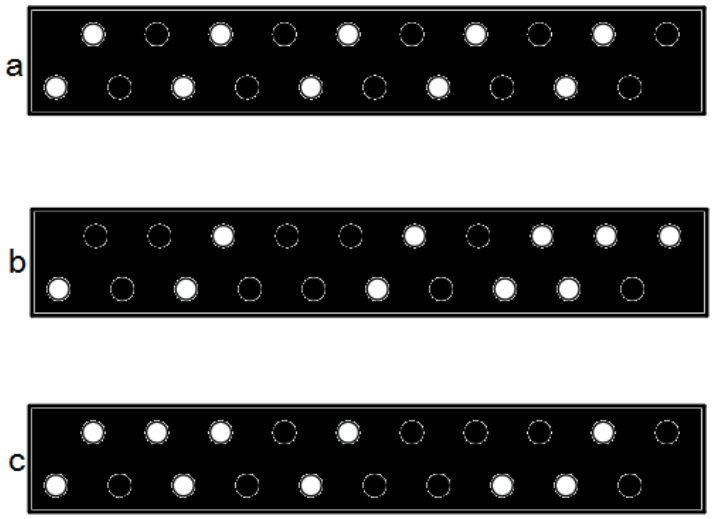


**Figure 0.12 Group 3 gas distributions, (a) 0.6-0.4 m/s, (b) 0.3-0.7 m/s, (c) 0.7-0.3 m/s**

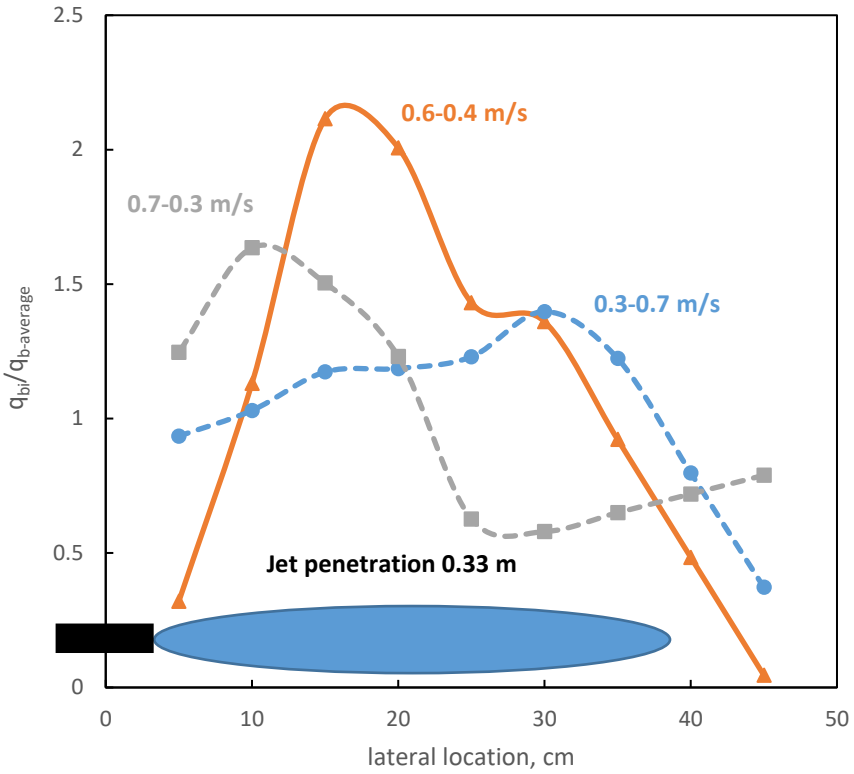


**Figure 0.13 Profiles of gas bubble flow for Group 3 gas distributions**

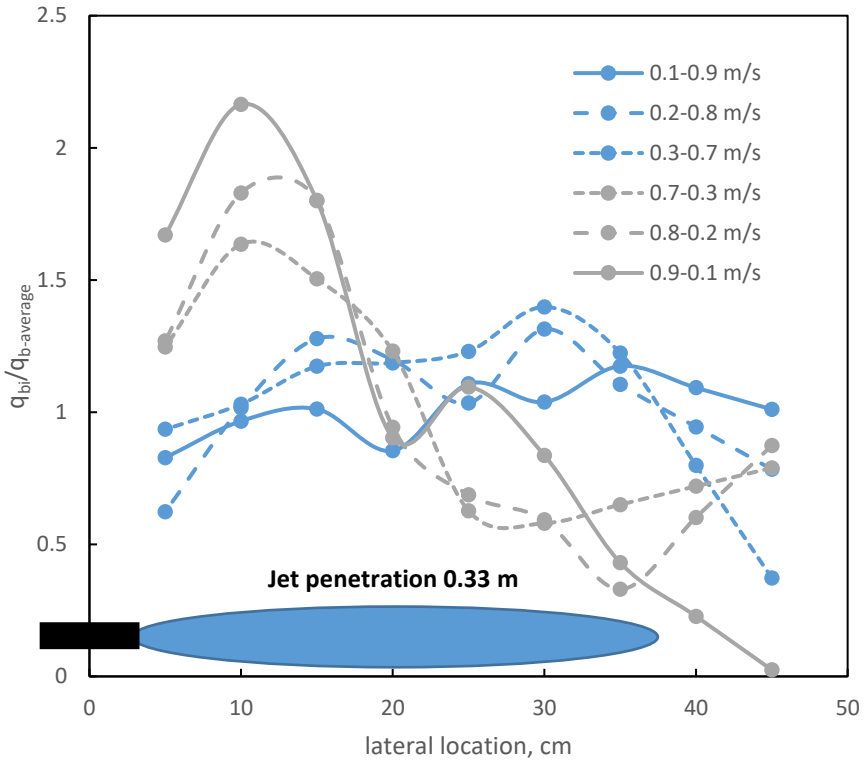


**Figure 0.14 Summary of bubble gas flow radial profiles of various gas distributions**

Because the gas distributors were located in an angled slope, the gas distribution in the fluidized bed was not symmetrical. Due to the hydrostatic pressure difference, the bubbles tend to shift to the left side of the bed (refer to figure 4.1). When the amount of gas initially put at the lower bank increases, bubble gas flowrate at the end of the jet increases gradually and an approximately flat profile was achieved. When the amount of gas initially put at the higher bank increases, bubble gas flowrate at the tip of the nozzle increases gradually while a peak of the gas bubble flux exists close to the left wall.

## 4.2.2 Confirmation of gas distribution by entrainment tests

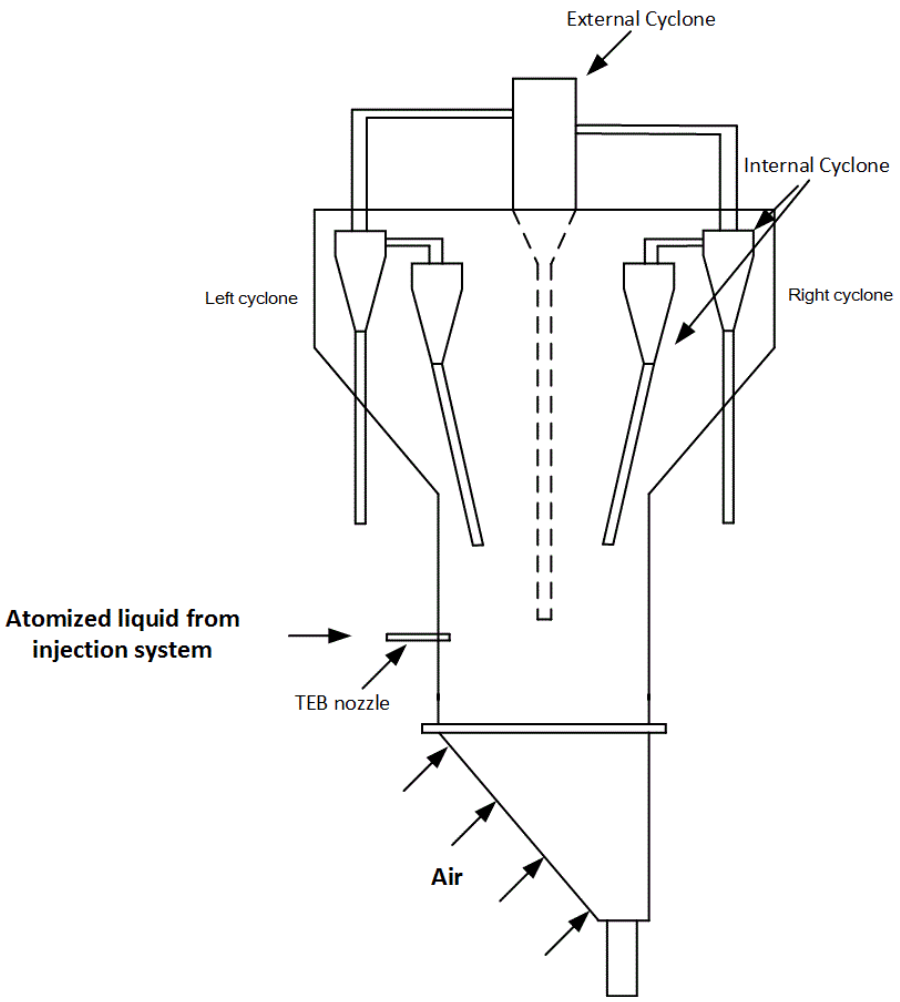


**Figure 0.15 schematic diagram of the high gas velocity fluidized bed**

There are 4 internal cyclones in the high gas velocity fluidized bed, which are symmetrically located in the upper section of the bed. The two cyclones on the left side (close to the higher bank) are identical to the two on the right side of the bed. Thus entrainment tests are used to confirm the inclination of bubble gas flow in the bed. Each experiment was run at the same superficial velocity (1 m/s) for 3 min.

**Table 0-1 Mass of solids entrained in left and right internal cyclones at different gas distributions**

| | gas distribution | | |
|---|---|---|---|
| | 0.6-0.4 m/s | 0.1-0.9 m/s | 0.9-0.1 m/s |
| mass of sand entrained in left cyclone, g | 800.5 | 1886 | 1809 |
| mass of sand entrained in right cyclone, g | 127 | 698 | 127 |
| $\frac{\text{mass of sand entrained in left cyclone}}{\text{mass of sand entrained in right cyclone}}$ | 6.3 | 2.7 | 14.2 |

The results show that when gas velocity is higher in the lower bank, the entrainment in the right cyclone has increased in comparison to that in the left cyclone. When gas velocity is higher in the higher bank, the entrainment in the left cyclone has increased compared to that in the right cyclone. For gas distribution 0.1-0.9 m/s, the ratio between the mass of sand entrained in right cyclone and the mass of sand entrained in right cyclone was expected to be approximately 1 since the radial profile is flat. The anomaly is due to the severe erosion of the left internal cyclone. Nonetheless the results are in consistence with the radial profiles of bubble gas flow obtained by triboelectricity measurement.

## 4.2.3 Effect of gas distribution on liquid distribution

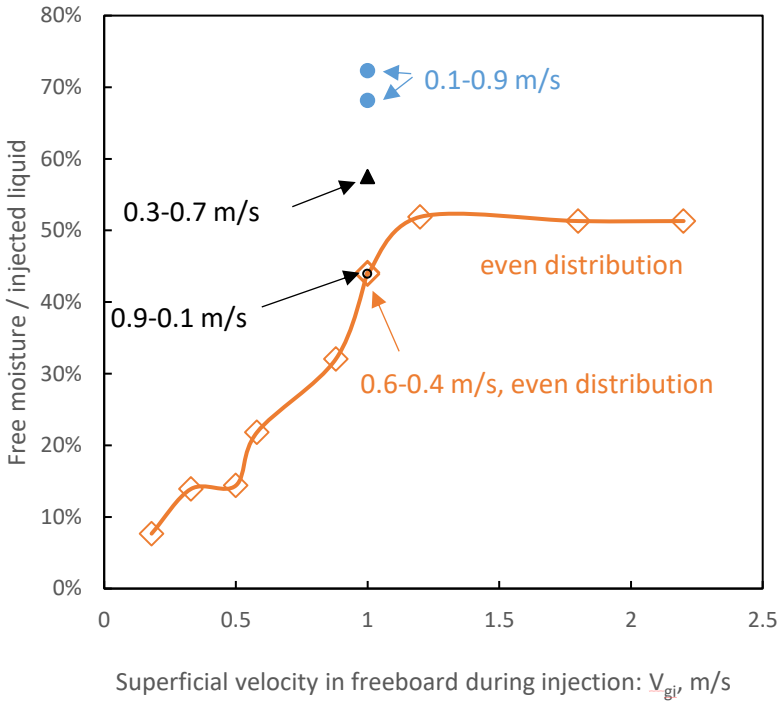


**Figure 0.16 Fraction of free moisture in mass of liquid injected (data for even distribution is obtained from section 3.2.2)**

The amount of free moisture increases drastically when the bubble gas flowrate becomes higher at the end of the jet. While increasing the bubble gas flowrate at the tip of the nozzle has no impact on the amount of free moisture. This result indicates that the agglomerates are majorly produced at the end of the jet.

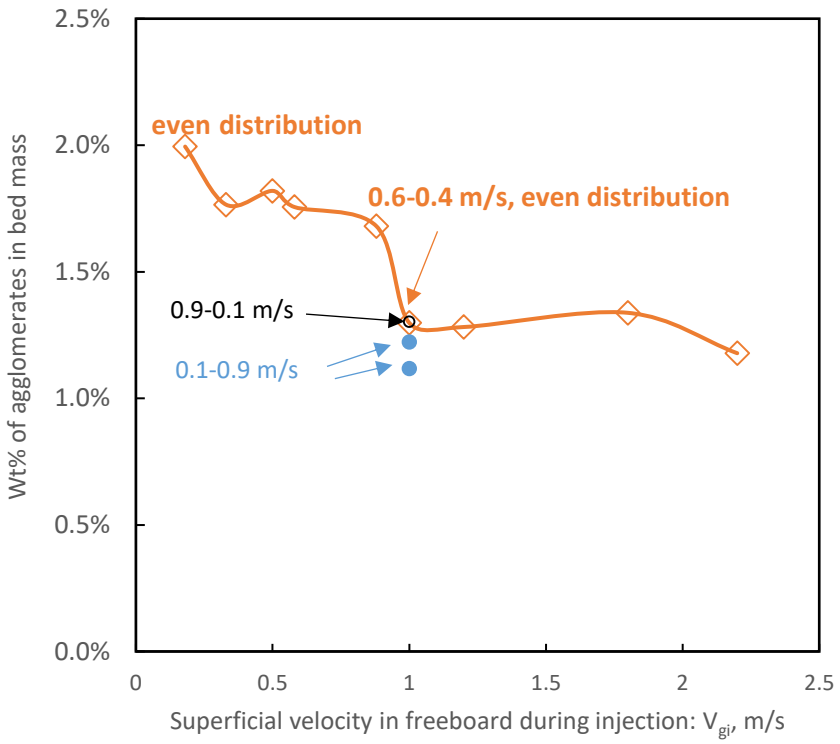


**Figure 0.17 weight percentage of agglomerates in bed mass**

The amount of agglomerates decreases when the bubble gas flowrate becomes higher at the end of the jet. While increasing the bubble gas flowrate at the tip of the nozzle has no impact on the amount of agglomerates. This result also shows that the agglomerates majorly formed at the end of the jet.

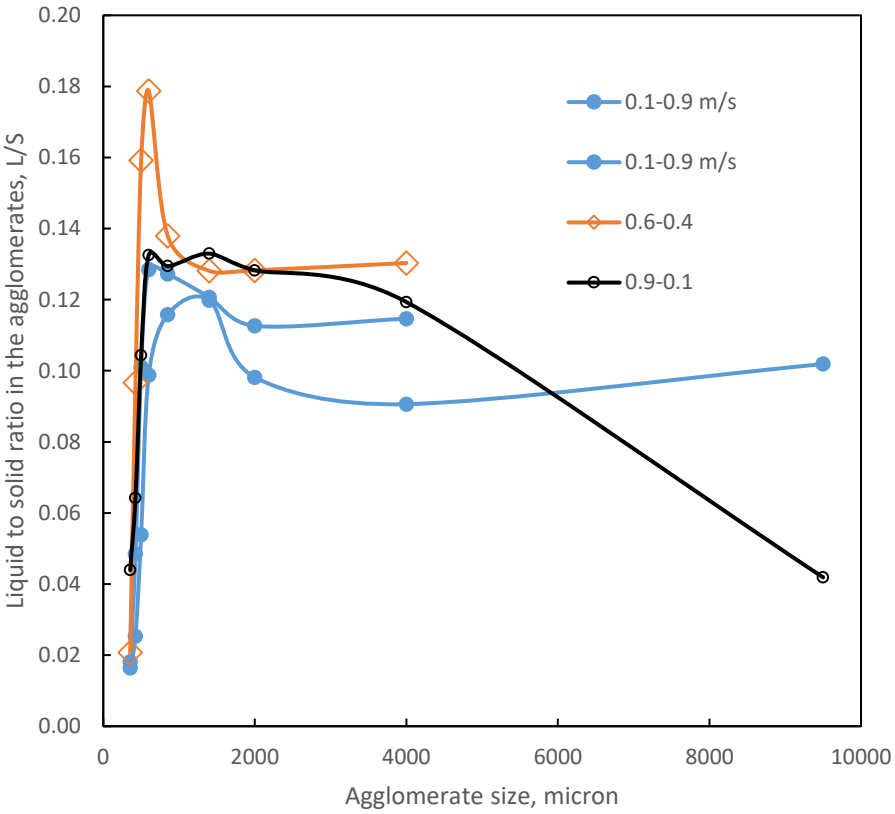


**Figure 0.18 liquid to solid ratio in agglomerates for gas distributions**

The liquid to solid ratio in agglomerates decreases when the bubble gas flowrate becomes higher at the end of the jet. While increasing the bubble gas flowrate at the tip of the nozzle has a minimal impact on the liquid to solid ratio in agglomerates.

# Effect of improvements in nozzle performance on the distribution of liquid in a fluidized bed for various bed hydrodynamics

The effect of jet stability on liquid distribution has been studied by several researchers previously. A nozzle performance index (NPI) based on conductance measurements in the fluidized bed was used to characterize the liquid-solid contact during injection[20]. From various researches, the pulsations of jets were reported to have a beneficial impact on the liquid distribution[21][22] on both small scale nozzles and industrial scale nozzles.

The effect of the atomization gas to liquid mass ratio (GLR) on liquid distribution has also been studied previously. NPIs based on different methods were utilized to characterize the liquid-solid contact[29][18]. Based on the geometry of nozzles, different impacts of GLR on the liquid distribution were reported.

In this study a high gas velocity fluidized bed with silica sand is used to investigate the effect of spray stability and gas to liquid ratio of injection (GLR). Pulsations in the spray are introduced by changing the geometry of the injection system. GLR is changed by changing the size of sonic nozzle for atomization gas and the upstream pressure by a regulator. The experiments performed to determine the impact of GLR were all conducted with stable sprays.

## 5.1 Experimental setup and methodology

### 5.1.1 Jet stability

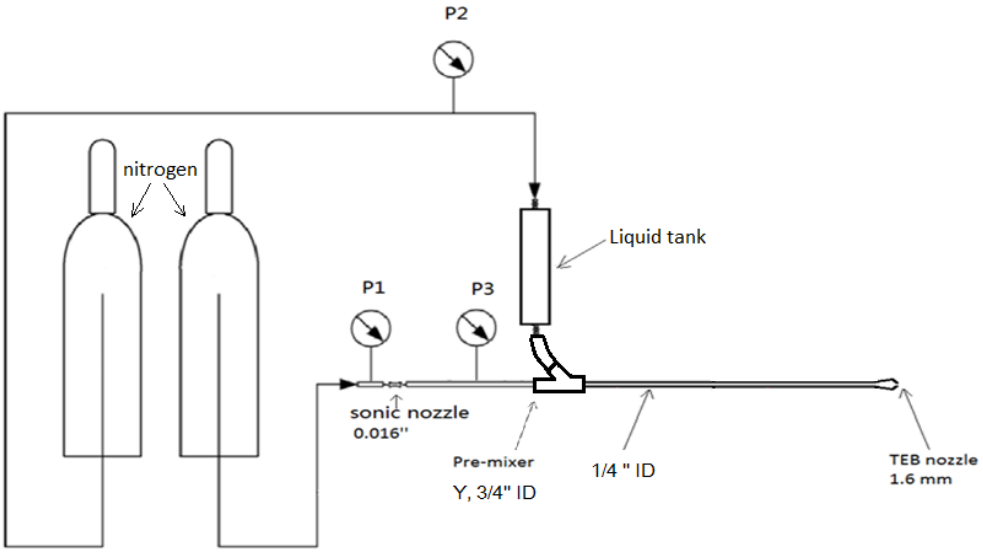


**Figure 0.1 Injection system for pulsating spray**

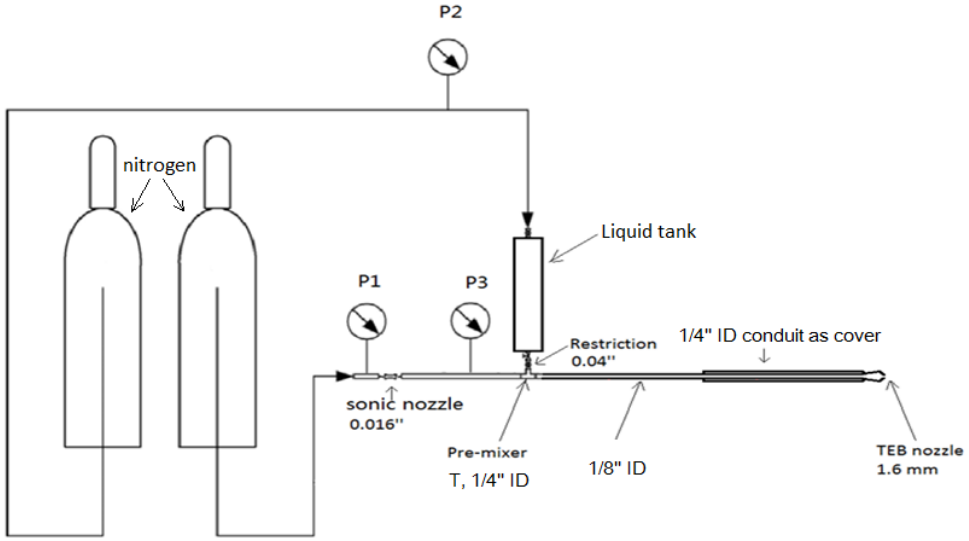


**Figure 0.2 Injection system for stable spray**

In figure 5.1 and figure 5.2, the systems for stable spray and pulsating spray are displayed. Three parts are different. In the injection system for pulsating spray, the pre-mixer for atomization gas and liquid is Y connector with an internal diameter of 19 mm (3/4 inch). No restriction was put below the tank and the conduit leading to the nozzle tip has an internal diameter of 6.35 mm (1/4 inch). In the injection system for stable spray, the pre-mixer for atomization gas and liquid is T connector with an internal diameter of 6.35 mm (1/4 inch). A restriction that has a diameter of 1.016 mm was installed below the tank. The conduit leading to the nozzle tip has an internal diameter of 3.175 mm (1/8 inch).

Previous studies by Ariyapadi [27] have shown that the key factor that affects the stability of a spray is the flow pattern of gas and liquid in the conduit upstream of the nozzle tip. Figure 5.3 shows the flow pattern map for gas-liquid flow in a horizontal conduit.

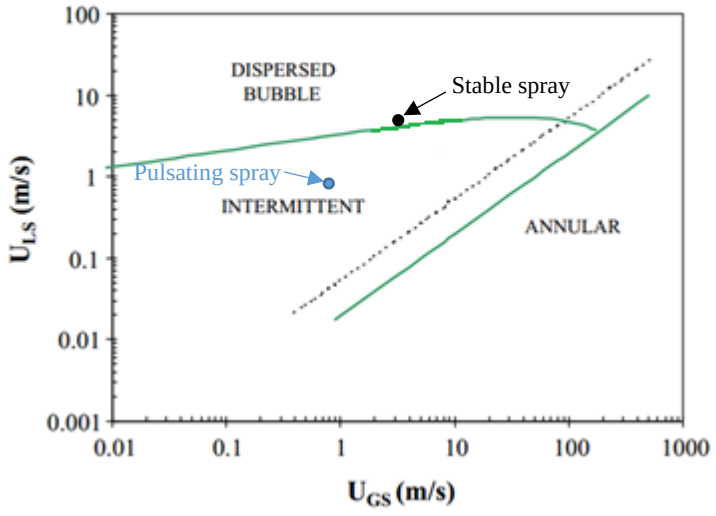


**Figure 0.3 Flow pattern map of Taitel and Dukler** [30]**. The dotted line refers to the modified transition line between the intermittent and annular regimes, as proposed by Barnea et al** [31]**.**

**Table 0-1 Linear velocities of liquid and atomization gas in different sizes of conduits**

| Conduit diameter 1/4 inch (unstable spray) | | | |
|---|---|---|---|
| Inner diameter of conduit, m | 0.00635 | Inner diameter of conduit, m | 0.00635 |
| Area, $m^2$ | 0.000032 | Area, $m^2$ | 0.000032 |
| Volume flowrate $m^3/s$ | 0.000024 | Volume flowrate $m^3/s$ | 0.00003 |
| $U_{LS}$, m/s | 0.76 | $U_{GS}$, m/s | 0.94 |
| Conduit diameter 1/8 inch (stable spray) | | | |
| Inner diameter of conduit, m | 0.003175 | Inner diameter of conduit, m | 0.003175 |
| Area, $m^2$ | 0.0000079 | Area, $m^2$ | 0.000079 |
| Volume flowrate $m^3/s$ | 0.000024 | Volume flowrate $m^3/s$ | 0.00003 |
| $U_{LS}$, m/s | 3.03 | $U_{GS}$, m/s | 3.77 |

The gas and liquid superficial velocities in the injection system for a stable spray is higher than in the system for a pulsating spray. When the $U_{GS}$ and $U_{LS}$ combination falls in the region of dispersed bubble, the flow has a tendency to be more stable. Open air injection shows that when the gas and liquid superficial velocity is in the disperse bubble region, the injection is improved by producing fewer pulsations. A regular video camera with a frequency of 1 frame every 30 ms is used to record the open air injection process. The pictures below show the expansion of the liquid jet during different times of injection. A more sophisticated analysis, developed in Chapter 2 (section 2.4), was used to characterize the spray stability.

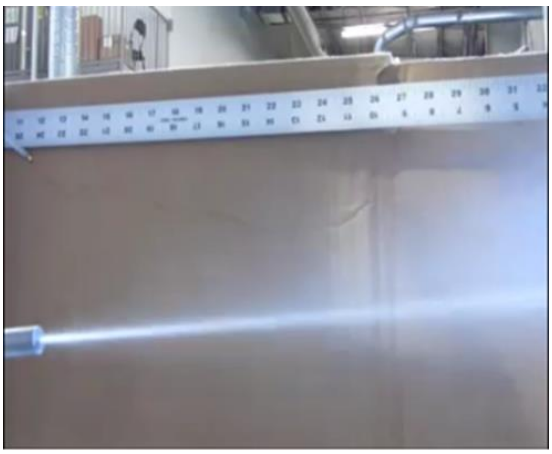

a. t=0.47 s

b. t=0.53 s

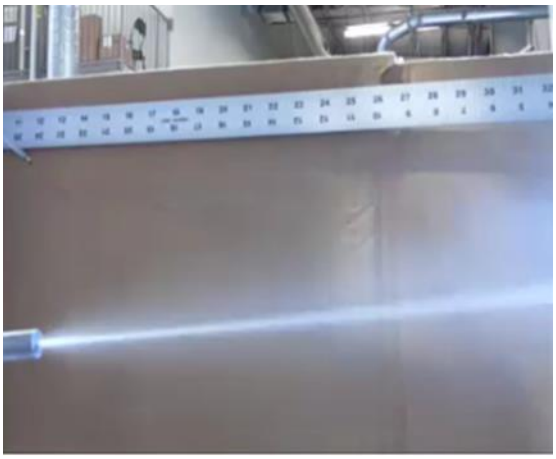

c. t= 0.57 s

d. t= 0.60 s

**Figure 0.4 Pictures of spray (pulsating spray, t=0 is the beginning of injection)**

## 5.1.2 Gas to liquid ratio (GLR)

In previous chapters, GLR was set at 2% for all injection experiments. In this study, GLR will be changed from 1% to 3.5%. The injection system used was the same as shown in Figure 5.2, which creates a relatively stable spray. First open air spray experiments were performed to verify the stability of the sprays. The Gum Arabic injection experiments were conducted subsequently to investigate the effect of different GLRs on the liquid-solid contact. The liquid flowrate was the same for all experiments and the gas-liquid flow through the spray nozzle throat was always in the sonic regime. $V_{gi}$ and $V_{gd}$ are kept constant at 0.68 m/s for all of these experiments.

## 5.1.3 Jet expansion angle

The jet expansion angle was measured in open air for different GLRs using the method described in section 2.5.

## 5.2 Results and discussion

### 5.2.1 Spray stability

$\eta/\bar{\eta}$ can effectively characterize the stability of different sprays. For a perfectly stable spray $\eta/\bar{\eta}$ should be equal to 1 constantly. In this way there is no need to calibrate for $\alpha_s$.

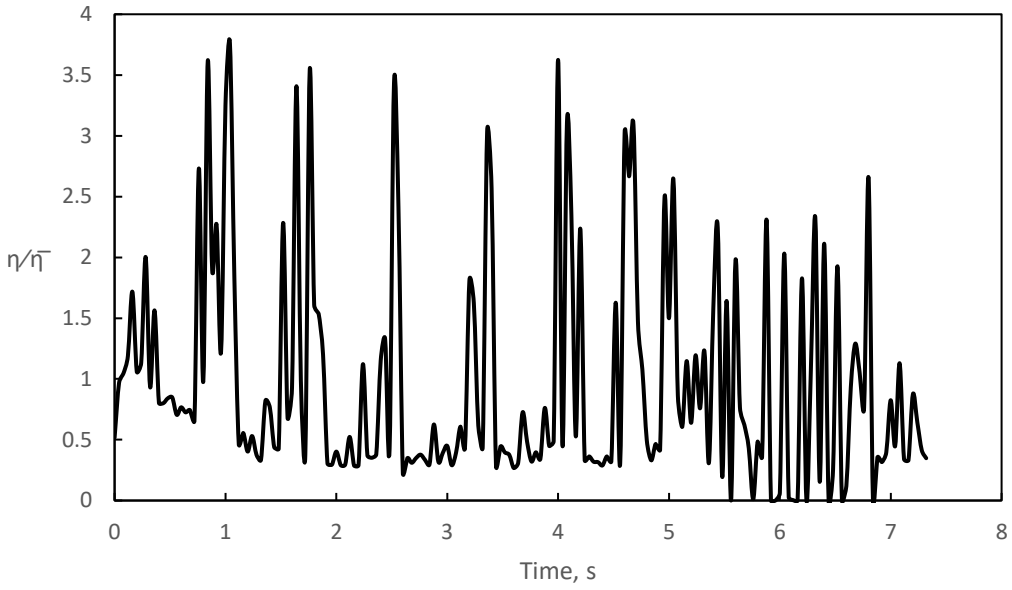


**Figure 0.5 Stability analysis for pulsating spray, GLR=2.2%, $F_L$=21.4 g/s**

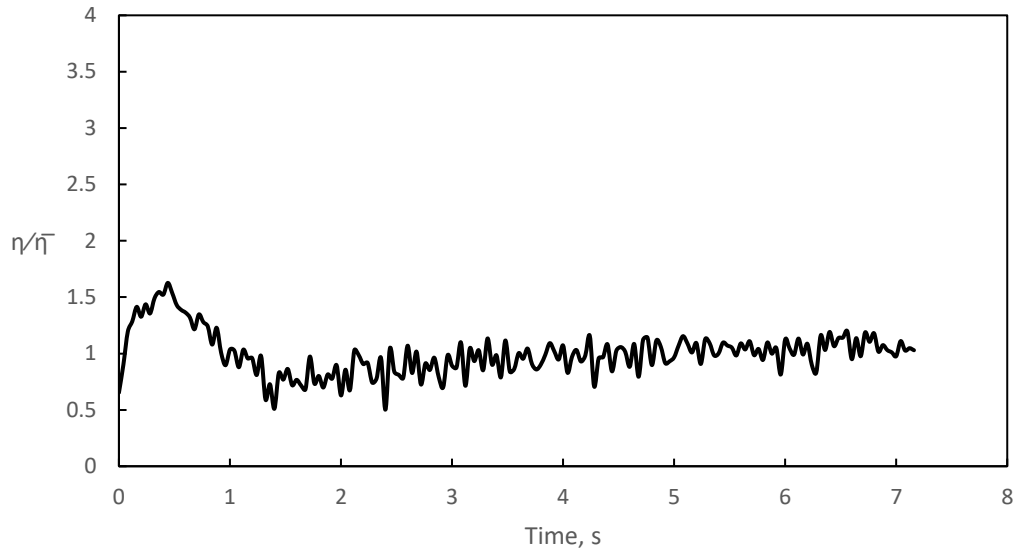


**Figure 0.6 Stability analysis for stable spray GLR=2.2%, $F_L$=21.4 g/s**

The frequency of pulsations in the pulsating spray is approximately 5 Hz. The magnitude of the fluctuations in the spray area is significantly higher than for the stable spray. At the beginning of the stable spray, a pulse is detected and afterwards the spray tends to stabilize at around $\eta/\bar{\eta}=1$.

## 5.2.2 Effect of spray stability on liquid distribution

Below shows the difference in free moisture, agglomerate mass and L/S of agglomerates for stable and unstable sprays at various gas velocities.

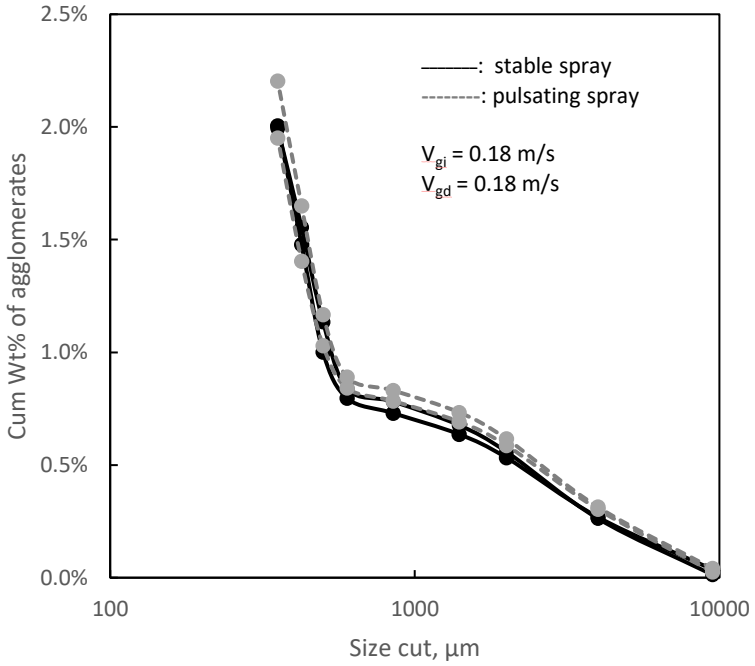


**Figure 0.7 Cumulative Wt% of agglomerates in bed mass GLR=2.2%, $F_L$=21.4 g/s (two experiments for each condition)**

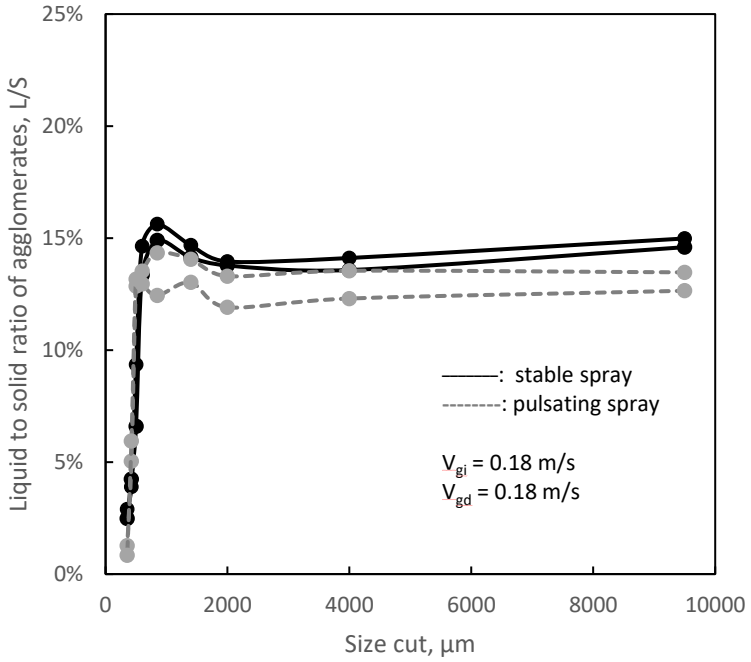


**Figure 0.8 Initial L/S ratio in agglomerates (g/g) GLR=2.2%, $F_L$=21.4 g/s**

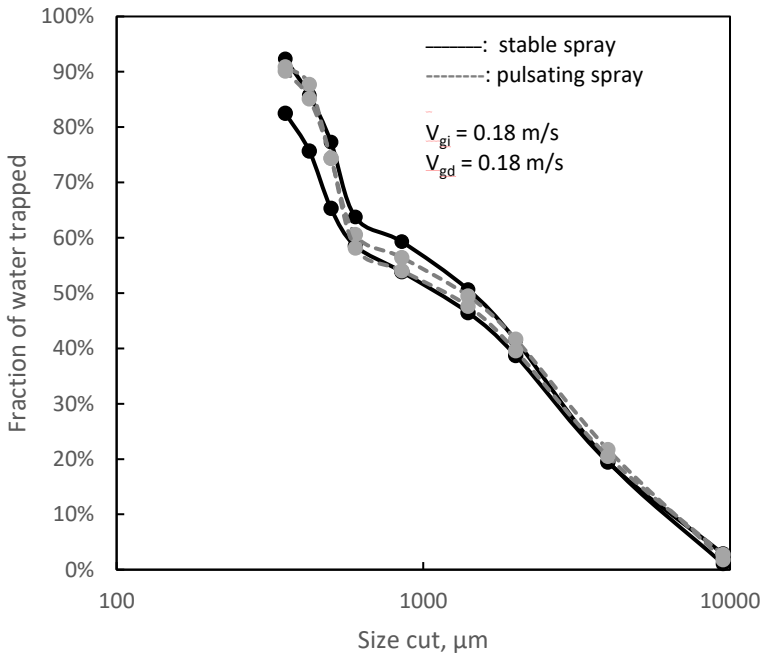


**Figure 0.9 Cumulative fraction of water trapped in agglomerates GLR=2.2%, $F_L$=21.4 g/s**

When the fluidization velocity during injection, $V_{gi}$, was 0.18 m/s and when the fluidization velocity during drying, $V_{gd}$, was 0.18 m/s, spray pulsation has a minimal impact on the free moisture and the liquid to solid ratio. Thus the free moisture is not affected in any significant manner. When the superficial velocity is low in both liquid injection stage and agglomerate drying stage, bed hydrodynamics is the dominant factor determining the liquid distribution.

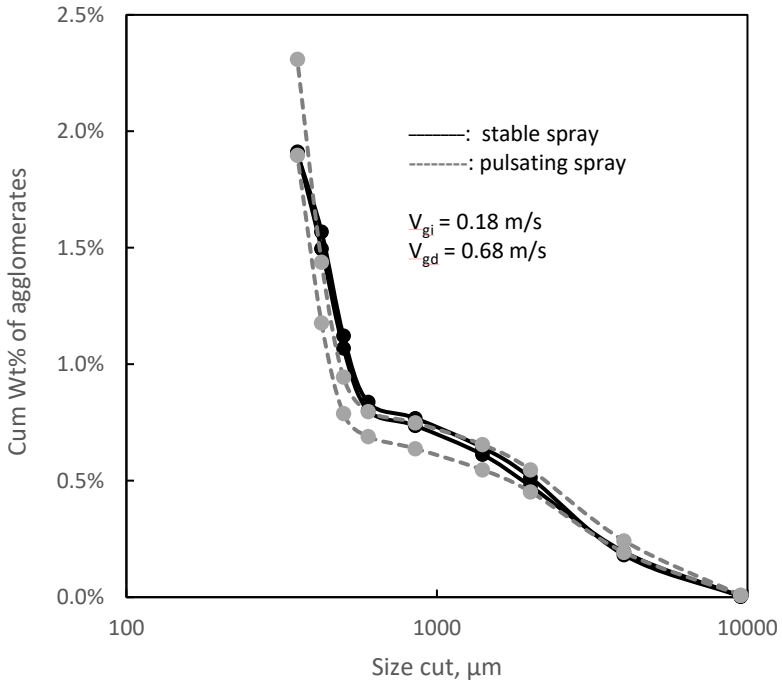


**Figure 0.10 Cumulative Wt% of agglomerates in bed mass GLR=2.2%, $F_L$=21.4 g/s**

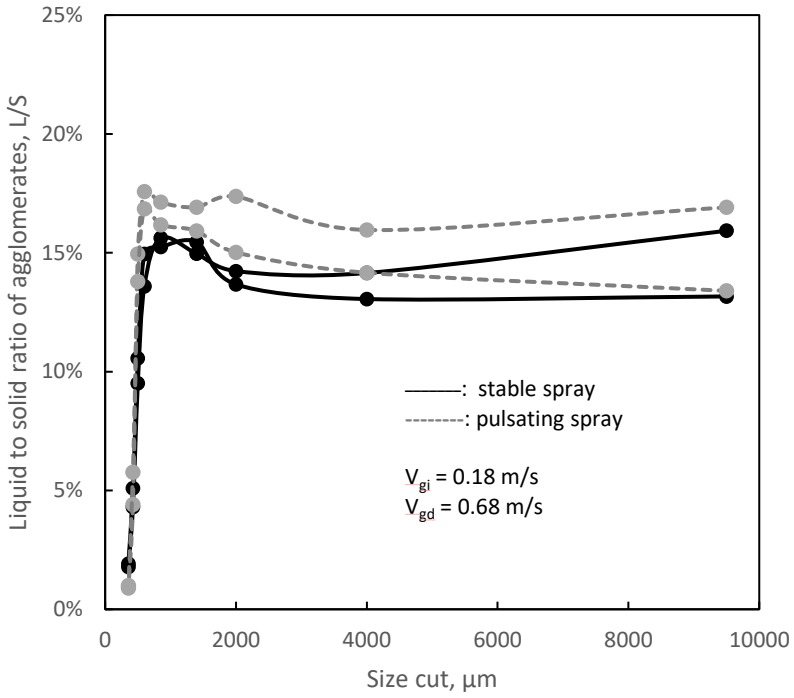


**Figure 0.11 Initial L/S ratio in agglomerates (g/g) GLR=2.2%, $F_L$=21.4 g/s**

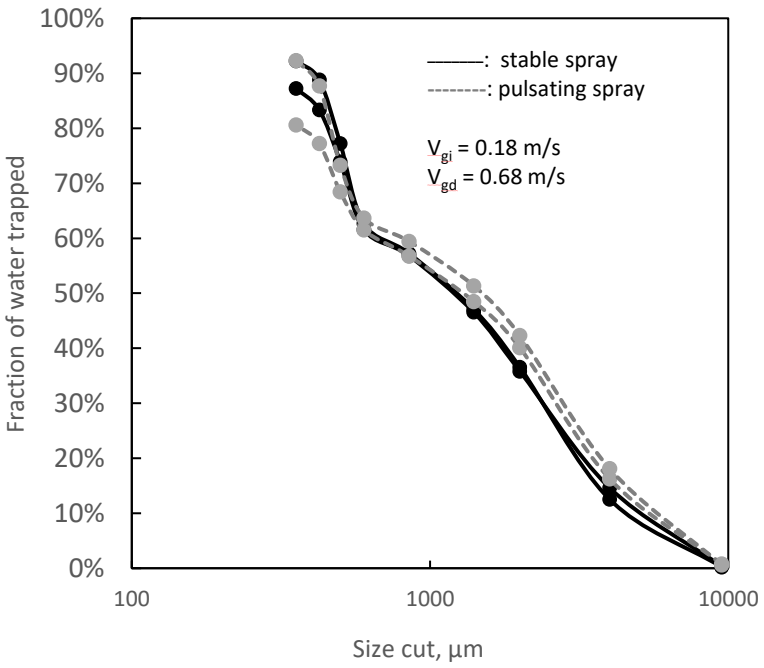


**Figure 0.12 Cumulative fraction of water trapped in agglomerates GLR=2.2%, $F_L$=21.4 g/s**

When $V_{gi}$=0.18 m/s and $V_{gd}$=0.68 m/s, the pulsation of spray also has a minimal impact on the free moisture and liquid to solid ratio. Thus the free moisture is not affected in a significant manner. The low superficial gas velocity is still the dominant factor affecting the liquid-solid contact.

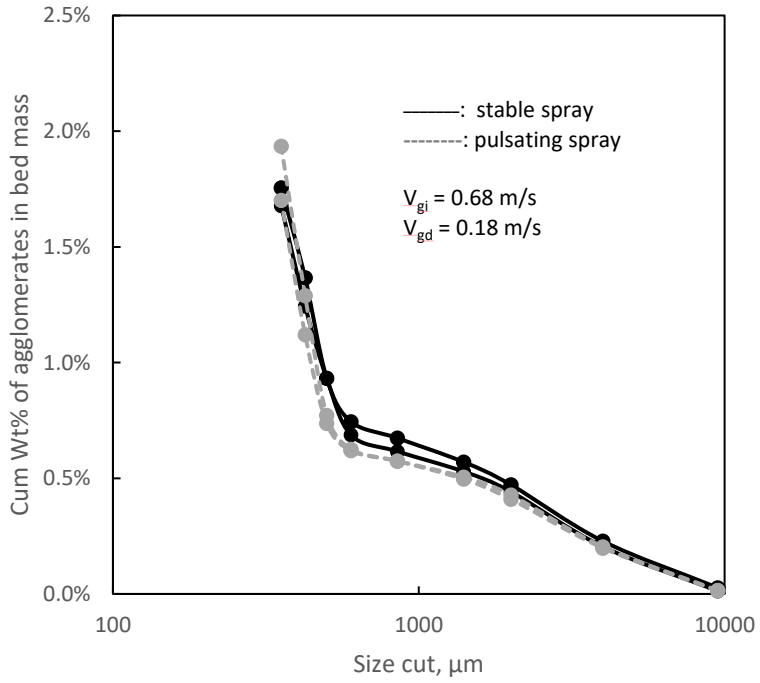


**Figure 0.13 Cumulative Wt% of agglomerates in bed mass GLR=2.2%, $F_L$=21.4 g/s**

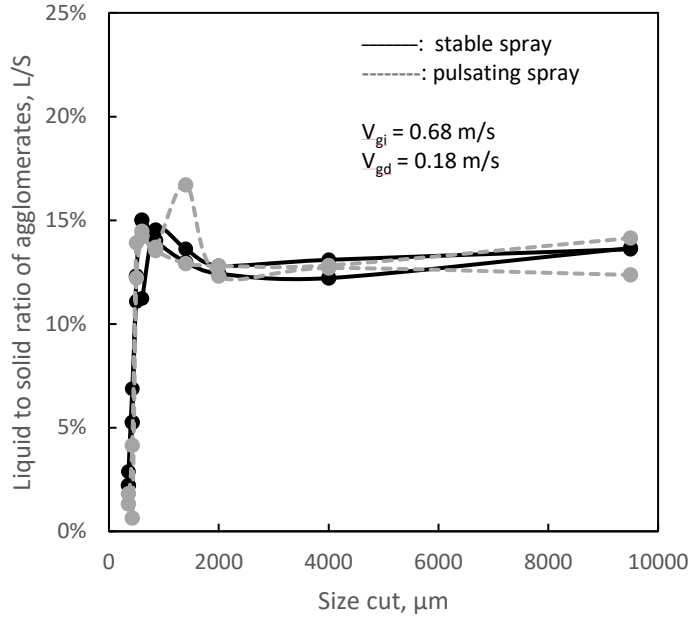


**Figure 0.14 Initial L/S ratio in agglomerates (g/g) GLR=2.2%, $F_L$=21.4 g/s**

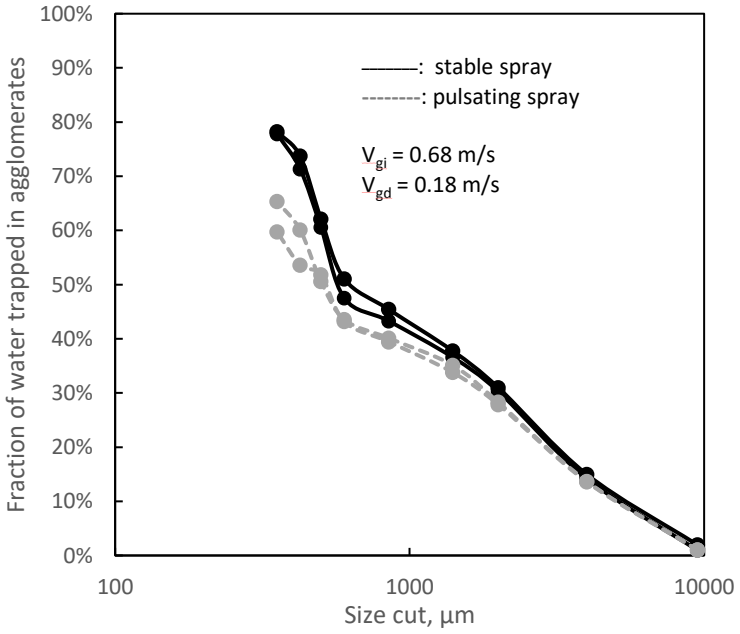


**Figure 0.15 Amount of water trapped in agglomerates GLR=2.2%, $F_L$=21.4 g/s**

When $V_{gi}$=0.68 m/s and $V_{gd}$=0.18 m/s, the pulsation of spray has a minimal impact on the amount of agglomerates. But for pulsating sprays, micro agglomerates have a lower liquid concentration which resulted in a higher free moisture.

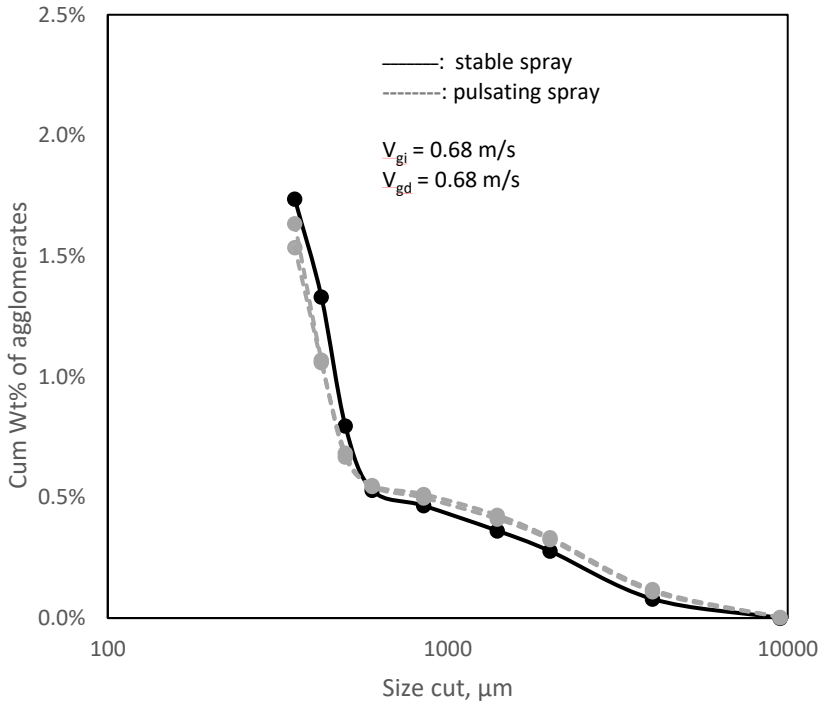


**Figure 0.16 Cumulative Wt% of agglomerates in bed mass GLR=2.2%, $F_L$=21.4 g/s**

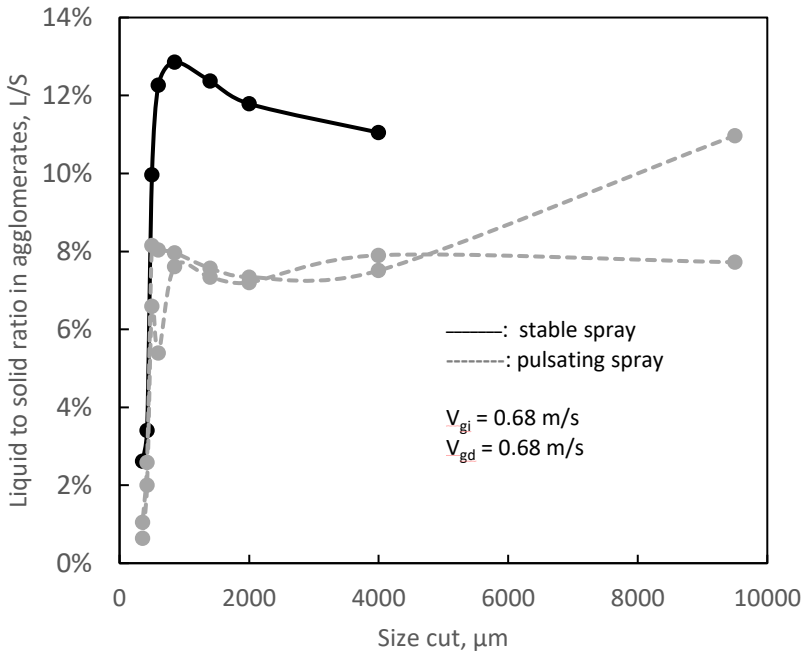


**Figure 0.17 Initial L/S ratio in agglomerates (g/g) GLR=2.2%, $F_L$=21.4 g/s**

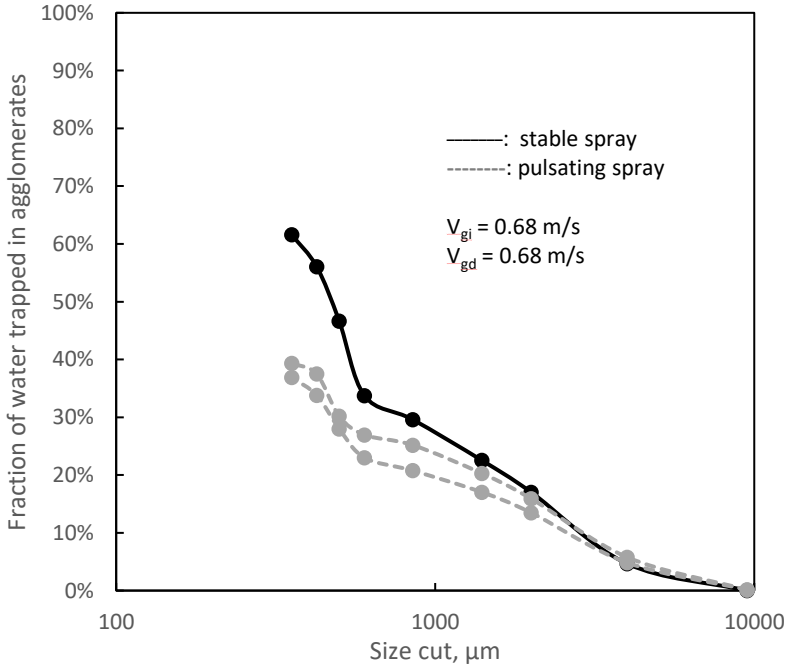


**Figure 0.18 Initial L/S ratio in agglomerates (g/g) GLR=2.2%, $F_L$=21.4 g/s**

When $V_{gi}$=0.68 m/s and $V_{gd}$=0.68 m/s, the bed hydrodynamics is beneficial for the liquid-solid contact of stable spray and also spray pulsation reduced the amount of agglomerates slightly. And for pulsating sprays, the agglomerates have a lower liquid concentration which resulted in a significantly larger free moisture. At a higher superficial gas velocity, jet pulsation becomes the dominant factor affecting liquid distribution.

**Table 0-2 Free moisture fraction for pulsating and stable spray at different conditions**

| Free moisture fraction at different conditions | | | | |
|---|---|---|---|---|
| $\frac{V_{gi}, m/s}{V_{gd}, m/s}$ | $\frac{0.18}{0.18}$ | $\frac{0.18}{0.68}$ | $\frac{0.68}{0.18}$ | $\frac{0.68}{0.68}$ |
| Pulsating Injections | 9.1-9.9 % | 9.4 -15.6 % | 34.6-40.3% | 63.1-65.2% |
| Stable Injections | 7.7-17.5% | 7.8-12.7% | 21.8%-22.2% | 38.4% |

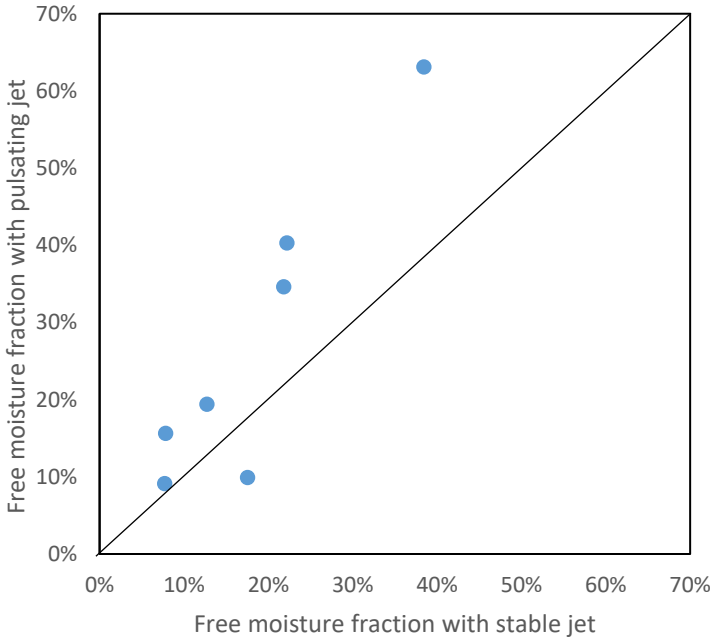


**Figure 0.19 Comparison between the amount of free moisture of stable spray and pulsating spray**

The comparison between the amount of free moisture of a stable spray and a pulsating spray indicates that when liquid-solid contact is improved by higher superficial velocities for a stable spray it is more beneficial to use pulsating sprays. Improvements in liquid distribution due to bed hydrodynamics and nozzle pulsations reinforce each other.

### 5.2.3 Effect of gas velocity on liquid distribution for pulsating spray

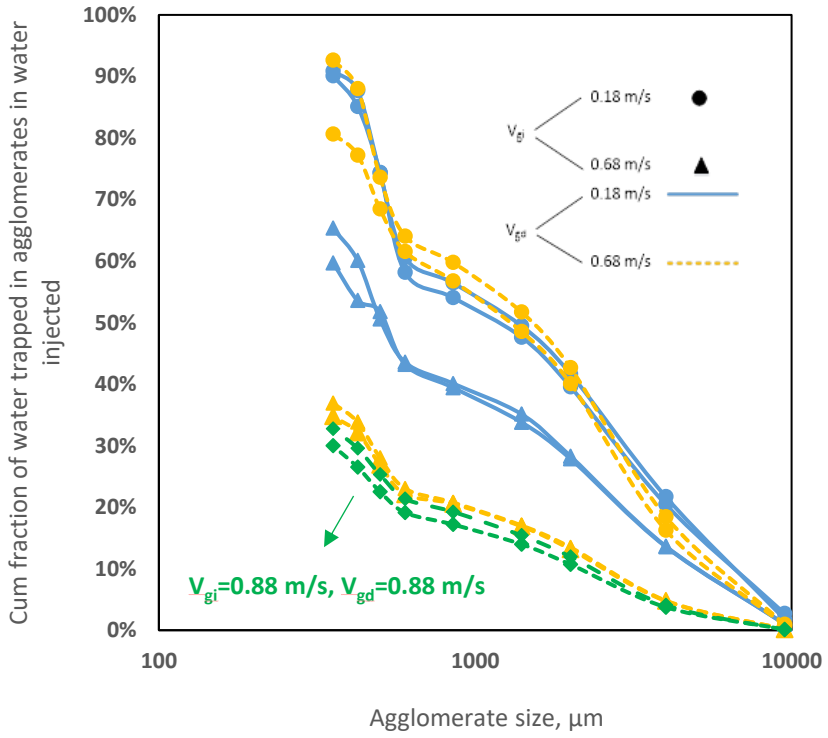


**Figure 0.20 Cumulative weight fraction of water trapped in agglomerates, GLR=2.2%, $F_L$=21.4 g/s**

The results of free moisture fraction show that both increasing $V_{gi}$ and $V_{gd}$ is beneficial for liquid-solid contact. When $V_{gi}$ is low, increasing $V_{gd}$ has quite limited impact on the amount of free moisture. When $V_{gi}$ is high, increasing $V_{gd}$ can greatly increase the amount of free moisture. When $V_{gd}$ is high, increasing $V_{gi}$ can also greatly increase the amount of free moisture.

## 5.2.4 Effect of GLR on liquid distribution

First open air injections were conducted to examine the stability of sprays at different GLRs. The same analysis method was used to characterize the stability of sprays. The injection durations were obtained from both video analysis and the pressure at the downstream of the sonic nozzle for atomization gas.

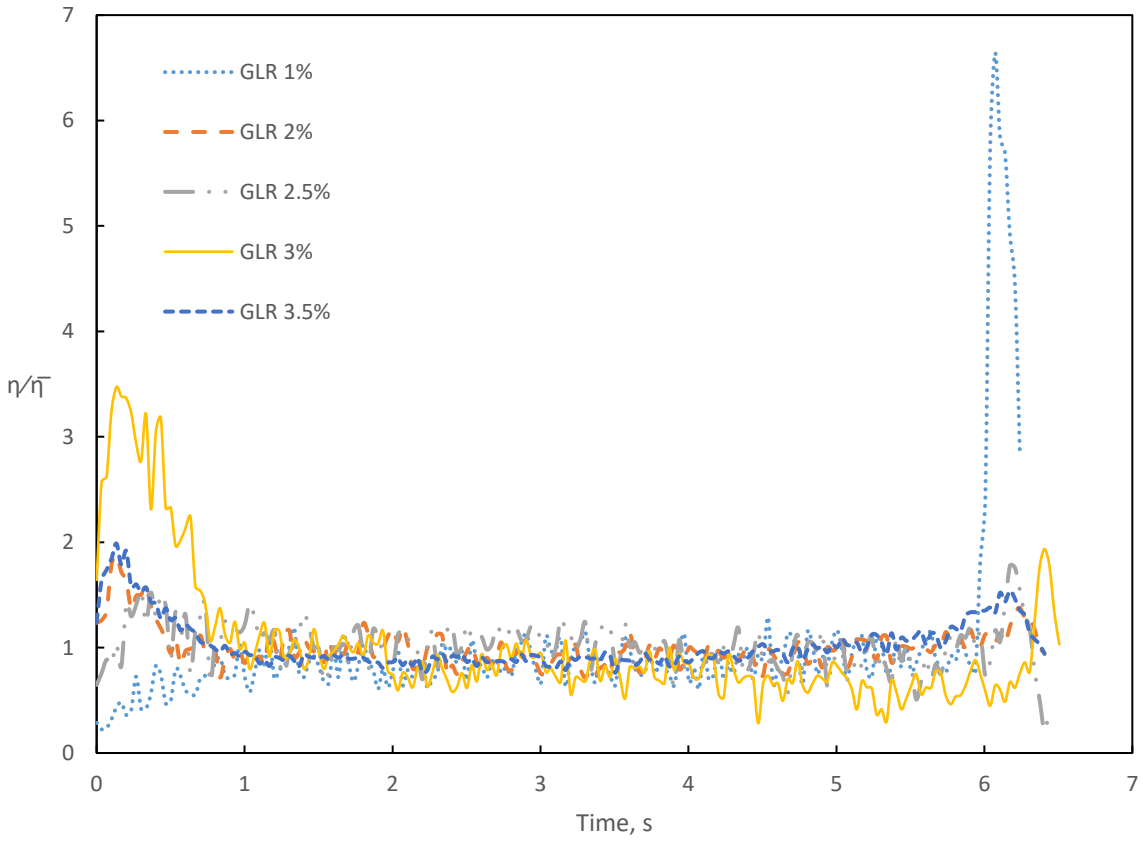


**Figure 0.21 Stability analysis for open air spray at various GLRs, $F_L$=23.4 g/s**

The results of video analysis indicate that for GLR = 1%, 2%, 2.5 %, 3% and 3.5% at a constant liquid flowrate, the sprays are all relatively stable. At the beginning or the end of the injections, a pulse usually occurs. The intensity of these pulses changes depending on the GLR. During the middle of the injection, the sprays are stable. Hence we can assume no impact of pulsations on liquid-solid contact.

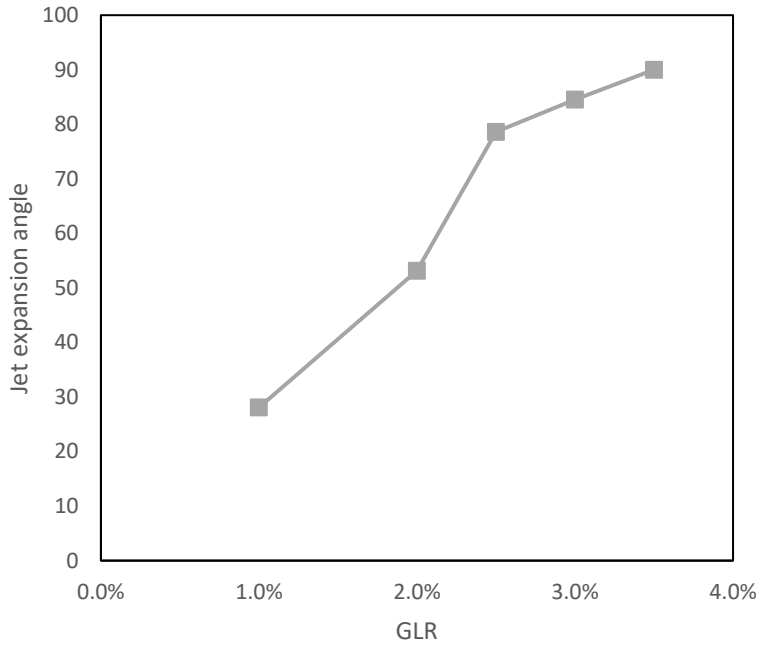


**Figure 0.22 Jet expansion angle for sprays of different GLRs in the open air**

The results in Figure 5.22 show that the jet expansion angle increases with the atomization gas to liquid ratio. As the gas flowrate increases in the spray, the liquid is distributed into a larger region, which is likely to be beneficial to liquid-solid contact.

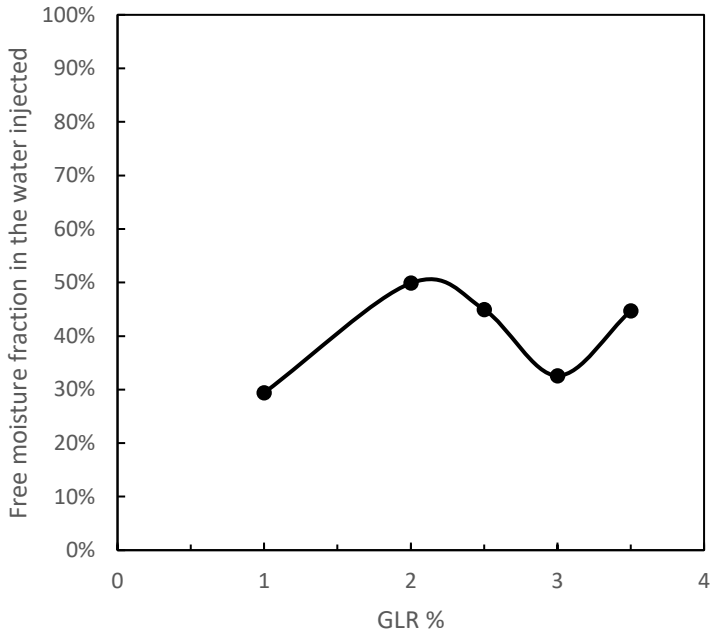


**Figure 0.23 Free moisture fraction in the water injected for different GLRs, $F_L$=23.4 g/s**

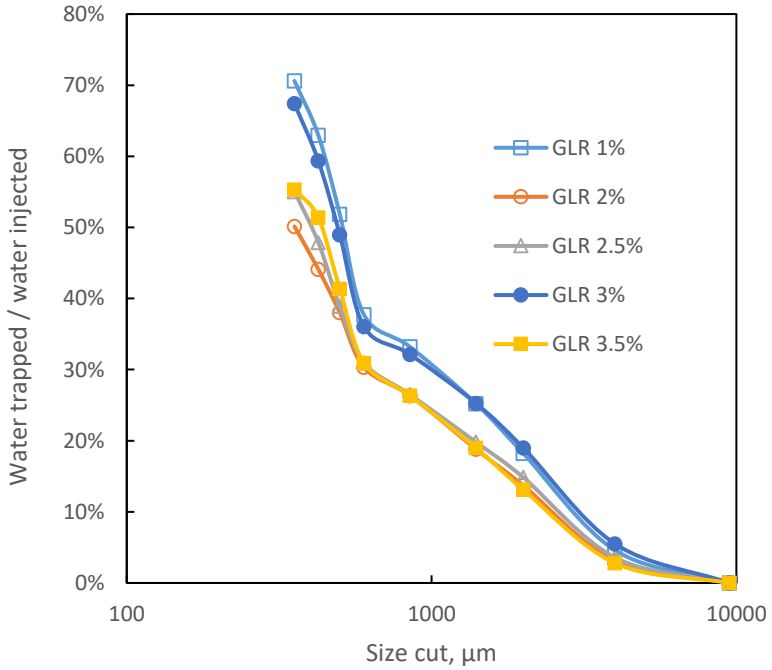


**Figure 0.24 Cumulative fraction of water trapped in agglomerates in total amount of water injected for different GLRs, $F_L$=23.4 g/s**

The results in figure 5.23 and 5.24 show that an increase of GLR from 1% to 2% improves the liquid distribution. Then with further increase in the GLR, the amount of free moisture shows a sharp drop, followed by a subsequent recovery for GLRs larger than 3%. An optimal GLR for liquid distribution exists at 2%. The results are similar to the conclusion reached by Leach et al. [18], who used a conductance method to characterize the liquid-solid contact.

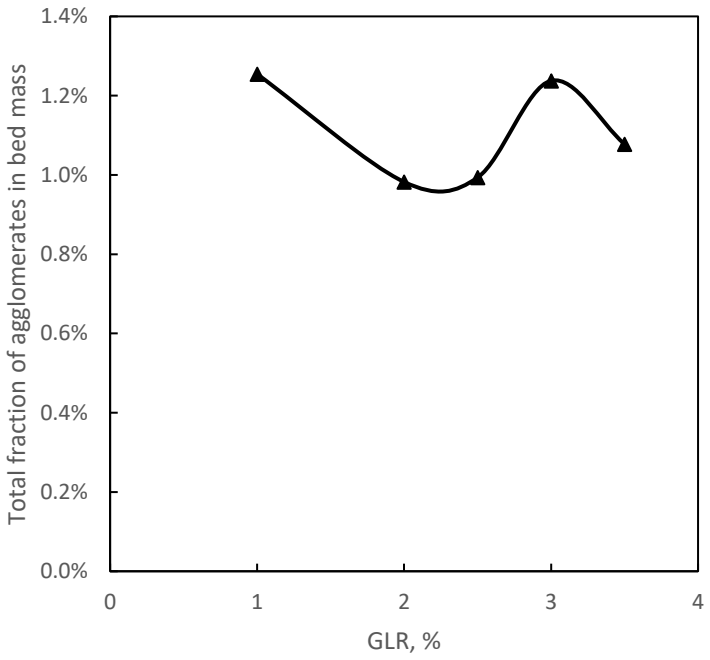


**Figure 0.25 Total fraction of agglomerates in bed mass for different GLRs, $F_L$=23.4 g/s**

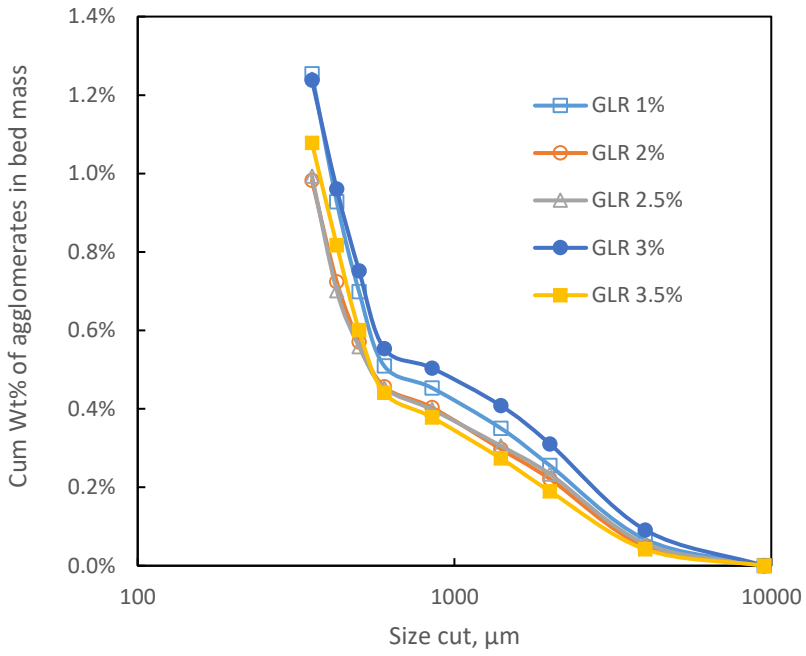


**Figure 0.26 Cumulative wt% of agglomerates in bed mass for different GLRs, $F_L$=23.4 g/s**

The results in figure 5.25 and 5.26 show that when the atomization gas to liquid ratio increases from 1% to 3.5%, the amount of agglomerates decreases first and reaches the lowest value at GLR=2% and afterwards increases. This is consistent with the results about the amount of free moisture. When the amount of free moisture increases, the amount of agglomerates decreases. Various reasons can account for the change in liquid-solid contact such as the size of liquid droplets. Further studies need to be continued to find the key factor affecting the liquid-solid contact when increasing the atomization gas flowrate.

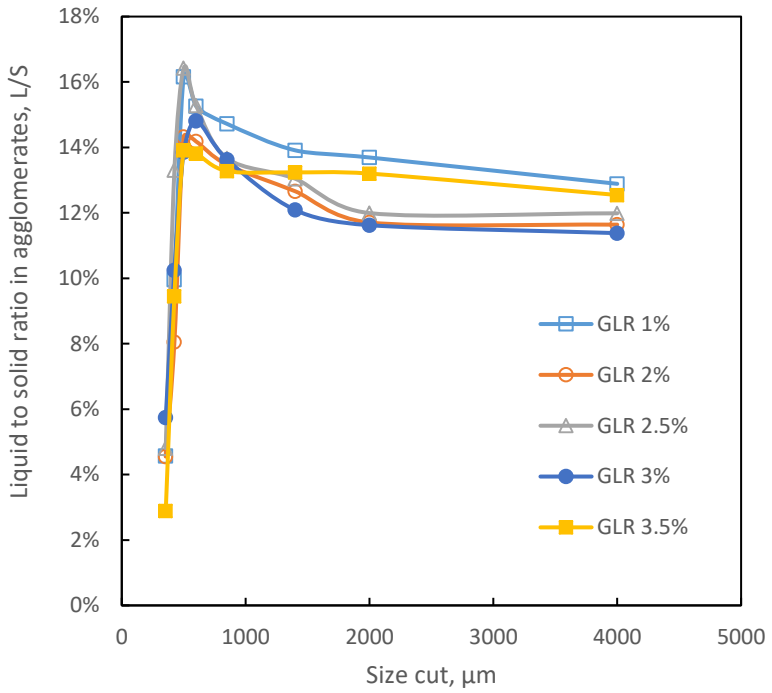


**Figure 0.27 Liquid to solid ratio in agglomerates for different GLRs, $F_L$=23.4 g/s**

Figure 5.27 shows that changing the GLR has no significant impact on the liquid to solid ratio in agglomerates. This suggests that when bed hydrodynamics and liquid flowrate are the same, changing the atomization gas to liquid ratio has a minimal impact on the liquid concentration in the agglomerates.

# Conclusions and Recommendations

## 6.1 Conclusions

— In a fluidized bed, both superficial velocities during liquid injection and during the subsequent agglomerate drying stage can greatly affect the liquid distribution.

1. Increasing the superficial velocity during liquid injection reduces the total amount of agglomerates and slightly decreases the liquid to solid ratio in agglomerates. After the superficial velocity reaches 1.2 m/s, the effect became minimal and the amount of free moisture ceased to increase.
2. Increasing the superficial velocity during the drying stage contributes to larger shear forces which facilitates the breakup of wet agglomerates. The liquid to solid ratio decreased in micro agglomerates but did not significantly change in macro agglomerates. The total amount of agglomerates also dropped as the superficial velocity increased.

— The triboelectricity method can be used effectively to measure the bubble gas flowrate in the bed when the initial gas distributions are different. When the superficial velocity is constant, the triboelectricity method indicates the concentration of gas bubbles in different lateral positions in the fluidized bed.

— Various in-bed gas distributions were created by changing the initial gas distribution. When the superficial velocity was constant, two types of gas distributions were used in comparison to the base case. Either the gas velocity at the beginning of jet was increased or the gas velocity at the end of jet was increased. The results from the gum Arabic injection experiments indicate that increasing the gas velocity at the beginning of the jet has negligible impact on the liquid distribution while increasing the gas velocity at the end of the jet improves the liquid distribution. Fewer agglomerates, with a relatively lower initial liquid to solid ratio, were produced with a higher gas velocity at the end of the jet.

— Pulsations in liquid sprays can be introduced by changing the geometry of the injection system. By changing the geometry of the injection system, the linear velocities of gas and liquid in the conduit leading to the spray nozzle change. Thus the flow can fall into different patterns according to the flow pattern map of Taitel and Dukler[29]. This results in changes in the spray.

— Pulsations improve liquid distribution when the fluidization velocity in either spray region or drying region is high.

— For a scaled down industrial type TEB nozzle, changing the atomization gas to liquid ratio has a strong effect on the liquid distribution. An optimal GLR exists at 2.5% which provides the highest free moisture in the bed and the fewest amount of agglomerates.

## 6.2 Recommendation

— Experiments using a scaled down industrial TEB nozzle have shown that increasing the superficial gas velocities during the injection phase and the agglomerate drying and breakup phase are both beneficial for liquid distribution. This corresponds to the spray region where injected feedstocks interact with coke particles and the agglomerate drying region where agglomerates are transported, dried and broken up in a Fluid Coker™. Thus either increasing the superficial gas velocity in the spray region or the agglomerate drying region can improve the liquid distribution in a Fluid Coker™.

— The results from the gum Arabic injection experiments using various gas distributions indicate that increasing the gas velocity at the beginning of the jet has no impact on the liquid distribution while increasing the gas velocity at the end of the jet improves the liquid distribution. In a Fluid Coker™, correspondingly more gas bubbles can be placed at the end of the spray jet, which is close to the center of the reactor, instead of at the region close to the wall in order to improve the liquid distribution.

— The effect of the atomization gas to liquid ratio was studied using a scaled down industrial type TEB nozzle. The amount of free moisture as a function of GLR is not monotonic while an optimal GLR for liquid-solid contact was found to be 2%. The expansion angles for sprays of different GLRs were also measured in the open air. Future studies about the correlation and GLR can be conducted on an industrial scale nozzle.

# References


[1] P. K. House, C. L. Briens, F. Berruti, and E. Chan, “Effect of spray nozzle design on liquid-solid contact in fluidized beds,” *Powder Technol.*, vol. 186, no. 1, pp. 89–98, 2008.

[2] N. E. Board(NEB), “Canada’s oil sands-a supply and market outlook to 2015,” Calcary, AB.

[3] R. W. Pfeiffer, D. S. Borey, and C. E. Jahnig, “Inventors fluid coking of heavy hydrocarbons,” *US Pat.*, 1959.

[4] D. G. Hammond, M. Jacobson, J. F. Pagel, M. C. Poole, R. C. Green, and W. Serrand, “Fluidized bed coking process.” Google Patents, 19-Aug-1997.

[5] X. Song, J. R. Grace, H. Bi, C. J. Lim, E. Chan, B. Knapper, and C. Mcknight, “Experimental Simulation of the Reactor Section of Fluid Cokers : Comparison of FCC and Fluid Coke Particles,” *Can. J. Chem. Eng.*, vol. 84, no. 2002, pp. 161–169, 2006.

[6] M. Mohagheghi, M. Hamidi, F. Berruti, C. Briens, and J. McMillan, “Study of the effect of local hydrodynamics on liquid distribution in a gas-solid fluidized bed using a capacitance method,” *Fuel*, vol. 107, pp. 236–245, 2013.

[7] K. Pougatch, M. Salcudean, and J. McMillan, “Three-dimensional numerical modelling of interactions between a gas–liquid jet and a fluidized bed,” *Chem. Eng. Sci.*, vol. 68, no. 1, pp. 258–277, 2012.

[8] C. B. Morales, “Development and Application of an Experimental Model for the Fluid Coking Process,” *M.Sc Thesis*, no. August, 2013.

[9] S. Weber, C. Briens, F. Berruti, E. Chan, and M. Gray, “Stability of agglomerates made from fluid coke at ambient temperature,” *Powder Technol.*, vol. 209, no. 1–3, pp. 53–64, 2011.

[10] S. Ariyapadi, D. W. Holdsworth, C. J. D. Norley, F. Berruti, and C. Briens, “Digital X-ray Imaging Technique to Study the Horizontal Injection of Gas-Liquid Jets into Fluidized

Beds," *Int. J. Chem. React. Eng.*, vol. 1, no. 1, 2003.

[11] S. Bruhns and J. Werther, "An investigation of the mechanism of liquid injection into fluidized beds," *AIChE J.*, vol. 51, no. 3, pp. 766–775, 2005.

[12] S. M. Iveson, J. D. Litster, K. Hapgood, and B. J. Ennis, "Nucleation, growth and breakage phenomena in agitated wet granulation processes: A review," *Powder Technol.*, vol. 117, no. 1–2, pp. 3–39, 2001.

[13] M. R. Gray, "Fundamentals of bitumen coking processes analogous to granulations: A critical review," *Can. J. Chem. Eng.*, vol. 80, no. 3, pp. 393–401, 2002.

[14] M. Farkhondehkavaki, M. Soleimani, M. Latifi, F. Berruti, C. Briens, and J. McMillan, "Characterization of moisture distribution in a fluidized bed," *Meas. J. Int. Meas. Confed.*, vol. 47, no. 1, pp. 150–160, 2014.

[15] T. E. Base, E. W. Chan, R. D. Kennett, and D. A. Emberley, "Nozzle for atomizing liquid in two phase flow." Google Patents, 21-Dec-1999.

[16] M. Ali Zirgachian, M. Soleimani, C. Briens, and F. Berruti, "Electric conductance method for the assessment of liquid-gas injection into a large gas-solid fluidized bed," *Meas. J. Int. Meas. Confed.*, vol. 46, no. 2, pp. 893–903, 2013.

[17] F. Portoghese, F. Berruti, C. Briens, and E. Chan, "Novel triboelectric method for characterizing the performance of nozzles injecting gas-atomized liquid into a fluidized bed," *Chem. Eng. Process. Process Intensif.*, vol. 46, no. 10, pp. 924–934, 2007.

[18] A. Leach, G. Chaplin, C. Briens, and F. Berruti, "Comparison of the performance of liquid-gas injection nozzles in a gas-solid fluidized bed," *Chem. Eng. Process. Process Intensif.*, vol. 48, no. 3, pp. 780–788, 2009.

[19] and F. B. Rana Sabouni, Aidan Leach, Cedric Briens, "Enhancement of the Liquid Feed Distribution in Gas-Solid Fluidized Beds by Nozzle Pulsation," *AIChE J.*, vol. Vol. 57, no. No.12, pp. 3344–3350, 2011.

[20] R. Sabouni, C. Briens, and F. Berruti, “Enhancement of the liquid feed distribution in gas solid fluidised beds by non-mechanically induced nozzle pulsations,” *Can. J. Chem. Eng.*, vol. 91, no. 6, pp. 1161–1167, 2013.

[21] R. Sabouni, F. Berruti, and C. Briens, “Comparison of the impact of flow pulsations on the performance of various liquid-gas injectors in a gas-solid fluidised bed,” *Can. J. Chem. Eng.*, vol. 90, no. 1, pp. 51–60, 2012.

[22] A. Leach, R. Sabouni, F. Berruti, and C. Briens, “Use of pulsations to enhance the distribution of liquid injected into fluidized particles with commercial-scale nozzles,” *AIChE J.*, vol. 59, no. 3, pp. 719–728, 2013.

[23] M. Leva, *Fluidization*. McGraw-Hill, 1959.

[24] M. Farkhondehkavaki, B. Engineering, and P. Studies, “Developing Novel Methods to Characterize Liquid Dispersion in a Fluidized Bed,” *Univ. West. Ontario*, 2012.

[25] L. A. P. Reyes, “Effect of Temperature and Successive Sprays on Liquid Distribution in Fluidized Beds.” The University of Western Ontario, 2015.

[26] C. Poynton, “Frequently asked questions about color,” *Retrieved June*, vol. 19, p. 2004, 1997.

[27] S. Ariyapadi, F. Berruti, C. Briens, B. Knapper, R. Skwarok, and E. Chan, “Stability of horizontal gas-liquid sprays in open-air and in a gas-solid fluidized bed,” *Powder Technol.*, vol. 155, no. 3, pp. 161–174, 2005.

[28] F. Benjelloun, R. Liegeois, and J. Vanderschuren, “Penetration length of horizontal gas jets into atmospheric fluidized beds,” *Proc. Fluid. Eng. Found. NY*, pp. 239–246, 1995.

[29] A. Leach, F. Portoghese, C. Briens, and F. Berruti, “A new and rapid method for the evaluation of the liquid-solid contact resulting from liquid injection into a fluidized bed,” *Powder Technol.*, vol. 184, no. 1, pp. 44–51, 2008.

[30] Y. Taitel and a E. Dukler, “A Model for Predicting Flow Regime Transitions Horizontal

and Near Horizontal Gas-liquid Flow," *AIChE J.*, vol. 22, no. 1, pp. 47–55, 1976.

[31] D. Barnea, Y. Luninskl, and Y. Taitel, "Flow Pattern in Horizontal and Vertical Two Phase Flow in Small Diameter Pipes," *Can. J. Chem. Eng.*, vol. 61, no. 5, pp. 617--620, 1983.

# Appendices

## Data Acquisition

```
//==============================================================================
==========================

//

// Title:       PinkBedDAQ.c

// Purpose:     DAQ for the Pink Bed

//

// Created on:  7/24/2014 at 4:02:00 PM by Francisco J. Sanchez, Ph.D..

// Copyright:   University of Western University. All Rights Reserved.

//

//==============================================================================
==========================



//==============================================================================
==========================

// Include files

//==============================================================================
==========================

#include <windows.h>

#include <formatio.h>

#include <toolbox.h>

#include <utility.h>
```

```
#include <ansi_c.h>

#include <math.h>

#include <stdio.h>

#include <stdlib.h>

#include <time.h>

#include <userint.h>

#include <OleAuto.h>

#include <cviauto.h>

#include <NIDAQmx.h>

#include <analysis.h>

#include <3DGraphCtrl.h>

#include <rs232.h>

#include <cviddc.h>

#include <userint.h>

#include "PinkBedDAQ.h"

//==============================================================================
============================

// Macros

//==============================================================================
============================

#define Pi 3.14159

//==============================================================================
============================
```

```
// Global Variables

//==============================================================================
==========================

char FileBrowser[300], TimeChar01[21], TimeChar02[21];

double M[12][1300000];

FILE *FileOfData01, *FileOfData02, *FileOfData03, *FileOfData04;

float64 Temperatures[4], Voltage[16], Voltage2[16000], Vrms, Vrms1s, Volt[1000], GraphValue[7];

int PlotAndSave = 0, PlotAndSaveFlag = 0;

int FunctionID;

int CVICALLBACK FastDAQ(void *FunctionData);

int GetVoltFlag=0;

int STFast=0;

int GetDataFast=0;

int CounterFast=0;

int EndFlag=0;

int mstest=1000;

int TMS=0;

// Test Save Data on Matrix


int32 SamplesPerChannelRead = 0, SamplesPerChannelRead2 = 0;

static int MainPanelHandle, Executable01; // Panel Handles

TaskHandle TemperatureHandle, PressureHandle, PressureHandle2;

time_t Clock; // Time and Date Variables
```

```
//==============================================================================
==========================

// Main Program

//==============================================================================
==========================

int main()

{

	// Open NI Max

	LaunchExecutableEx ("c:\\Program Files (x86)\\National Instruments\\MAX\\NIMax.exe",
LE_SHOWMINIMIZED, &Executable01);

	Sleep (7000);

	// Schedule Thread

	MainPanelHandle = LoadPanel (0,"PinkBedDAQ.uir", MAINPANEL);

	DisplayPanel(MainPanelHandle);

	// Open the Hardware Channels

	//DAQmxLoadTask ("Dev01Temp", &TemperatureHandle);

	DAQmxLoadTask ("Dev02Voltage", &PressureHandle);

	//DAQmxLoadTask ("Dev03Voltage", &PressureHandle2);

	// Create a Thread

	GetVoltFlag=1;

	CmtScheduleThreadPoolFunction (DEFAULT_THREAD_POOL_HANDLE, FastDAQ, NULL,
&FunctionID);

	RunUserInterface ();

	return 0;
```

```
}

//==============================================================================
==========================

//Take DAQ Fast

int CVICALLBACK FastDAQ(void *FunctionData)

{

	int i=0,j=0;

	SYSTEMTIME LT01;

	CmtSetCurrentThreadPriority(15);

	while (GetVoltFlag == 1)

	{

		// Get Voltage Values

		DAQmxReadAnalogF64 (PressureHandle, DAQmx_Val_Auto, 1,
DAQmx_Val_GroupByChannel, Voltage, 16, &SamplesPerChannelRead, 0);

		// Conductivity

		for (i=0; i<=998; i++)

			Volt[i]=Volt[i+1];

		Volt[999]=Voltage[6];

		Vrms=0;

		for (i=0; i<=999; i++)

			Vrms=Vrms+(pow(Volt[i],2))/1000;

		Vrms=sqrt(Vrms);

		//Vrms=Voltage[6];//Remove Vrms
```

```
Vrms1s=Vrms;
if (PlotAndSaveFlag == 1)
{
// Get Time
GetLocalTime (&LT01);
memset (TimeChar01, 0, 21);
sprintf (TimeChar01, "%2d %s %2d %s %2d %s %3d", LT01.wHour, ":",
LT01.wMinute, ":", LT01.wSecond, ":", LT01.wMilliseconds);
// Print on File
fprintf (FileOfData01,
"%12s %3s %9.2lf %9.2lf %9.2lf %9.2lf %9.2lf %9.2lf %9.2lf %9.2lf\n",
TimeChar01, " |", Voltage[0], Voltage[1], Voltage[2], Voltage[3],
Voltage[4], Voltage[5], Voltage[6], Vrms, Voltage[7]);
Sleep (1);
}
if (GetDataFast == 1)
{
SetPanelAttribute (MainPanelHandle, ATTR_DIMMED, 1);
while (CounterFast<=STFast)
{
// Get Time
DAQmxReadAnalogF64 (PressureHandle, DAQmx_Val_Auto, 1,
DAQmx_Val_GroupByChannel, Voltage, 16, &SamplesPerChannelRead, 0);
GetLocalTime (&LT01);
```

```
memset (TimeChar01, 0, 21);

sprintf (TimeChar01, "%2d %s %2d %s %2d %s %3d", LT01.wHour, ":",
LT01.wMinute, ":", LT01.wSecond, ":", LT01.wMilliseconds);

if (mstest != LT01.wMilliseconds)

{

    mstest=LT01.wMilliseconds;

    // Print on File

    fprintf (FileOfData03,
"%12s %3s %9.2lf %9.2lf %9.2lf %9.2lf %9.2lf %9.2lf %9.2lf %9.2lf\n",

                                    TimeChar01, " |", Voltage[0], Voltage[1],
Voltage[2], Voltage[3], Voltage[4], Voltage[5], Voltage[6], Vrms1s, Voltage[7]);

    if (CounterFast==STFast)

    {

        GetDataFast=0;

        EndFlag=1;

    }

    CounterFast++;

}/*

if (mstest != LT01.wMilliseconds)

{

    mstest=LT01.wMilliseconds;

    // Save on Matrix

    M[0][j]=LT01.wHour; M[1][j]=LT01.wMinute;
M[2][j]=LT01.wSecond;M[3][j]=LT01.wMilliseconds;
```

```
                                        M[4][j]=Voltage[0]; M[5][j]=Voltage[1]; M[6][j]=Voltage[2];
M[7][j]=Voltage[3]; M[8][j]=Voltage[4];

                                        M[9][j]=Voltage[5]; M[10][j]=Voltage[6]; M[7][j]=Vrms;

                                        if (CounterFast == STFast)

                                        {

                                                GetDataFast=0;

                                                EndFlag=1;

                                        }

                                        CounterFast++;

                                        j++;

                                }  */

                        }

                }

                if (GetDataFast == 0 && PlotAndSaveFlag == 0)

                {

                        j=0;

                        SetPanelAttribute (MainPanelHandle, ATTR_DIMMED, 0);

                        if (EndFlag == 1)

                        {

                                EndFlag=0;

                                /*for (j=0; j<=STFast;j++)

                                {
```

```
                                        fprintf (FileOfData03,
"%2.0lf %3s %2.0lf %3s %2.0lf %3s %3.0lf %3s %9.2lf %9.2lf %9.2lf %9.2lf %9.2lf %9.2lf %9.2lf %9.2lf \n",

                                                                M[0][j], ":", M[1][j], ":", M[2][j], ":", M[3][j], " | ",
M[4][j], M[5][j], M[6][j], M[7][j], M[8][j], M[9][j], M[10][j], M[11][j]);

                                        } */

                                        fclose (FileOfData03);

                                }

                        }

        }

        return 0;

}

// Write File Name

void WriteFileTitle()

{

        char FileName[256], WriteFileName[256];

        // Ask for Pressures File Name

        memset (FileName, 0, 256);

        memset (WriteFileName, 0, 256);

        PromptPopup ("Save File As", "Type the name for the file", FileName, 255);

        CopyString (WriteFileName, 0, "c:/DAQ File/", 0, -1);

        strcat (WriteFileName, FileName);

        strcat (WriteFileName, "-Pressures");

        strcat (WriteFileName, ".txt");
```

```
        // Open Pressure File and Print Titles
        FileOfData01 = fopen(WriteFileName, "w");
        fprintf (FileOfData01, "%11s %10s %9s %9s %9s %9s %9s %9s %9s %9s %9s %9s \n\n",
                                "Time", " | ", " V-01 ", " V-02 ", " V-03 ", " V-04 ", " V-05 ", " V-06 ", " V-07 ", "
Vrms ", " V-08 ");
        /*/ Ask for Temperature File Name
        memset (WriteFileName, 0, 256);
        CopyString (WriteFileName, 0, "c:/DAQ File/", 0, -1);
        strcat (WriteFileName, FileName);
        strcat (WriteFileName, "-Temperature");
        strcat (WriteFileName, ".txt");
        // Open Temparature File and Print Titles
        FileOfData02 = fopen(WriteFileName, "w");
        fprintf (FileOfData02, "%11s %10s %9s %9s %9s %9s %9s \n\n",
                                "Time", " | ", " T-01 ", " T-02 ", " T-03 ", " T-04 "); */
        memset (WriteFileName, 0, 256);
        CopyString (WriteFileName, 0, "c:/DAQ File/", 0, -1);
        strcat (WriteFileName, FileName);
        strcat (WriteFileName, "-Tribo");
        strcat (WriteFileName, ".txt");
        // Open Pressure File and Print Titles
        FileOfData04 = fopen(WriteFileName, "w");
```

```
        fprintf (FileOfData04,
"%14s %10s %9s %9s %9s %9s %9s %9s %9s %9s %9s %9s %9s %9s %9s %9s %9s %9s %9s\n\n",
                                "Time", " V-01 ", " V-02 ", " V-03 ", " V-04 ", " V-05 ", " V-06 ", " V-07 ", " V-08 ",
                                                                " V-09 ", " V-10 ", " V-11 ", " V-12 ", " V-13 ", " V-14
", " V-15 ", " V-16 ");
}
// Write File Name Fast
void WriteFileTitle2()
{
        char FileName[256], WriteFileName[256];
        // Ask for File Name
        memset (FileName, 0, 256);
        memset (WriteFileName, 0, 256);
        PromptPopup ("Save File As", "Type the name for the file", FileName, 255);
        CopyString (WriteFileName, 0, "c:/DAQ File/", 0, -1);
        strcat (WriteFileName, FileName);
        strcat (WriteFileName, "-Fast");
        strcat (WriteFileName, ".txt");
        // Open Pressure File and Print Titles
        FileOfData03 = fopen(WriteFileName, "w");
        fprintf (FileOfData03, "%11s %10s %9s %9s %9s %9s %9s %9s %9s %9s %9s \n\n",
                                "Time", " | ", " V-01 ", " V-02 ", " V-03 ", " V-04 ", " V-05 ", " V-06 ", " V-07 ", "
Vrms ", " V-08 ");
```

```
	memset (FileName, 0, 256);
	PromptPopup ("Sampling Time", "How many minutes is the run?", FileName, 255);
	STFast=atoi(FileName);
	STFast=STFast*60*1000;
	CounterFast=0;
}
//==============================================================================
==========================
// Timers
//==============================================================================
==========================
// Date, Time and Temperature - 1 Second Event
int CVICALLBACK Clock_Time (int panel, int control, int event, void *callbackData,
                                                        int eventData1, int eventData2)
{
	switch (event)
	{
		case EVENT_TIMER_TICK:
			int ii;
			SYSTEMTIME LT02;
			if (GetDataFast==0)
			{
				// Time on Screen
```

```
                    Clock = time(NULL);

                    SetCtrlVal (MainPanelHandle, MAINPANEL_DATEANDTIME,
asctime(localtime(&Clock)));

                    // Get Temperature Values

                    // DAQmxReadAnalogF64 (TemperatureHandle, DAQmx_Val_Auto, 1,
DAQmx_Val_GroupByChannel, Temperatures, 4, &SamplesPerChannelRead, 0);

                    // Print Temperatures on Screen

                    /*SetCtrlVal (MainPanelHandle, MAINPANEL_NT01, Temperatures[0]);

                    SetCtrlVal (MainPanelHandle, MAINPANEL_NT02, Temperatures[1]);

                    SetCtrlVal (MainPanelHandle, MAINPANEL_NT03, Temperatures[2]);

                    SetCtrlVal (MainPanelHandle, MAINPANEL_NT04, Temperatures[3]);  */

                    // Print Voltage on Screen

                    SetCtrlVal (MainPanelHandle, MAINPANEL_NP01, Voltage[0]);

                    SetCtrlVal (MainPanelHandle, MAINPANEL_NP02, Voltage[1]);

                    SetCtrlVal (MainPanelHandle, MAINPANEL_NP03, Voltage[2]);

                    SetCtrlVal (MainPanelHandle, MAINPANEL_NP04, Voltage[3]);

                    SetCtrlVal (MainPanelHandle, MAINPANEL_NP05, Voltage[4]);

                    SetCtrlVal (MainPanelHandle, MAINPANEL_NP06, Voltage[5]);

                    SetCtrlVal (MainPanelHandle, MAINPANEL_NP07, Vrms1s);

                    SetCtrlVal (MainPanelHandle, MAINPANEL_NP08, Voltage[7]);

                    //DAQmxReadAnalogF64 (PressureHandle2, DAQmx_Val_Auto, 1,
DAQmx_Val_GroupByScanNumber, Voltage2, 16000, &SamplesPerChannelRead2, 0);

                    // Plot on Graph
```

```
if (PlotAndSaveFlag == 1)
{
    GraphValue[0]=Voltage[0];
    GraphValue[1]=Voltage[1];
    GraphValue[2]=Voltage[2];
    GraphValue[3]=Voltage[3];
    GraphValue[4]=Voltage[4];
    GraphValue[5]=Voltage[5];
    GraphValue[6]=Vrms1s;
    //PlotStripChart (MainPanelHandle, MAINPANEL_SC01,
Temperatures, 4, 0, 0, VAL_DOUBLE);
    PlotStripChart (MainPanelHandle, MAINPANEL_SC02, GraphValue,
7, 0, 0, VAL_DOUBLE);
    // Save Temperatures to File
    /*GetLocalTime (&LT02);
    memset (TimeChar02, 0, 21);
    sprintf (TimeChar02, "%2d %s %2d %s %2d %s %3d", LT02.wHour,
":", LT02.wMinute, ":", LT02.wSecond, ":", LT02.wMilliseconds);
    fprintf (FileOfData02, "%12s %3s %9.2lf %9.2lf %9.2lf %9.2lf\n",
        TimeChar02, " |", Temperatures[0], Temperatures[1],
Temperatures[2], Temperatures[3]);
*/
    for (ii=0; ii<=999; ii++)
    {
```

```
                                        fprintf (FileOfData04,
"%14d %9.4lf %9.4lf %9.4lf %9.4lf %9.4lf %9.4lf %9.4lf %9.4lf %9.4lf %9.4lf %9.4lf %9.4lf %9.4l
f %9.4lf \n",
                                                1000*TMS+ii,
                                                Voltage2[16*ii+0], Voltage2[16*ii+1],
Voltage2[16*ii+2], Voltage2[16*ii+3],
                                                        Voltage2[16*ii+4], Voltage2[16*ii+5],
Voltage2[16*ii+6], Voltage2[16*ii+7],
                                                        Voltage2[16*ii+8], Voltage2[16*ii+9],
Voltage2[16*ii+10], Voltage2[16*ii+11],
                                                        Voltage2[16*ii+12], Voltage2[16*ii+13],
Voltage2[16*ii+14], Voltage2[16*ii+15]);
                                        }
                                        TMS++;
                                }
                        }
                        break;
        }
        return 0;
}
//=============================================================================================
=========================
// Buttons
//=============================================================================================
=========================
// Close Main Program
```

```
int CVICALLBACK End_Program (int panel, int control, int event,
		void *callbackData, int eventData1, int eventData2)
{
	switch (event)
	{
		case EVENT_COMMIT:
			GetVoltFlag = 0;
			// Terminate Executable
			TerminateExecutable (Executable01);
			// Open the Hardware Channels
			//DAQmxClearTask (TemperatureHandle);
			DAQmxClearTask (PressureHandle);
			DAQmxClearTask (PressureHandle2);
			// Quit Program
			QuitUserInterface (0);
			break;
	}
	return 0;
}
// Open File
int CVICALLBACK Open_File (int panel, int control, int event,
		void *callbackData, int eventData1, int eventData2)
```

```
{
	switch (event)
	{
		case EVENT_COMMIT:
			FileSelectPopup ("c:\\DAQ File", "*.*", "*.*", "Select File to Open",
VAL_SELECT_BUTTON, 0, 0, 0, 0, FileBrowser);
			OpenDocumentInDefaultViewer (FileBrowser, 2);
			break;
	}
	return 0;
}
// Open File Explorer
int CVICALLBACK Open_File_Explorer (int panel, int control, int event,
		void *callbackData, int eventData1, int eventData2)
{
	switch (event)
	{
		case EVENT_COMMIT:
			LaunchExecutable ("c:\\Windows\\explorer.exe");
			break;
	}
	return 0;
}
```

```
// Start Fast Sampling

int CVICALLBACK Start_Fast_Sampling (int panel, int control, int event,

		void *callbackData, int eventData1, int eventData2)

{

	switch (event)

	{

		case EVENT_COMMIT:

			WriteFileTitle2();

			MessagePopup ("Storing Data Fast", "Press OK to Start Sampling");

			OpenCom(4,"COM4");

			Sleep(1500);

			ComWrt(4, "0", 1);

			Sleep(1500);

			CloseCom(4);

			GetDataFast=1;

			break;

	}

	return 0;

}



//============================================================================
==========================

// Switches
```

```
//==============================================================================
==========================

//Plot and Save to File

int CVICALLBACK Binary_Switch_01 (int panel, int control, int event,

		void *callbackData, int eventData1, int eventData2)

{

	switch (event)

	{

		case EVENT_COMMIT:

			GetCtrlVal (MainPanelHandle, MAINPANEL_BS01, &PlotAndSave);

			if (PlotAndSave==1)

			{

				// Clear Strip Charts

				ClearStripChart (MainPanelHandle, MAINPANEL_SC01);

				ClearStripChart (MainPanelHandle, MAINPANEL_SC02);

				// Create the name of the File to Write

				WriteFileTitle();

				// Call Arduino

				OpenCom(4,"COM4");

				Sleep(1500);

				ComWrt(4, "0", 1);

				Sleep(1500);

				CloseCom(4);
```

```
                    PlotAndSaveFlag = 1;
                    // Change Software Attributes
                    SetCtrlAttribute (MainPanelHandle, MAINPANEL_BENDPROGRAM,
ATTR_DIMMED, 1);
                    TMS=0;
                }
                else
                {
                    // Stop Writing of File
                    PlotAndSaveFlag = 0;
                    fclose (FileOfData01);
                    fclose (FileOfData04);
                    //fclose (FileOfData02);
                    // Change Softw Attributes
                    SetCtrlAttribute (MainPanelHandle, MAINPANEL_BENDPROGRAM,
ATTR_DIMMED, 0);
                }
                break;
        }
        return 0;
}

//Injection Valve
```

```
int CVICALLBACK BS_Injection_Valve (int panel, int control, int event,
		void *callbackData, int eventData1, int eventData2)
{
	switch (event)
	{
		case EVENT_COMMIT:
			int InjectionValve=0;
			GetCtrlVal (MainPanelHandle, MAINPANEL_BSINJECTIONVALVE,
&InjectionValve);
			if(InjectionValve==1)
			{
				OpenCom(4,"COM4");
				Sleep(1500);
				ComWrt(4, "1", 1);
				Sleep(1500);
				CloseCom(4);
			}
			else
			{
				OpenCom(4,"COM4");
				Sleep(1500);
				ComWrt(4, "2", 1);
				Sleep(1500);
```

```
                CloseCom(4);
            }
            break;
        }
        return 0;
}

// Fluidization Valve
int CVICALLBACK BS_Fluidization_Valve (int panel, int control, int event,
        void *callbackData, int eventData1, int eventData2)
{
    switch (event)
    {
        case EVENT_COMMIT:
            int FluidizationValve=0;
            GetCtrlVal (MainPanelHandle, MAINPANEL_BSFLUIDVALVE, &FluidizationValve);
            if(FluidizationValve==1)
            {
                OpenCom(4,"COM4");
                Sleep(1500);
                ComWrt(4, "3", 1);
                Sleep(1500);
```

```
                CloseCom(4);
            }
            else
            {
                OpenCom(4,"COM4");
                Sleep(1500);
                ComWrt(4, "4", 1);
                Sleep(1500);
                CloseCom(4);
            }
            break;
        }
        return 0;
}
```

## Arduino

```
//Global Variables
int T01=30000; // Time Before Increasing Vg
int T02=30000; // Time Before Injection
int T03=8000; // Duration of valve below tank opening
int T04=5000; // Time before Reducing Vg
int T05=17000;
```

```
int inByte;


void setup()
{
  //Open Port
  Serial.begin(9600);
  pinMode(2,OUTPUT);
  pinMode(3,OUTPUT);
  analogWrite(2,255);
  analogWrite(3,255);
}


void loop()
{
  if (Serial.available()>0)
  {
    inByte = Serial.read();
    if(inByte == '0')
    {
      delay(T01);
      delay(T01);
      analogWrite(2,0);
```

```
  delay(T02);
  analogWrite(3,0);
  delay(T03);
  analogWrite(3,255);
  delay(T04);
  delay(T01);
  delay(T01);
  delay(T05);
  analogWrite(2,255);

}
if(inByte == '1')
{
  analogWrite(3,0);
}
if(inByte == '2')
{
  analogWrite(3,255);
}
if(inByte == '3')
{
  analogWrite(2,0);
```

```
    }
    if(inByte == '4')
    {
      analogWrite(2,255);
    }
  }
}
```

# Matlab Programs

## Pixel values

```
function VideoAnalysis()
    %*********************************************************************
    %Title: ColorAnalysis.m
    %Purpose: Analyze the stability of spray jets videos
    %Created: 15/April/2016 by Dr. Francisco J. Sanchez Careaga
    %*********************************************************************
    %
    %Global Variables
    %
    %Get Intensity Matrix from the Complete Histogram Data in Matlab Workspace
    %
```

```
clc;

MatrixRedComp=evalin('base','SimOutRedComplete.signals.values');

MatrixRedComp=squeeze(MatrixRedComp);

MatrixGreenComp=evalin('base','SimOutGreenComplete.signals.values');

MatrixGreenComp=squeeze(MatrixGreenComp);

MatrixBlueComp=evalin('base','SimOutBlueComplete.signals.values');

MatrixBlueComp=squeeze(MatrixBlueComp);

MatrixTimeComp=evalin('base','SimOutRedComplete.time');

MatrixTimeComp=squeeze(MatrixTimeComp);

MatrixIntComp=evalin('base','SimOutIntComplete.signals.values');

MatrixIntComp=squeeze(MatrixIntComp);

Ysize=size(MatrixIntComp,1);

Xsize=size(MatrixIntComp,2);

Tsize=size(MatrixIntComp,3);

%Note, the axis are backwards.

fprintf('\n');

fprintf('Size of the Matrix and Frames \n');

fprintf('X=0 & Y=0 at top left corner \n');

fprintf('It moves on Y axis first, X axis second, and Frame axis third \n');

fprintf('The Size of Matrix X is: %d\n', Xsize);

fprintf('The Size of Matrix Y is: %d\n', Ysize);

fprintf('Number of Frames is: %d\n', Tsize);
```

```
fprintf('\n');

fprintf('Intensity formula\n');

fprintf('Intensity = 0.2989*R + 0.5870*G + 0.1140*B \n');

fprintf('\n');

fprintf('Start Time\n');

format shortg;

ST=clock;

fprintf('Start Time  (hh:mm:ss): %d : %d : %2.3f \n\n', ST(4), ST(5), ST(6));

InPer =0.0;

fprintf ('%7.1f %% Completed\n',InPer);

%Open Files

%Complete Results

FileOfData=fopen('Results 1C.txt', 'wt');

fprintf(FileOfData, '%7s %7s %7s %7s %7s %7s %7s \n', 'Frame', 'X', 'Y', 'R', 'G', 'B', 'I');

%Red

FileOfDataR=fopen('Results 2R.txt', 'wt');

fprintf(FileOfDataR, '%7s \n', 'R');

%Green

FileOfDataG=fopen('Results 3G.txt', 'wt');

fprintf(FileOfDataG, '%7s \n', 'G');

%Blue

FileOfDataB=fopen('Results 4B.txt', 'wt');
```

```
fprintf(FileOfDataB, '%7s \n', 'B');

%Intensity

FileOfDataI=fopen('Results 5I.txt', 'wt');

fprintf(FileOfDataI, '%7s \n', 'I');

%Read and write to file

for i=1:Tsize

   for j=1:Xsize

      for k=1:Ysize

         %fprintf(FileOfData, '%7d %7d %7d %7.3f %7.3f %7.3f %7.3f \n', i, j, k, MatrixRedComp(k,j,i),
MatrixGreenComp(k,j,i), MatrixBlueComp(k,j,i), MatrixIntComp(k,j,i));

         fprintf(FileOfDataR, '%7.3f \n', MatrixRedComp(k,j,i));

         fprintf(FileOfDataG, '%7.3f \n', MatrixGreenComp(k,j,i));

         fprintf(FileOfDataB, '%7.3f \n', MatrixBlueComp(k,j,i));

         fprintf(FileOfDataI, '%7.3f \n', MatrixIntComp(k,j,i));

      end

   end

   fprintf('\b\b\b
```

```
    fclose (FileOfDataB);

    fclose (FileOfDataI);

    %Final notes

    fprintf('\n');

    fprintf('Finish Time\n');

    format shortg;

    FT=clock;

    fprintf('Finish Time (hh:mm:ss): %d : %d : %2.3f \n', FT(4), FT(5), FT(6));

    fprintf('\n');

    fprintf('...Done! \n\n');

end
```

## Pixel values-Simulink

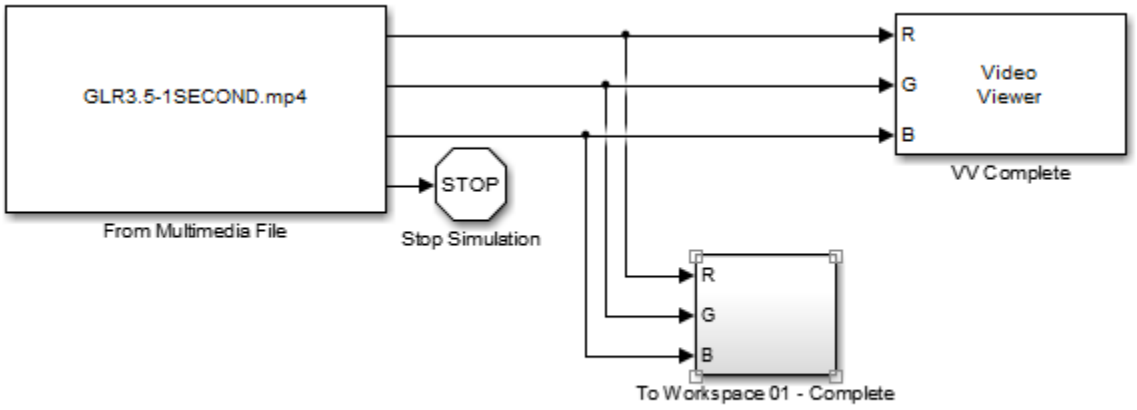

# Color analysis

```
function ColorAnalysis()
    %************************************************************************
    %Title: ColorAnalysis.m
    %Purpose: Analyze the stability of spray jets videos
    %Created: 25/Sep/2015 by Dr. Francisco J. Sanchez Careaga
    %************************************************************************
    %
    %Global Variables
    %
    %Get Intensity Matrix from the Complete Histogram Data in Matlab Workspace
    %
    IntMatHistComp=evalin('base','SimOutBWComplete.signals.values');
    IntMatHistComp=squeeze(IntMatHistComp);
    IntTimeMatHistComp=evalin('base','SimOutBWComplete.time');
    IntTimeMatHistComp=squeeze(IntTimeMatHistComp);
    IntMatrixC=zeros(size(IntTimeMatHistComp,1),size(IntMatHistComp,1)+1);
    for i=1:size(IntTimeMatHistComp,1)
        IntMatrixC(i,1)=IntTimeMatHistComp(i,1);
        for j=1:size(IntMatHistComp,1)
            IntMatrixC(i,j+1)=IntMatHistComp(j,i);
```

```
    end
end
IntMatCHeader = cell(1,size(IntMatHistComp,1)+1);
IntMatCHeader{1}='Time';
for i=2:size(IntMatHistComp,1)+1
    IntMatCHeader{i}=['Ch-' num2str(sprintf('%03d',i-1))];
end
IntMatCNotes = cell(1,1);
IntMatCNotes{1}='Intensity Formula = 0.2989 * R + 0.5870 * G + 0.1140 * B';
FileName01 = 'Results 01 - Intensity Histogram Analysis.xlsx';
 xlswrite(FileName01,IntMatCNotes, 'Sheet1', 'A1');
xlswrite(FileName01,IntMatCHeader, 'Intensity Data-Complete', 'A1');
xlswrite(FileName01,IntMatrixC,'Intensity Data-Complete', 'A2');
%
%Get Intensity Matrix from the Zoom Histogram Data in Matlab Workspace
%
IntMatHistZoom=evalin('base','SimOutBWZoom.signals.values');
IntMatHistZoom=squeeze(IntMatHistZoom);
IntTimeMatHistZoom=evalin('base','SimOutBWZoom.time');
IntTimeMatHistZoom=squeeze(IntTimeMatHistZoom);
IntMatrixZ=zeros(size(IntTimeMatHistZoom,1),size(IntMatHistZoom,1)+1);
for i=1:size(IntTimeMatHistZoom,1)
```

```
    IntMatrixZ(i,1)=IntTimeMatHistZoom(i,1);
    for j=1:size(IntMatHistZoom,1)
        IntMatrixZ(i,j+1)=IntMatHistZoom(j,i);
    end
end
IntMatZHeader = cell(1,size(IntMatHistZoom,1)+1);
IntMatZHeader{1}='Time';
for i=2:size(IntMatHistZoom,1)+1
    IntMatZHeader{i}=['Ch-' num2str(sprintf('%03d',i-1))];
end
xlswrite(FileName01,IntMatZHeader, 'Intensity Data-Zoom', 'A1');
xlswrite(FileName01,IntMatrixZ,'Intensity Data-Zoom', 'A2');
%
%Get RGB Matrix from the Complete Histogram Data in Matlab Workspace
%
ColorMatHistComp=evalin('base','SimOutColorHistComplete.signals.values');
RedComp=ColorMatHistComp(:,1,:);
GreenComp=ColorMatHistComp(:,2,:);
BlueComp=ColorMatHistComp(:,3,:);
RedComp=squeeze(RedComp);
GreenComp=squeeze(GreenComp);
BlueComp=squeeze(BlueComp);
```

```
ColorTimeMatHistComp=evalin('base','SimOutColorHistComplete.time');

ColorTimeMatHistComp=squeeze(ColorTimeMatHistComp);

RedMatrixC=zeros(size(ColorTimeMatHistComp,1),size(RedComp,1)+1);

GreenMatrixC=zeros(size(ColorTimeMatHistComp,1),size(GreenComp,1)+1);

BlueMatrixC=zeros(size(ColorTimeMatHistComp,1),size(BlueComp,1)+1);

for i=1:size(ColorTimeMatHistComp,1)

   RedMatrixC(i,1)=ColorTimeMatHistComp(i,1);

   GreenMatrixC(i,1)=ColorTimeMatHistComp(i,1);

   BlueMatrixC(i,1)=ColorTimeMatHistComp(i,1);

   for j=1:size(RedComp,1)

      RedMatrixC(i,j+1)=RedComp(j,i);

   end

   for j=1:size(GreenComp,1)

      GreenMatrixC(i,j+1)=GreenComp(j,i);

   end

   for j=1:size(BlueComp,1)

      BlueMatrixC(i,j+1)=BlueComp(j,i);

   end

end

ColorMatCHeader = cell(1,size(RedComp,1)+1);

ColorMatCHeader{1}='Time';

for i=2:size(RedComp,1)+1
```

```
    ColorMatCHeader{i}=['Ch-' num2str(sprintf('%03d',i-1))];
end
FileName02 = 'Results 02 - Color Histogram Analysis.xlsx';
xlswrite(FileName02,ColorMatCHeader, '01-Red Data-Complete', 'A1');
xlswrite(FileName02,RedMatrixC,'01-Red Data-Complete', 'A2');
xlswrite(FileName02,ColorMatCHeader, '02-Green Data-Complete', 'A1');
xlswrite(FileName02,GreenMatrixC,'02-Green Data-Complete', 'A2');
xlswrite(FileName02,ColorMatCHeader, '03-Blue Data-Complete', 'A1');
xlswrite(FileName02,BlueMatrixC,'03-Blue Data-Complete', 'A2');
%
%Get RGB Matrix from the Zoom Histogram Data in Matlab Workspace
%
ColorMatHistZoom=evalin('base','SimOutColorHistZoom.signals.values');
RedZoom=ColorMatHistZoom(:,1,:);
GreenZoom=ColorMatHistZoom(:,2,:);
BlueZoom=ColorMatHistZoom(:,3,:);
RedZoom=squeeze(RedZoom);
GreenZoom=squeeze(GreenZoom);
BlueZoom=squeeze(BlueZoom);
ColorTimeMatHistZoom=evalin('base','SimOutColorHistZoom.time');
ColorTimeMatHistZoom=squeeze(ColorTimeMatHistZoom);
RedMatrixZ=zeros(size(ColorTimeMatHistZoom,1),size(RedZoom,1)+1);
```

```
GreenMatrixZ=zeros(size(ColorTimeMatHistZoom,1),size(GreenZoom,1)+1);
BlueMatrixZ=zeros(size(ColorTimeMatHistZoom,1),size(BlueZoom,1)+1);
for i=1:size(ColorTimeMatHistZoom,1)
    RedMatrixZ(i,1)=ColorTimeMatHistZoom(i,1);
    GreenMatrixZ(i,1)=ColorTimeMatHistZoom(i,1);
    BlueMatrixZ(i,1)=ColorTimeMatHistZoom(i,1);
    for j=1:size(RedZoom,1)
        RedMatrixZ(i,j+1)=RedZoom(j,i);
    end
    for j=1:size(GreenZoom,1)
        GreenMatrixZ(i,j+1)=GreenZoom(j,i);
    end
    for j=1:size(BlueZoom,1)
        BlueMatrixZ(i,j+1)=BlueZoom(j,i);
    end
end
ColorMatZHeader = cell(1,size(RedZoom,1)+1);
ColorMatZHeader{1}='Time';
for i=2:size(RedZoom,1)+1
    ColorMatZHeader{i}=['Ch-' num2str(sprintf('%03d',i-1))];
end
xlswrite(FileName02,ColorMatZHeader, '04-Red Data-Zoom', 'A1');
```

```
    xlswrite(FileName02,RedMatrixZ,'04-Red Data-Zoom', 'A2');

    xlswrite(FileName02,ColorMatZHeader, '05-Green Data-Zoom', 'A1');

    xlswrite(FileName02,GreenMatrixZ,'05-Green Data-Zoom', 'A2');

    xlswrite(FileName02,ColorMatZHeader, '06-Blue Data-Zoom', 'A1');

    xlswrite(FileName02,BlueMatrixZ,'06-Blue Data-Zoom', 'A2');

    return

end
```

# Color analysis-Simulink

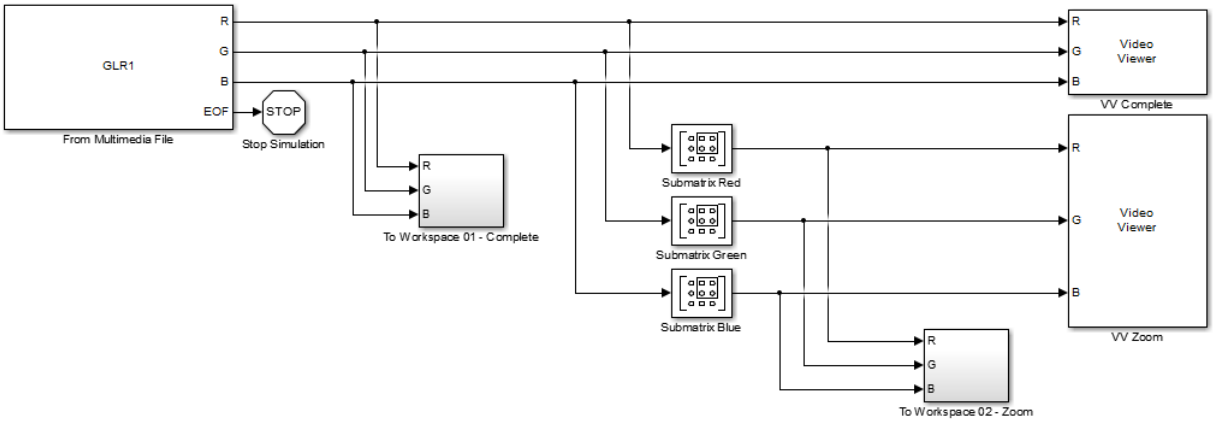

# Curriculum Vitae

| | |
|---|---|
| Name: | Lingchao Li |
| Post-secondary Education and Degrees: | The University of Western Ontario, London, Ontario, Canada<br>2014-2016 M.E.Sc.<br><br>China University of Petroleum (East China), Tsingtao, Shandong, China<br>2008-2012 B.Eng. |
| Honours and Awards: | NSERC Canada Graduate Scholarship |
| Related Work Experience: | Research assistant<br>China University of Petroleum (East China)<br>2012-2014 |